# THE EFFECT OF SWITCHABLE ADDITIVES ON COLLOIDAL INTERACTIONS FOUND IN OIL SANDS

by

Ying Yin Lau

A thesis submitted to the Department of Chemistry

in conformity with the requirements for the degree of

Master of Science

Queen's University

Kingston, Ontario, Canada

September 2010

# Abstract

This thesis describes an investigation of how carbon dioxide triggered switchable additives affect colloidal interactions found in oil sands, in an effort to identify potential candidates for industrial use.

Chemical force spectrometry was used to evaluate adhesion forces present in model oil sand systems. Organic/mineral and mineral/mineral interactions were investigated in the presence of cationic and anionic switchable surfactants, as well as switchable ionic strength additives. Of the additives studied, cationic switchable surfactants caused the greatest change in adhesion force between solutions free of $CO_2$ and solutions saturated with $CO_2$. These trends were consistent across all of the systems examined.

The effect of switchable additives on clay suspension behavior was studied by zeta potential measurements. The stability of clay suspensions are a problem in tailings disposal because fine mineral matter in recycled process water are detrimental to bitumen extraction. Cationic and anionic switchable surfactants were investigated, as were switchable ionic strength additives. Switchable ionic strength additives demonstrated the ability to suppress clay zeta potential to nearly zero upon exposure to $CO_2$. It was demonstrated that destabilization of clay suspensions can be achieved upon exposure of aqueous solutions containing the additives to $CO_2$.

# Acknowledgements

I would like to thank my two supervisors, Dr. Hugh Horton and Dr. Philip Jessop for their guidance and support through this project. I was fortunate enough to work under two brilliant and caring teachers, each bringing their own expertise and style to both my research and my education and growth as a chemist.

Many thanks need to be extended to Shell and NSERC for funding the research, and OGS for funding my second year of studies. In particular, the team at Shell has been most useful for their discussions and advice.

I would also like to acknowledge the faculty and staff at Queen's University for their assistance in this process. Thank you to Dr. Oleschuk and Dr. Liu for agreeing to be my supervisory committee. Thanks to Lindsay Hull and Ted Ison for allowing me to use their facilities and to Dr. Ruiyao Wang for answering all of my XPS questions. I would also like to extend a very special thank you to Dr. Igor Kozin. Dr. Kozin helped me set up several experiments and he was always helpful in discussion with any of my analytical chemistry issues that arose.

Thanks to the members of the Horton and Jessop group, past and present, for their encouragement and support through this project. These were the people who made each and everyday spent in the lab a joy. This experience would not have been the same without their friendship, consult, and generosity. Namaste.

**Horton Group**
Peiling
Alyza
Kevin
Mohammed
Hanif

**Jessop Group**
Dominik
Lam
Trisha
Catherine
Christoph
Elize
Sean
Keith
Chen
Darrell
Alaina
Amy
Vanessa
Andrew
Jitendra
Masa
Lauren
Candace

I am also deeply indebted to all the people at home on the rainy coast for their contribution of keeping me grounded and sane. Thanks to Kaz for always being on the other end of the phone to bring positivity into my life. I am especially grateful to my best friend Matthew for bringing me sunny days when cumulonimbus clouds hung over my head.

Lastly, I would like to acknowledge my family for everything that has led me to this accomplishment in my life. My brother Wei continues to keep me in touch with my inner child and always reminds me to keep things light and carefree. Thanks to my parents for their inspiration, motivation, and love. This thesis is dedicated to them for giving me the education and the opportunities that they never had. 谢 谢。

# Table of Contents

# List of Figures

# List of Tables

# List of Symbols and Abbreviations

| | |
|---|---|
| δ | chemical shifts in parts per million |
| Å | angstrom(s) |
| AFM | atomic force microscopy |
| ATR | attenuated total reflection |
| atm | atmosphere |
| CFS | chemical force spectrometry |
| CHAPS | 3-[(3-cholamidopropyl)dimethylammonio]-1-propanesulfonate |
| $cm^{-1}$ | wavenumbers |
| CTAB | cetyl trimethylammonium bromide |
| d | doublet |
| DMSO | dimethylsulfoxide |
| EI | electron impact |
| eV | electrovolts |
| FT | Fourier transform |
| h | hour(s) |
| Hz | hertz |
| IR | infrared |
| m | multiplet |
| M | molar |
| μm | micrometers |
| mM | millimolar |
| min | minute(s) |

| | |
|---|---|
| mol | mole(s) |
| mmol | millimole(s) |
| MS | mass spectrometry |
| mS $cm^{-1}$ | milliseimens per centimeter |
| mV | millivolts |
| nm | nanometers |
| NMR | nuclear magnetic resonance |
| nN | nanonewtons |
| ppm | parts per million |
| rpm | rotations per minute |
| s | second(s) |
| SAM | self assembled monolayer |
| SDS | sodium dodecyl sulfate |
| STM | scanning tunneling microscopy |
| UHV | ultrahigh vacuum |
| UPS | ultraviolet electron spectroscopy |
| vol | volume |
| wt | weight |
| XPS | x-ray photoelectron spectroscopy |

# 1. Introduction

## 1.1. Oil Sands

### 1.1.1 Introduction

Oil sands are sand beds saturated with viscous, high density bitumen. They represent one of the largest mining operations in the world today.[1,2] The amount of oil that can be recovered from the sands is on par with the world's total discovered medium and light gravity oils. Oil sands can be found in a variety of locations worldwide, but 91% of the world's oil sands deposits can be found in Canada and Venezuela. In Canada, the largest site is the Alberta Athabasca deposit and it is estimated to contain 600 billion barrels of bitumen. In comparison, a large oil field in Saudi Arabia (Ghawar) is estimated to contain 150 billion barrels.[3] Thus, mining of the Alberta oil sands has a tremendous socioeconomic effect on both Canada and the world.

Current industrial operations employ large volumes of water to extract bitumen from sand.[4] The National Energy Board reports that production of one barrel of bitumen from the Alberta oil sands requires 2-4.5 barrels of water, primarily supplied by the Athabasca River. The extraction gives rise to tailings consisting of coarse sands, mineral fines, and process water, which are deposited into man-made tailing ponds. Fine mineral tailings can take up to several years to consolidate into a solid layer, which makes recycling the water difficult. This is a major environmental problem, as the land on which these tailing ponds are created cannot be reclaimed for many years.

### 1.1.2 Oil Sands Structure

The Alberta oil sands are composed of bitumen (9-13%), water (3-7%), and mineral solids (80-85%), consisting of quartz sand, mica flakes, and mineral fines (Figure 1.1).[5] The mineral fines are predominately clays and they make up 15-30% of the mineral solids content. In addition, they are defined as being less than 40 microns in diameter. The clay minerals are predominately illite and kaolinite clay, but a small amount of montmorillonite clay is also found.[6]

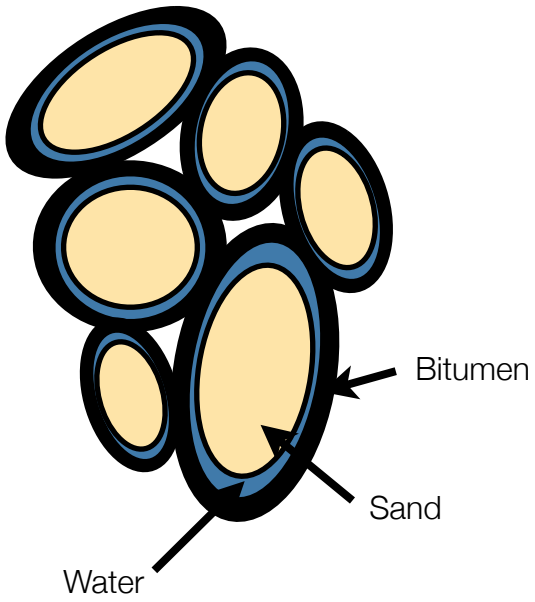


**Figure 1.1** Proposed oil sands structure[7]

It is postulated that the Alberta oil sands are hydrophilic and there is an envelope of water surrounding each grain of sand (Figure 1.1).[7] Although this hypothesis is widely accepted, there lacks experimental evidence as proof and thus, it is still a point of contention. The water wet theory was derived during the early

years of oil sands mining and two supporting points were presented. Dr. Karl Clark, who is credited with developing the current hot water method of extraction, observed with a microscope that when oil sand samples were cut, the oil envelopes were not cleanly exposed, but instead were sheared away.[8] Also, Clark suggests that since clean quartz and silicate materials are hydrophilic, it is more likely that water will wet these surfaces as opposed to bitumen. In agreement with Clark's findings, was work done by Ball which showed that dry heating of the oil sands does not result in separation of bitumen from the mineral surfaces.[9] He suggested that dry heat causes the water envelope to evaporate leaving behind an oil residue adhered to the sand surface. Takamura proposed a structure that is widely accepted today;[10] a water layer approximately 10 nm thick forms a film on the sand surfaces. This water film is stabilized by electrical double layer forces and destabilized by van der Waals forces. Although it is still unproven, most of the oil sands researchers accept the water wet model of oil sands structure proposed by Takamura.[3,7] However, it is still important to note that further investigations need to be conducted to obtain more direct experimental evidence.

### 1.1.3 Clay Structure and Chemistry

Clays are phyllosilicate materials.[11,12] They are made up to two dimensional arrays of silicon-oxygen tetrahedra layers and aluminum-or magnesium-oxygen-hydroxyl octahedra layers. As mentioned previously, the main types of clay fines found in oil sands are montmorillonite, kaolinite, and illite.[6]

Within the tetrahedral layer, $Si^{4+}$ cations form polyhedra with four oxygen atoms (Figure 1.2).[12] The oxygen anions are shared between cations either in the same tetrahedral layer or in the adjacent octahedral layer to maintain charge neutrality. Similarly, in the octahedral layer $Al^{3+}$ ions are surrounded by six oxygen atoms which are also shared by surrounding cations (Figure 1.3). In both the tetrahedral and the octahedral layers, the oxygen atoms may be oxygen anions or hydroxyl groups. The presence of hydroxyl groups in the crystal lattice gives rise to some of the acid-base properties of these minerals because they are amphoteric in nature.

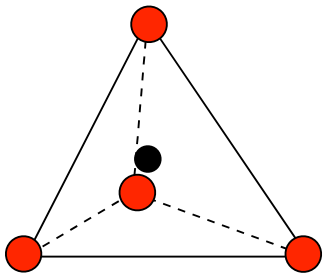

**Figure 1.2** Silica-oxygen tetrahedron in clay minerals

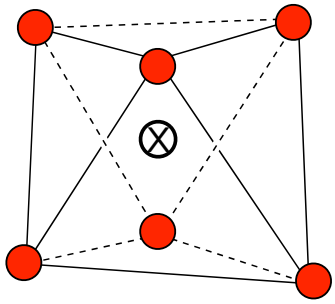

**Figure 1.3** Aluminum-oxygen octahedron

Random substitution of $Si^{4+}$ and $Al^{3+}$ with other cations is known as isomorphous substitution.[12] These substitutions can result in charge imbalances within the clay structure. Often this is compensated by integration of cations such as $Na^{+}$ and $K^{+}$ between the unit layers.

Montmorillonite has a 2:1 structure, consisting of 2 tetrahedral layers for every octahedral layer (Figure 1.4).[11,12] Its empirical formula is $(Na,Ca)_{0.33}(Al, Mg, Fe^{2+})_2Si_4O_{10}(OH)_2 \cdot nH_2O$. Within the tetrahedral sheet, there is random substitution of $Si^{4+}$ with $Al^{3+}$ and in the octahedral sheet there may be substitution of $Al^{3+}$ by a variety of divalent cations such as $Mg^{2+}$, $Fe^{2+}$, and $Zn^{2+}$. This results in a crystal lattice that has an excess of negative charge. Adsorption of cations such as $Na^{+}$ and $Ca^{2+}$ on the surface of the layers offsets the charge build up from isomorphous substitution, but these cations can easily be exchanged when in solution. For this reason, montmorillonite is known as a swelling clay and has properties that differ from kaolinite and illite. These exchangeable cations give rise to a large absorption capacity of ions from a solution.

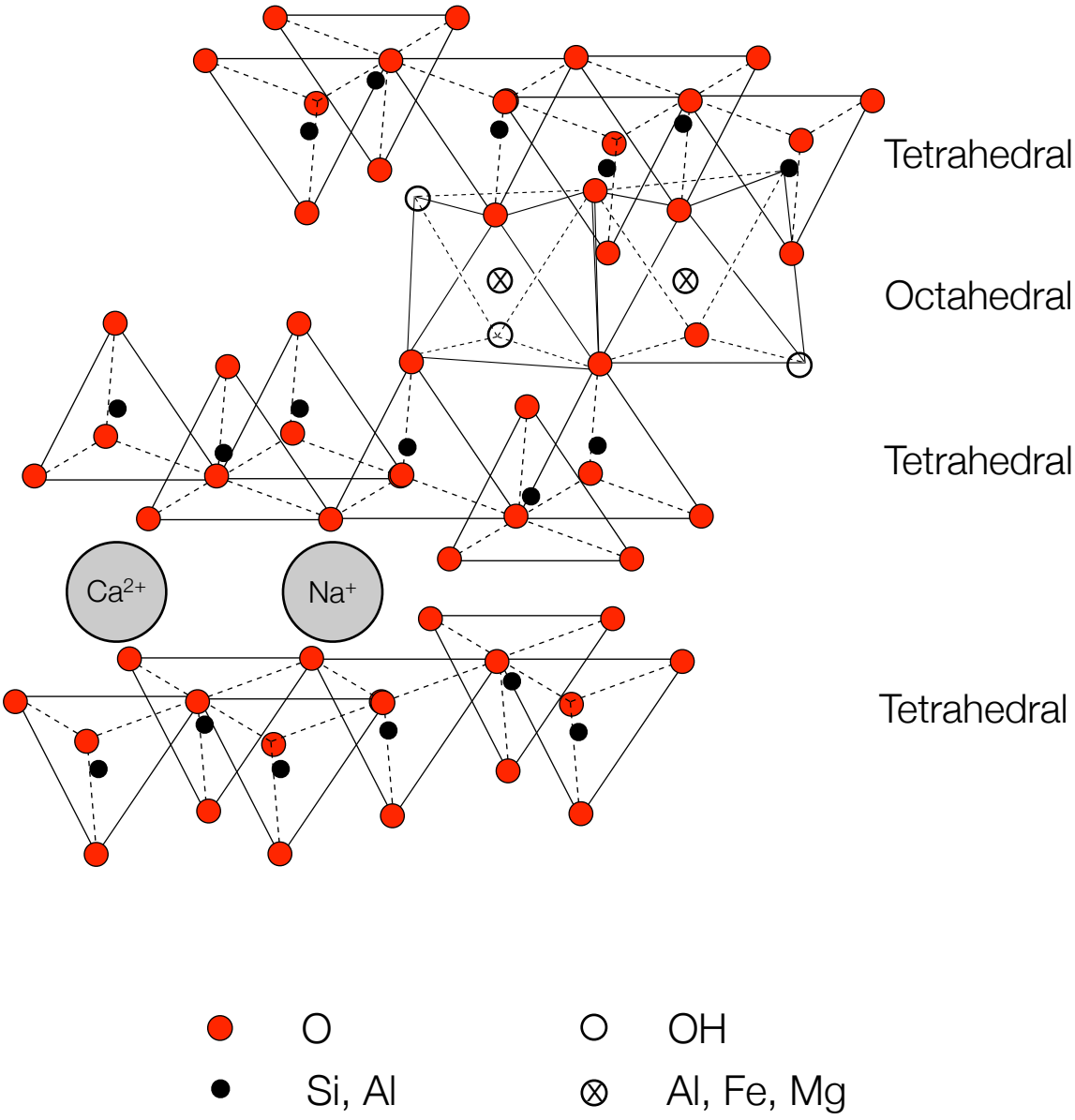


**Figure 1.4** Montmorillonite clay structure[11,12]

Montmorillonite is reported to have a unique pH-independent surface charge.[13] The basal plane contains very few amphoteric hydroxyl sites and thus retains a constant charge if the clays are submerged in solution. The amphoteric sites of this clay are situated on the edge surfaces, which make up approximately 1%

of the total surface area; therefore, changes in surface charge with varying pH are not typically observed with this clay.

The empirical formula for kaolinite is $Al_2Si_2O_5(OH)_4$.[11,12] It is a 1:1 (tetrahedral: octahedral) layered material that does not contain very high levels of isomorphous substitution (Figure 1.5). There are some substitutions of $Al^{3+}$ for $Si^{4+}$ in the tetrahedral sheet and $Mg^{2+}$ for $Al^{3+}$in the alumina octahedral sheet, resulting in an overall negatively charged crystal lattice. Charge compensating cations such as $K^+$ adsorb onto the surface of the clay and are not integrated into the layers, so therefore, kaolinite is known as a non-swelling clay.

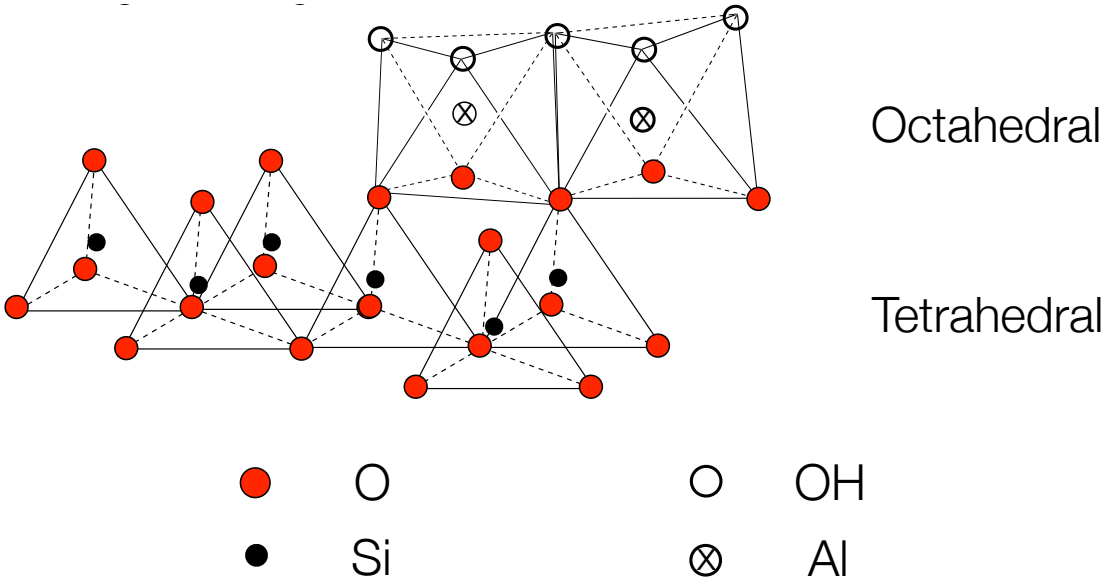


**Figure 1.5** Kaolinite clay structure[11,12]

In suspension, the basal planes of kaolinite are commonly assumed to be permanently negatively charged due to the isomorphous substitutions, whereas the

charge of the edge surface is pH dependent.[14] Recent work by Gupta and Miller has shown that both the tetrahedral silica layers and the octahedral alumina layers exhibit changes in surface charge with varying pH. Through surface force measurements, they revealed that the silica tetrahedral face is negatively charged in solutions with pH greater than 4, whereas the alumina octahedral face is positively charged in solutions with pH less than 6, but negatively charged at pH greater than 8. These surface charge dependencies on pH are attributed to amphoteric hydroxyl defects in the crystal lattice.

Like kaolinite, illite is also a non-swelling clay.[11,12] Its empirical formula is $K_{0.8\text{-}0.9}(Al, Fe, Mg)_2(Si, Al)_4O_{10}(OH)_2$. The clay has a 2:1 structure, consisting of 2 tetrahedral layers for every octahedral layer (Figure 1.6). There are more isomorphous substitutions in illite than in kaolinite, with some $Fe^{3+}$, $Mg^{2+}$, $Fe^{2+}$ substitutions in the octahedral sheet and some $Al^{3+}$ in the tetrahedral sheet. Potassium ions are tightly integrated between the layers to compensate for charge imbalance and unlike in the case of montmorillonite, they do not exchange to yield a swelling clay.[11,12] As a result of isomorphous substitutions, the basal surfaces are considered to be permanently negatively charged, whereas most of the amphoteric sites are situated on the edge surfaces and become more negatively charged with increasing pH.[15]

The surface of illite clay is reported to be acidic under aqueous conditions due to the presence of surface hydroxyl sites.[15,16] Ding et al. were able to show experimentally that addition of illite clay to aqueous solutions causes the solution pH to drop[15]. For oil sands processing water, a decrease in pH from 8 to 6 was observed

with the addition of 5% by weight of clay. Illite clay is more acidic under these conditions compared with kaolinite and montmorillonite, but the reason for this behaviour is still unclear.[16]

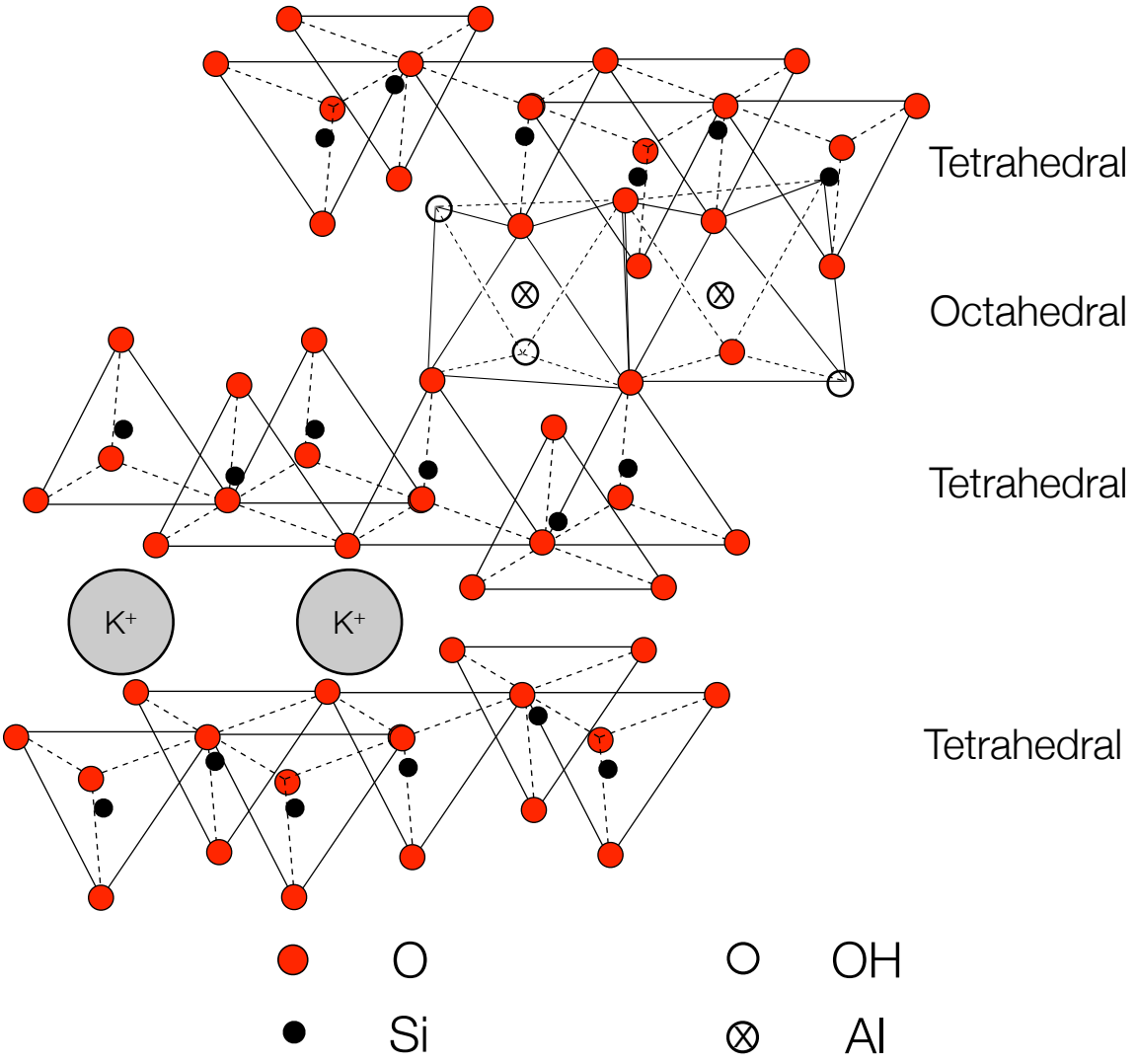


**Figure 1.6** Illite clay structure[11,12]

Like the clays mentioned above, mica is a phyllosilicate, but is defined as a mineral and not a clay because it forms large tabular crystals and not fine grains.[11,12]

However, structurally micas and clays are very similar. Muscovite mica, $KAl_2(AlSi_3)O_{10}(OH)_2$, is an example illustrated below (Figure 1.7) and rarely deviates from its empirical formula. Structurally, muscovite mica is similar to illite clay, but differs slightly in chemical composition. It is also a 2:1 mineral. Both muscovite mica and illite cleave on the {001} plane to reveal similar surfaces upon cleavage; however, muscovite is often used as a substrate for surface science as it cleaves to give a molecularly smooth sample. For every three $Si^{4+}$ in the tetrahedral layer, there is a substitution of $Al^{3+}$ which leads to a buildup of negative charge. The charge imbalance is resolved by the integration of $K^+$ between the layers. The basal surface of muscovite mica is generally considered to be permanently negatively charged in aqueous solutions due to the $Al^{3+}$ isomorphous substitution, whereas, the charge of edge surface is more pH dependent due to a greater number of amphoteric sites.[17]

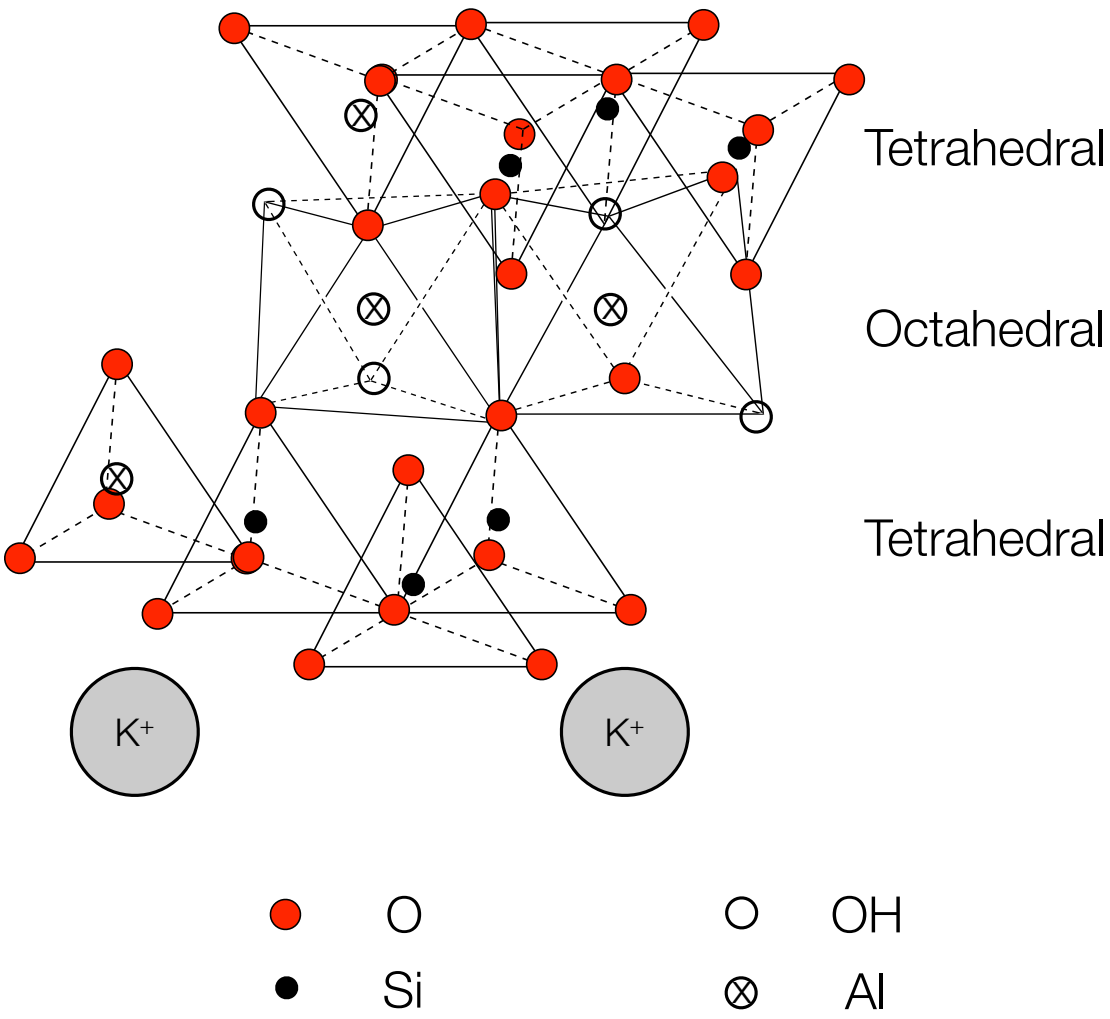


**Figure 1.7** Muscovite mica structure[11,12]

### 1.1.4 Bitumen

Bitumen is a complex mixture of hydrocarbons, polyaromatics, heterocycles, and trace amounts of inorganic salts and oxides.[18] The exact chemical composition is dependent on the deposit the bitumen was recovered from, but most bitumens contain 82-88% carbon, 8-11% hydrogen, 0-1.5% oxygen, 0-1% nitrogen, and 0-6%

sulfur. Infrared spectroscopy has identified the presence of organic functionalities such as carboxylic acids, sulfonic acids, amides, and esters. Under alkaline conditions, the carboxylic acids and the sulfonic acids are deprotonated to form natural surfactants from the bitumen.[3] Saponification of esters can also occur under these conditions.

Bitumen can be separated into four broad classes known as saturates, aromatics, resins, and asphaltenes (Figure 1.8).[18] These groups arise from the techniques used for separation and are not exact chemical entities. Two components, asphaltenes and maltenes (consisting of saturates, aromatics, and resins) can be identified through n-heptane precipitation.[13] Maltenes are soluble in n-heptane, whereas asphaltenes will precipitate as black or brown solids. Column chromatography using silica gel or alumina is used to separate the maltenes fraction into its three constituents: saturates, aromatics, and resins.

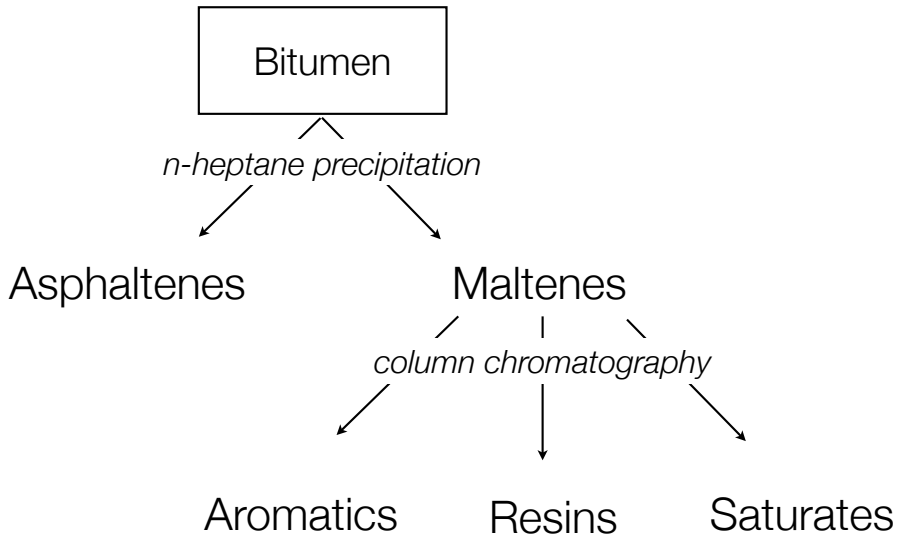


**Figure 1.8** Components of bitumen[18]

Asphaltenes make up 5-25% of bitumen by weight.[18] This is a class of highly polar, aromatic compounds containing some nitrogen, sulphur, and oxygen (Figure 1.9). They are typically of higher molecular weight than maltenes, with a wide range of weights from 600-300000 g/mol. The viscosity of bitumen is strongly dependent on the asphaltenes content; bitumen with higher asphaltenes content has a higher viscosity than bitumen with lower asphaltenes content.

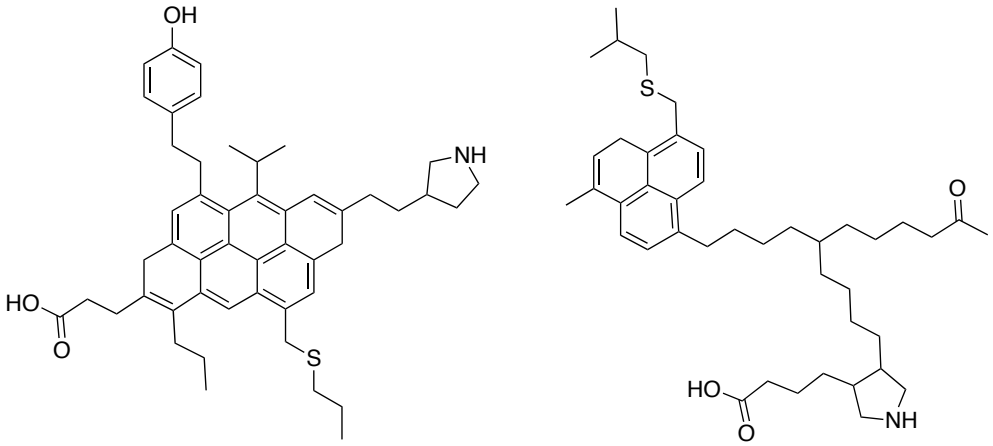


**Figure 1.9** Typical asphaltenes structures[18]

Resins are organic molecules containing small amounts of oxygen, sulfur, and nitrogen.[18] They typically have molecular weights from 500-50000 g/mol. This is a very polar constituent of bitumen and display strong adhesive properties. In addition, they act as dispersants for asphaltenes.

Aromatics make up approximately 40-65% of bitumen by weight and they dissolve other hydrocarbons.[18] Compared to asphaltenes and resins, they have a lower average molecular weight of 300-2000 g/mol. They are a mixture of polyaromatic organic compounds and hydrocarbon chains (Figure 1.10).

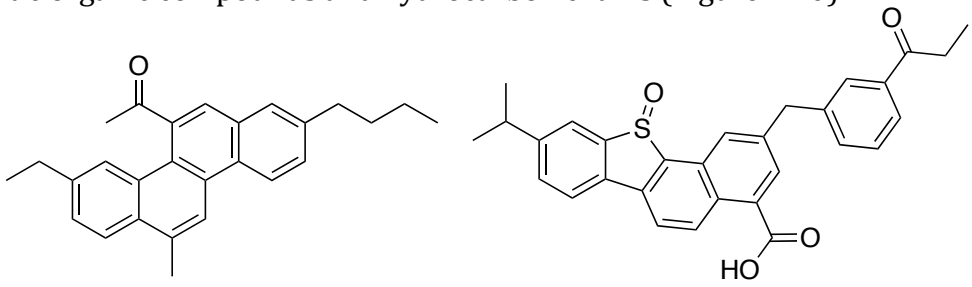


**Figure 1.10** Typical aromatic structures[18]

Saturates are straight and branched aliphatic hydrocarbons with some alkyl-aromatics (Figure 1.11).[18] They make up 5-20% of bitumen by weight and the average molecular weight of compounds in this class is similar to that of the aromatics (300-2000 g/mol).

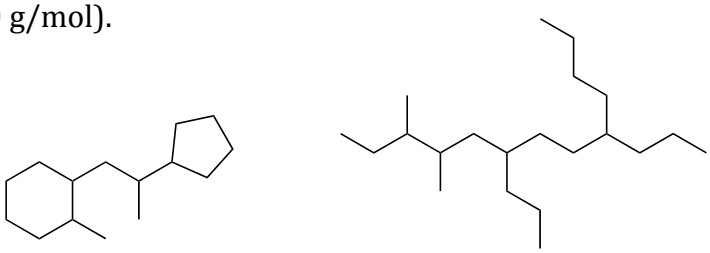

**Figure 1.11** Typical saturate structures[18]

## 1.2 Oil Sands Extraction

### 1.2.1 Oil Sands Extraction

The main method of oil sands extraction was developed by Dr. Karl Clark in the 1920s. This general method has remained in use since inception, although some minor changes have been made to increase efficiency and lower cost.[8, 19]

Of the tonnes of oil sands present in the Athabasca deposit, only 20% is considered to be surface mineable.[20] For the surface mineable oil sands there is less than 50 m of overburden and therefore, the oil sands may be mined in an open pit mine with trucks and shovels. The rest of the oil sands deposit lies too deep to be excavated in this manner and requires *in situ* techniques to recover the bitumen, as opposed to the hot water extraction method described below (Figure 1.12).

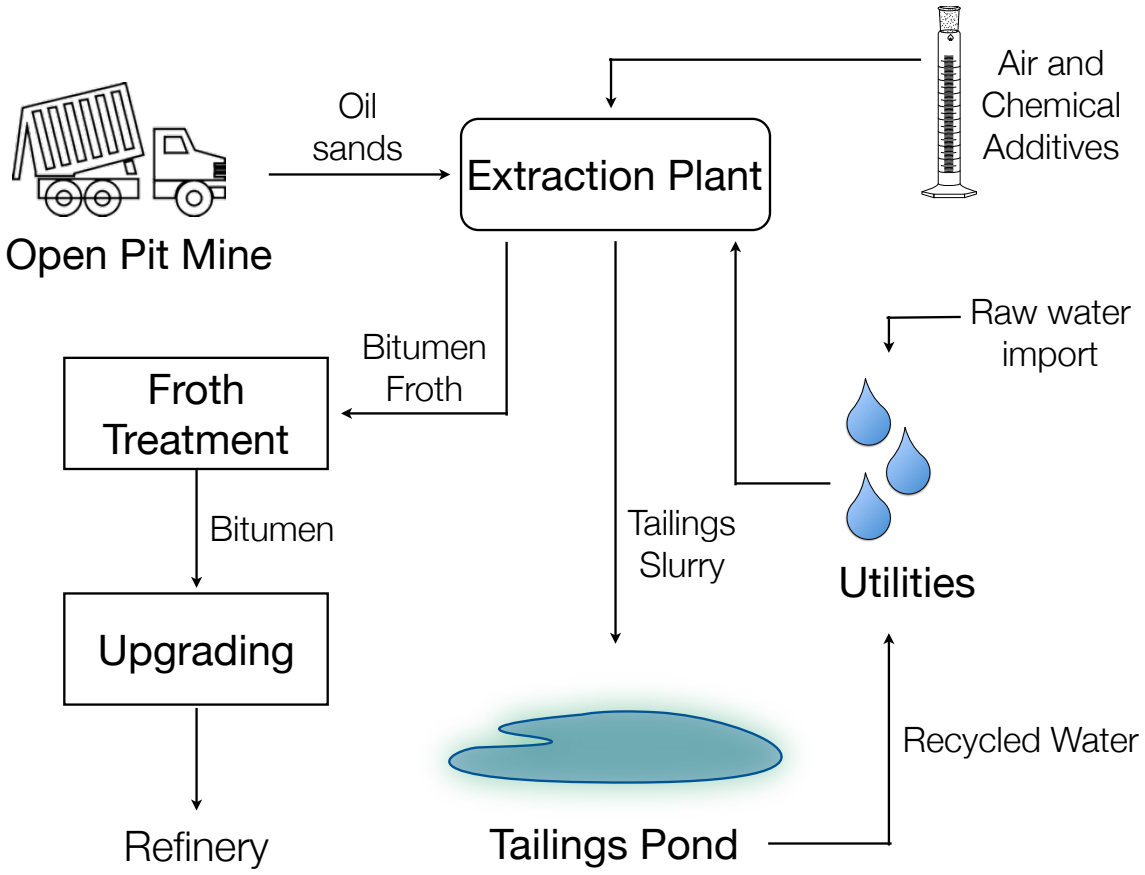


**Figure 1.12** General scheme for processing of surface mineable oil sands[19]

The processing of surface mineable oil sands begins with the removal of the material from the open pit mine and transport to the extraction plant (Figure 1.12).[19] At the extraction plant, large lumps of ore are crushed for size reduction and water is added to form the slurry. This water is a mixture of recycled process water from the tailings pond and fresh water from nearby sources such as the Athabasca River. It is also warmed to 30-35°C prior to slurry preparation, as elevated temperatures facilitate bitumen liberation. The slurry mixture is then moved to hydrotransport pipelines where chemical additives are added to aid with bitumen separation from

the sands. Common additives that improve bitumen recovery include inorganic bases such as NaOH and surfactants. Liberation of bitumen from sand is dependent on disrupting the balance of forces that cause bitumen to attach to the sand grains and forces pulling the bitumen off of the sand. Chemical additives, processing temperature, and mechanical agitation are all factors which affect the rate at which bitumen separation occurs.

Once the processing slurry is prepared, it is aerated.[19] Aeration of the slurry is crucial for bitumen floatation and recovery as bitumen is generally the same density as water over the temperature ranges employed for bitumen extraction. The liberated bitumen attaches itself to the available air bubbles and floats to the top. The attachment of air bubbles to bitumen is a thermodynamically favourable process as both the air bubbles and bitumen are hydrophobic in the absence of contamination. The aerated slurry is transported into large gravity separation vessels where the aerated bitumen froth is skimmed off the top and processed. The heavier solids such as sand and other mineral matter sink to the bottom of the vessel and are removed and sent to tailings ponds. The mixture in the middle consisting of solids, clay fines, and bitumen is further processed to improve recovery. Further information about tailings ponds may be found in Chapter 1.3 of this thesis.

Bitumen-bubble attachment is dependent on the size of the air bubbles introduced into the processing slurry.[8] Smaller bubbles (0.01-0.6 mm in diameter) have been reported to attach to bitumen more effectively than larger bubbles (~1 mm in diameter), and this is reflected through comparatively higher bitumen recovery with smaller bubbles.[8,19]

The aerated bitumen froth is a complex dispersion of oil, water, gas, and solids.[21] During the treatment process water and fine solids are removed by first diluting the froth with heated naphtha followed by centrifuging or using lamella settlers. Most of the water may be removed in this manner, but water that is emulsified in the bitumen is much more difficult to get rid of.[22] Emulsions are stabilized by asphaltenes and mineral fines that are present in the multi-phase bitumen froth. Surfactants can be added to promote coalescence of the emulsified water, but the resulting mixture still needs to be centrifuged and distilled to recover the naphtha diluent. As a whole, this process is energy intensive and process conditions have yet to be optimized simply because froth treatment issues are not as well studied as the bitumen extraction process, which more strongly affects the overall bitumen loss in this industrial process.

### 1.2.2 Temperature Effects

One of the main modifications to Clark's Hot Water Extraction Process is the reduction in slurry temperature over the years. Clark reported typical water temperatures of 80-85°C,[23] but this has been greatly reduced in recent years without adverse effects on bitumen recovery. 35-50°C is the slurry temperature range which current operations use.[24] These changes have lowered both thermal energy consumption and greenhouse gas emissions of oil sands operations; thus, leading to a reduction in operating costs.

The control of slurry temperature appears to influence many aspects of bitumen/sand separation. Amongst the properties affected include, but are not

limited to, bitumen viscosity, surface zeta potentials, and the kinetics of bitumen recovery.[24]

Reduction in bitumen viscosity with increasing temperature was postulated to be a main contributor to the increase in bitumen recovery with increasing temperature. In 1983, Hupka et al. demonstrated that there is a dependence on bitumen recovery on viscosity.[25] In this work, oil sands of various geographical origins were diluted with kerosene to adjust the viscosity of the oil sands. They were able to conclude that not only is viscosity dependent on the origin of the oil sands, but that recovery was reduced dramatically with bitumen viscosity greater than 3 Pa·S. Above this threshold value, the recovery rate in most cases was above 80%. They concluded that viscosity is a parameter that influences both the liberation and the aeration processes of extraction and without the increase of slurry temperature or the addition of a diluent, the bitumen remains adhered to the sand grains.

Not only does temperature affect bitumen viscosity, but temperature dependence of the zeta potentials of both silica and bitumen were reported by Long et al.[26] That is, increasingly negative zeta potentials were measured with increase in temperature from 20-45°C. This was attributed to dissociation of carboxyl and sulfonate on the bitumen surface and silanol groups on silica. With increasingly negative zeta potentials, an increase of electrostatic repulsion was observed between bitumen and silica with increasing temperature. In addition, carboxyl and sulfonate groups dissociate to form surfactants, which reduce interfacial tension and contribute to the increase in bitumen recovery observed.

The changes in physicochemical properties discussed above likely contribute to the increase in bitumen recovery kinetics observed with increasing temperature. For both good processing ore and poor processing ore, an increase in rate of bitumen recovery was observed when the water temperature was increased from 25°C to 50°C. This again, demonstrates the importance of slurry temperature on oil sands extraction.[27] Although other attempts have been made to further reduce operating temperatures, they have not been successful without sacrificing bitumen recovery.[24]

### 1.2.3 pH Effects

Bitumen extraction is typically conducted under weakly alkaline conditions.[8] Process water pH modifications are generally accomplished through the use of strong inorganic bases such as NaOH; this has been the practice since the method was originally developed. However, there is an optimal concentration of NaOH that results in the maximum bitumen recovery. Finding the optimal base concentration for processing is not trivial, as it is dependent on the nature of the ore being extracted. Schramm and Smith showed that although average and lean ores show an increase in bitumen recovery with increasing NaOH added, bitumen rich ores do not.[28] In fact, recovery decreases with the addition of base. For average ores, recovery was improved with increasing NaOH addition, but decreased if too much was added. This work demonstrated that although alkaline conditions generally improve bitumen recovery, the addition of too much base can be detrimental in some cases and maximum recovery does not occur at the same pH for all of the ores studied.

The addition of NaOH is postulated to improve recovery by ionizing organic acids in bitumen to produce "natural" surfactant species.[29] The surfactants serve to improve bitumen liberation by decreasing the interfacial tension between the oil and the mineral surfaces. Indeed, Schramm and Smith show that free surfactant concentration in the process water was an important parameter for high recovery rates.[28] However, it is also thought that increasingly alkaline conditions change the surface charges of both bitumen and solids, making both more negatively charged. This intensifies the electrostatic repulsion at the interface and therefore, facilitates bitumen removal.[30]

### 1.2.4 Divalent cations

As early as 1935, divalent metal cations such as $Ca^{2+}$ and $Mg^{2+}$ have been reported to have a detrimental effect on bitumen recovery.[8] Divalent cations decrease the surface charge of negatively charged bitumen and sand through absorption onto the surfaces. This decreases long range electrostatic repulsion between bitumen and sand, resulting in a reduction in recovery due to a stronger adhesion between the two surfaces.[31]

Kasongo et al. studied the effect of $Ca^{2+}$ and $Mg^{2+}$ on bitumen recovery in the presence and in the absence of 1 wt% clays (illite, kaolinite, or montmorillonite).[32] They found that the presence of calcium (1 mM) or clay alone only had a slight adverse affect on bitumen recovery, but a sharp reduction was observed when both calcium and montmorillonite were present in the processing water. The same effect

was observed with magnesium, indicating that the effect observed was a result of the valency of the cation, and not the nature of the metal ion.

Calcium can cause clays, particularly montmorillonite, to strongly attach to bitumen surfaces.[33,34] This is known as slime coating. Reduction of bitumen recovery ensues because slime coating impedes both coagulation of bitumen droplets and attachment to air bubbles.

### 1.2.5 Surfactants and other process aids

Surfactants have previously been shown to be effective process aids during extraction, improving bitumen recovery.[3] These may be naturally liberated from the bitumen as carboxylates, sulfonates, or sulfates into the aqueous phase through the addition of sodium hydroxide[35] or they may be commercially available additives.[36] The presence of surfactants results in the lowering of the interfacial tension between bitumen and water, by making the bitumen surface more hydrophilic, thereby facilitating removal of the bitumen film from the sand surface.[3] Bitumen recovery using surfactants as process aids is a pH dependent process regardless of whether naturally liberated or externally added surfactants are employed.[19]

Rowe and coworkers studied the effects of commercial surfactants on bitumen recovery as a function of pH.[36] Their findings showed that Triton X-100, CHAPS, and SDS show an increase in bitumen recovery with increasing pH. CHAPS and SDS are both anionic surfactants whereas Triton X-100 is a nonionic surfactant. The latter gave the best performance out of the commercial surfactants studied. However, when a cationic surfactant CTAB was used during extraction, the percent

oil recovered decreased with increasing pH. Rowe et al.[36] suggest that in the case of the cationic surfactant, there were changes in the solid surface hydrophobicity through surfactant absorption by means of electrostatic interactions with the oil/ mineral surfaces. Thus, surfactant absorption must also be considered when using surfactants for bitumen extraction.

## 1.3. Tailings

### 1.3.1 Tailings Disposal

Following bitumen extraction, the remaining solids (consisting of sand and clay) and process water are pumped to large tailings ponds for consolidation of the solid matter.[19] The tailings can be considered to have two components, a solid fraction of sand and a fluid part termed "sludge".[37] This sludge arises from the alkaline pH conditions of the process water during bitumen extraction. The addition of inorganic bases improves bitumen recovery during extraction, but keep the clay fines dispersed in the process water.

In the tailing ponds, the sand rapidly settles into the bottom of the pond.[38] The sludge layer lies above the solids layer and at the pond surface is a clear water layer which can be reused in the extraction process. The sludge layer of the pond gives rise to the general problem with tailings disposal. That is, the water contains too much suspended clay that does not settle to yield clear pond water that can be recycled or a solid compact surface that is desirable for disposal.

### 1.3.2 pH Effects

For bitumen extraction, the processing water ideally has an alkaline pH to facilitate bitumen literation.[8,28,29] However, for tailings disposal clay consolidation ideally occurs under acidic conditions,[39] leading to issues involving recycling the process water as the conditions desired in one step of the process is undesired in another.

Long et al. investigated the pH effect on illite-illite clay interactions.[39] Using atomic force microscopy, they were able to show that at pH 8.3, repulsive long range interaction forces were observed, but at pH 2.9, the repulsive forces are very small and attractive forces were measured. Suspensions of illite clay in water were stable at pH 8.3, but settled at pH 2.9. This work illustrated the importance of acidic aqueous conditions to tailings disposal.

### 1.3.3 Divalent Cations

Divalent cations such as $Ca^{2+}$ have been identified as detrimental to bitumen recovery in the presence of clays due to absorption onto bitumen surfaces.[8] On the other hand, divalent cations have been shown to improve clay settling in tailings. Addition of gypsum, $CaSO_4$, to tailings is known as the consolidated tailings process. Both Suncor and Syncrude are currently using this method to treat their tailings.[19] Generally, high loadings of gypsum are required (800-1200 ppm) which results in an increase of the ionic strength of the process water. Ions contributing to this increase include $Ca^{2+}$, $SO_4^{-2}$ (from gypsum), and $Na^+$ from $Ca^{2+}$ ion exchange with the clays.[40] This increase in ionic strength of the process water will ultimately effect the bitumen

extraction stage of the process if the water is to be used again.[41] For example, the presence of $Ca^{2+}$ will adversely affect bitumen recovery, as discussed previously.[8]

### 1.3.4 Polymer Flocculants

Paste technology is another tailings treatment process that aims to accelerate settling of clay fines.[42,43] Here, polymer flocculants are added to the tailings water. A variety of commercially available flocculants have been studied, but it was found that high molecular weight polymers with medium charge densities had the best performance. Polymers with molecular weights less than 1 million Daltons behaved as dispersants and improved bitumen extraction, but did not aid in the settling process. Conversely, polymers with molecular weights higher than 15 million Daltons accelerated tailings setting, but had a detrimental effect on the bitumen froth quality.[42] The best polymer flocculant for both bitumen recovery and tailings has been identified as a partially hydrolyzed polyacrylamide (HPAM) with a charge density of 30% and a molecular weight of 17.5 million Daltons. The commercial name for this additive is Percol 727.[43,44]

Percol 727 is most effective for accelerating settling of fines at low pH, but this is the pH range in which clays tend to coagulate even without the polymer flocculant present.[45] At alkaline pH conditions, such as those required for bitumen extraction, the clay fines form a stable suspension in the presence of Percol 727. Settling is accelerated when both Percol 727 and gypsum are present under these conditions.

Although polymer flocculants have been shown to be effective process aids in the tailings process, the effect of residual flocculants in the process water on bitumen extraction has yet to be identified.[42]

## 1.4 $CO_2$ Mediated Switchable Chemistry

### 1.4.1 Switchable Surfactants

Switchable surfactants with properties controlled by addition or removal of $CO_2$ were first reported by Jessop and coworkers in 2006.[46] They demonstrated that long chain alkyl amidines can reversibly switch between a demulsifier form and a surface active form using $CO_2$ as an external trigger. Treatment of aqueous solutions of these amidine compounds with 1 atmosphere of $CO_2$ affords the amidinium bicarbonate salt, which is a surfactant. When the solution is flushed with an inert gas ($N_2$, Ar, or air) to remove the $CO_2$, the process is reversed to transform the surfactant back to its demulsifier form (Figure 1.13).

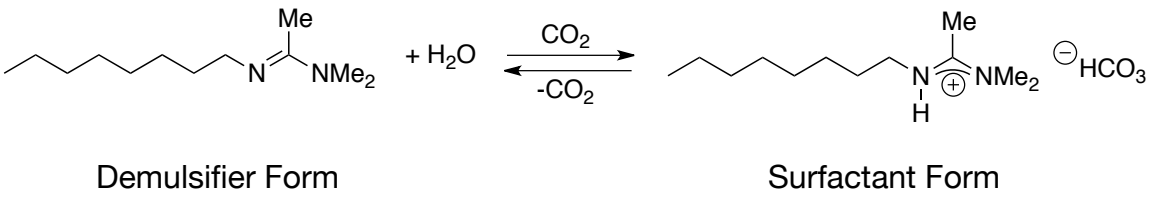


**Figure 1.13** An example of a cationic switchable surfactant

Switchable surfactants were designed with the purpose of improving industrial processes where emulsions are desired in one step of the operation and undesired in another.[46] Many potential applications have been proposed and identified. Aqueous solutions containing switchable surfactants have demonstrated ability to stabilize water/alkane emulsions for potential crude oil applications. They also have demonstrated utility for emulsion polymerization.

The success with the switchable surfactants discussed above prompted the development of a complementary new class of anionic switchable surfactants.[47] In contrast to the cationic switchable surfactants, the anionic switchable surfactants are surface active in aqueous solutions in the absence of $CO_2$. Upon exposure to 1 atmosphere of $CO_2$ the molecule becomes surface inactive. Again this process may be reverted to transform the surfactant back to its original state and restore its original surfactant properties upon flushing the solution with an inert gas. An example of a anionic switchable surfactant is shown below (Figure 1.14).

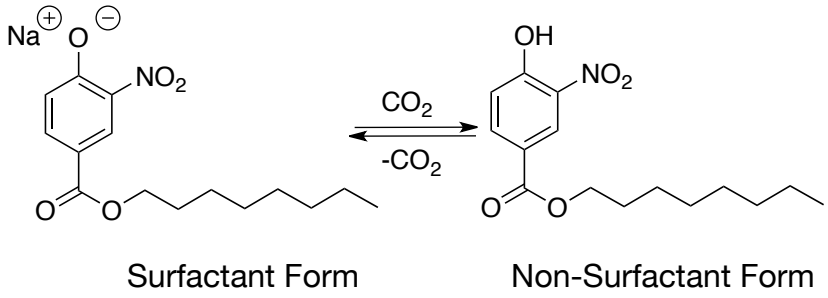


**Figure 1.14** An example of an anionic switchable surfactant

### 1.4.2 Switchable Water Additives

Water is often used as a solvent in industry, but is expensive to decontaminate before disposal. Common methods to separate solutes from water include distillation[48] and pervaporation;[49] these processes are expensive in energy, time, and materials. One effective method of separating organic solutes from water is to increase the ionic strength of the aqueous solution by dissolution of an electrolyte such as NaCl, thereby reducing the solubility of the dissolved organic solute.[50] However, the resulting aqueous salt solution is difficult to desalinate before re-use or disposal making the entire process costly.

One method to circumvent the expenses associated with using water as a solvent is to use a process that allows for reversible switching from an aqueous solution of low ionic strength to one of high ionic strength though the introduction of a trigger. The first aqueous solution of switchable ionic strength, "switchable water", has recently been reported in the literature.[51] This work employs tertiary amines dissolved in water, which are uncharged in solution and have zero ionic strength prior to the introduction of $CO_2$. Upon saturation of the solution with $CO_2$, the formation of ammonium hydrogen carbonate occurs and the ionic strength is significantly increased from that of the original sample. The process can be reversed through moderate heating and sparging with $N_2$ or air to remove the dissolved carbon dioxide (Figure 1.15).

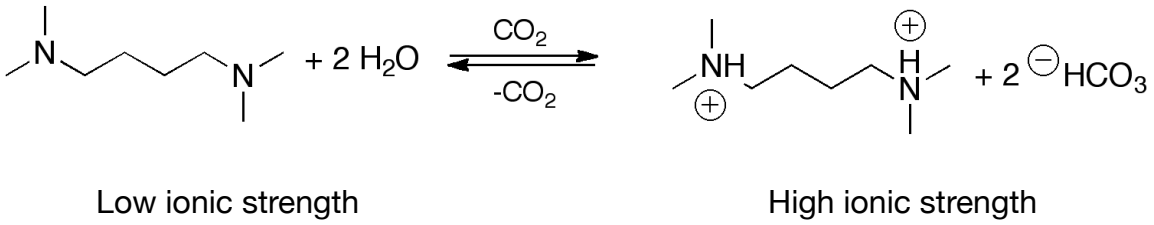


**Figure 1.15** An example of a switchable ionic strength additive

Changes in the ionic strength of solutions containing these switchable water additives was clearly illustrated via conductivity studies.[51] When a 1:1 (v/v) solution of the diamine pictured above (Figure 1.4) and water was saturated with $CO_2$ an increase from nearly zero conductivity (0.006 mS $cm^{-1}$) to up to 22 mS $cm^{-1}$ was observed.

Currently, one practical application of this technology has been identified. That is, these additives have been shown to reversibly separate THF from water through the application of $CO_2$.[51] Other applications and new additives are currently being investigated.

## 1.5 Surface Characterization Methods

### 1.5.1 Atomic Force Microscopy

Atomic force microscopy (AFM) is a surface characterization technique invented in 1986 by Bining, Quate and Gerber.[52] It may be used to achieve topographic imaging of non-conductive surfaces of, under ideal conditions, the atomic level scale. This overcame the limitation of its precursor, Scanning Tunneling Microscopy (STM), that monitors a tunneling current between a nanofabricated tip

and conducting substrate surface, limiting the range of substrates available. AFM can also be used to measure forces as a function of distance between the tip and the sample.

Figure 1.16 illustrates the basic principle of operation for an atomic force microscope.[49] A laser beam is focused on the tip of a cantilever. Application of a voltage to the piezoelectric scanner initiates movement of the sample towards the tip. When the sample is brought close enough to the tip, atomic forces between the tip and the sample or changes in surface topography cause deflection of the cantilever. These changes are detected through monitoring the laser beam reflected from the back surface of the cantilever by a photodiode detector. Topographic data may be obtained by subtracting the (C+D) signal from the (A+B) signal where subtracting the (B+D) signal from the (A+C) signal provides information pertaining to lateral frictional forces the tip experiences as it scans over the sample surface.

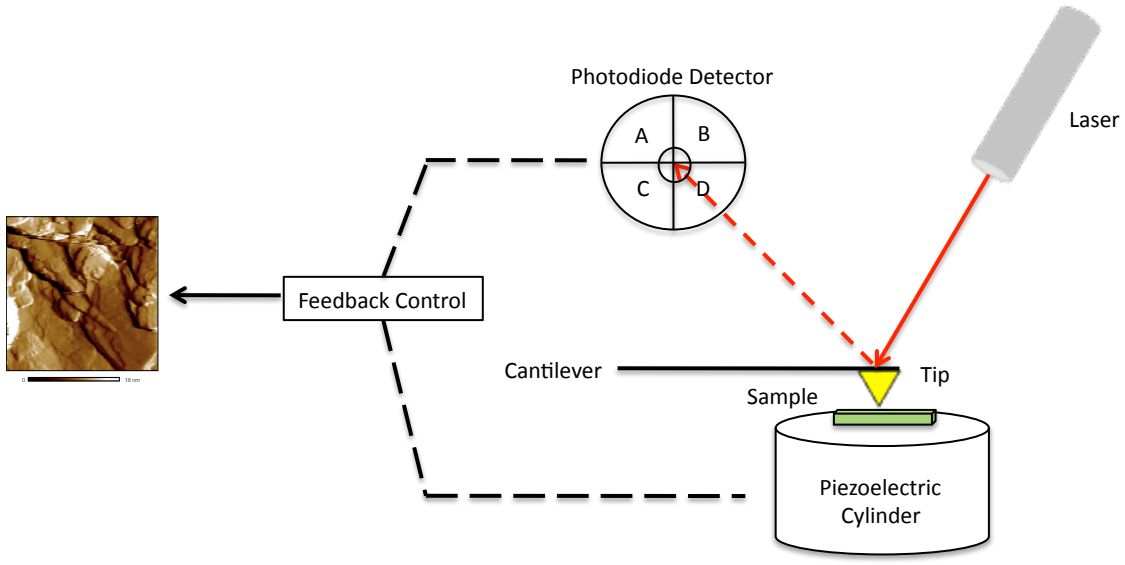


**Figure 1.16** Schematic illustration of an atomic force microscope[49]

Two major modes of operation are available for surface investigations using AFM: static contact mode and dynamic mode.[49] The latter is further divided into amplitude modulation (AM-AFM) and frequency modulation (FM-AFM).

In static contact mode, the deflection of the cantilever is translated into force through Hooke's Law (Equation 1)

$$F = kx \qquad [1]$$

where F is the calculated adhesion force, k is the spring constant of the cantilever, and x is the measured normal displacement of the cantilever.[53] This interaction between the tip and the sample can be rendered into an imaging signal to acquire topographical information about the sample surface

AM-AFM, known commercially as tapping mode AFM, is often used to probe soft surfaces such as polymers and biological samples.[54] Here, a stiff cantilever is oscillating at a fixed amplitude and a fixed frequency, usually at its resonant frequency, and is positioned just above the surface being investigated. As a result, the tip is only in contact with the surface for a brief period of time, theoretically resulting in lesser substrate damage by the tip. Changes in the oscillation amplitude of the cantilever is detected and used to map out tip-surface interactions.

Similar to the previously described AFM mode of operation, FM-AFM also requires oscillation of the cantilever at its resonance frequency.[55] Changes in the frequency of oscillation due to tip-surface interaction are detected and translated into topographical images or force gradient information. However, unlike AM-AFM,

FM-AFM can be operated in ultra high vacuum conditions to improve the sensitivity of the technique.

### 1.5.2 Chemical Force Microscopy

Chemical force microscopy (CFM) is an AFM technique where the AFM tip is chemically modified by covalent attachment of organic molecules; thereby allowing for forces between specific functional groups and a specified substrate to be probed. CFM may be used to probe forces between different molecular groups, determine local pKa values of acid and base groups, and study the ionization states of specific functional groups distributed on a surface.[56]

A common method of chemical modification of AFM tips is through the self assembly of monolayers of functionalized organic thiols onto a gold coated AFM tip. The thiol end of the molecule forms a covalent bond with the gold surface and the other end of the molecule is available for interaction with the desired substrate (Panel A, Figure 1.17).[57] The mechanism for generating a typical force distance curve consists of a full approach-withdraw cycle (Figure 1.17).

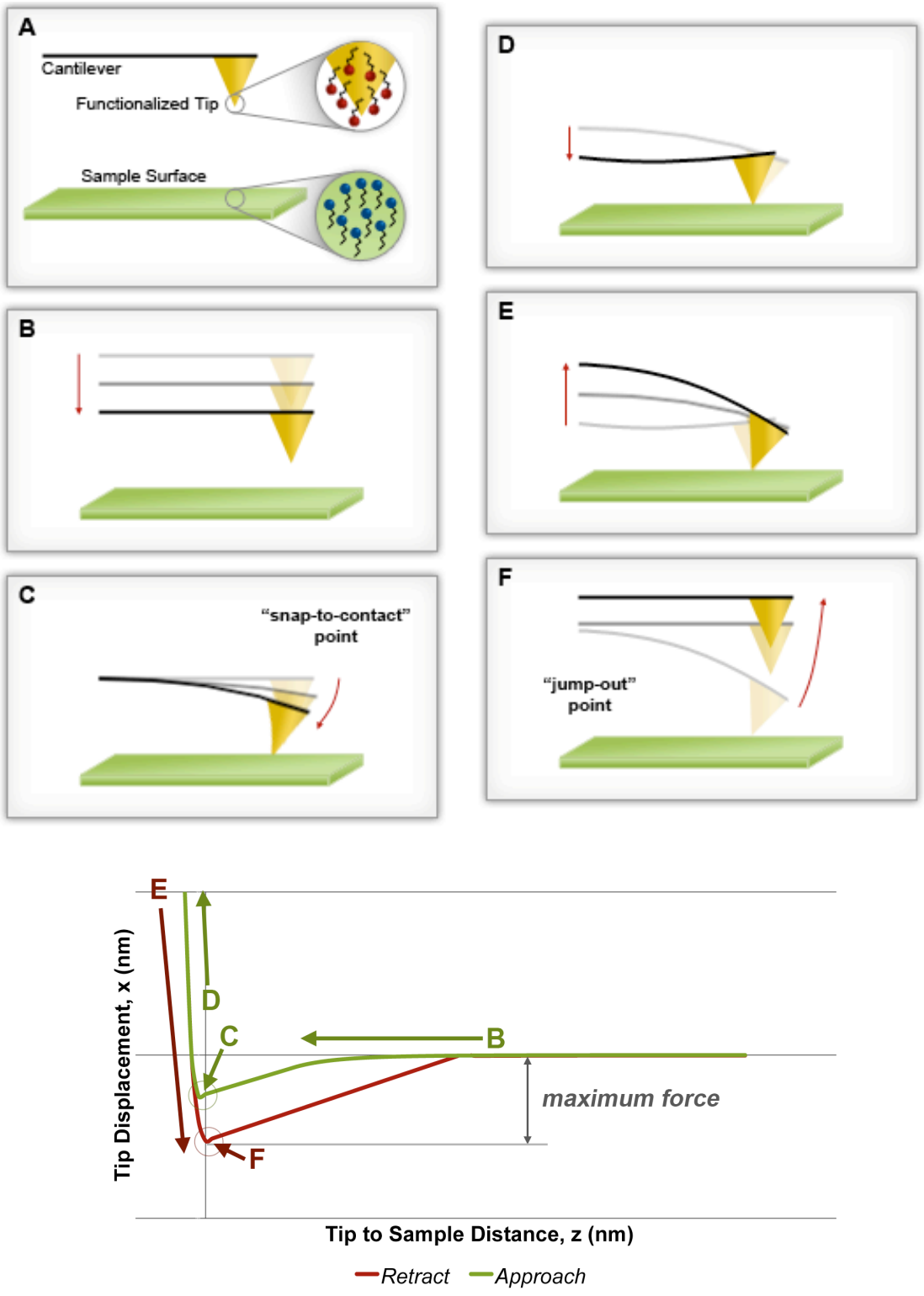


**Figure 1.17** Schematic representation of chemical force microscopy

First, the functionalized tip is brought close to the sample surface through the use of a piezoelectric scanner.[58,59] When the tip is far away from the sample there is no interaction between the tip and the sample and the cantilever experiences no displacement. However, when the tip and the sample are brought close enough together to the point where the gradient of total attractive forces surpasses the force constant of the cantilever, the tip jumps to contact with the sample (Panel C, Figure 1.17). This is known as the "snap-to-contact" point and the cantilever exhibits a negative displacement from its non-interacting state. When the tip and the sample are brought too close together, electronic repulsions from the two surfaces begin to dominate and the cantilever begins to experience a positive deviation from its non-interacting state (Panel D, Figure 1.17). This sequence is plotted together as the approach curve. The sequence is reversed to generate a curve. From the repulsive regime, the sample brought away from the tip into a region where attractive forces between the tip and the sample begin to dominate over the repulsive forces (Panel E, Figure 1.17). As the distance between the tip and the sample continues to increase, at some distance the gradient of total attractive forces will not be enough to surpass the force constant of the cantilever and the cantilever will return back to its non-interacting state (Panel F, Figure 1.17).

The well depth of the withdraw curve is measured and used to calculate the adhesion force observed between the functionalized AFM tip and the substrate using Hooke's Law.[53]

### 1.5.3 X-Ray Photoelectron Spectroscopy

X-Ray Photoelectron Spectroscopy (XPS) is an analytical tool used to study the chemical composition and electronic state of surfaces.[60] It can be used to study almost all elements except hydrogen and helium. XPS is a surface characterization method that can be used to probe 5-50 Å (or 2-20 atomic layers) deep. It is typically a non-destructive method, unless the samples are X-ray sensitive. As the system is under ultra high vacuum (UHV), samples must also be UHV compatible.

The basic theory behind the analysis is the photoelectron effect.[61] When a sample is irradiated, absorption of energy results in the emission of electrons. However, the kinetic energy of these ejected electrons are independent of the intensity of irradiation. This is because elements have a characteristic threshold frequency ($\upsilon_o$), and if this frequency is not met, then no electrons are ejected from the surface. However, above $\upsilon_o$ there is a linear relationship between the kinetic energy of the emitted electrons and the frequency of irradiation. Therefore, the following relationship between kinetic energy and frequency of incident radiation can be expressed if $\upsilon \geq \varphi$ (Equation 2).

$$KE = h\upsilon - \varphi \qquad [2]$$

During analysis, a monochromatic beam of X-rays irradiates the sample surface, resulting in emission of electrons from the surface (Figure 1.18).[62] For XPS, the core electrons are ejected. Valence level electrons are better studied using ultraviolet electron spectroscopy (UPS) due to the relatively low resolution

(approximately 1 eV) of the incident X-rays. The ejected electrons travel into a hemispherical electron analyzer where they are separated by their kinetic energies and sent to a electron multiplier detector to be counted. The kinetic energies of the electrons can be used to identify specific corresponding elements using Equation 2. Because the ejected electrons are counted, they are used to quantify relative concentrations of elements present in the sample. Chemical states of elements can also be determined because the kinetic energies of the emitted electrons are dependent on both the element's oxidation number and the relative polarizability of its surrounding environment.

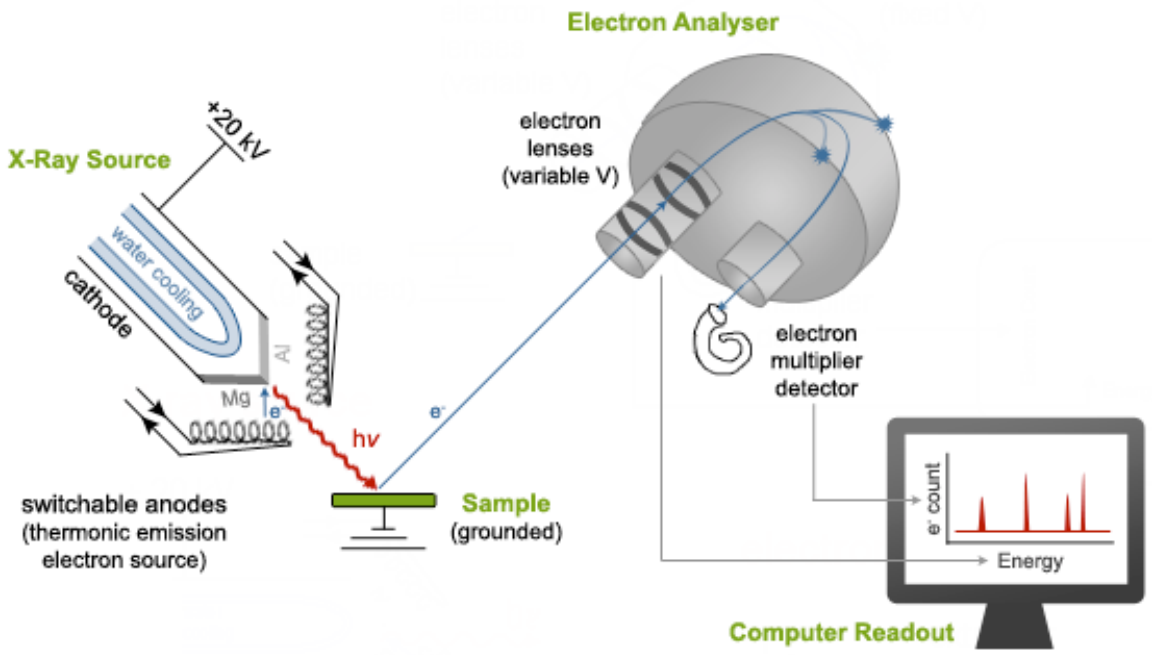


**Figure 1.18** Schematic representation of X-ray photoelectron spectroscopy

### 1.5.4 Zeta Potential Measurements

A charged particle in solution will affect the distribution of ions in solution surrounding the particle (Figure 1.19).[63,64] There will be an increase in concentration of counter ions of opposite charge to the surface near the interfacial region. Ions strongly bound with the particle surface comprise what is known as the Stern layer. Other ions which are loosely associated with the surface form the diffuse layer, which is generally considered to be electrically neutral. The two layers mentioned together are known as the electrical double layer. The boundary between the Stern layer and the diffuse layer is known as the slipping plane. The potential difference at the slipping plane is defined as the zeta potential.

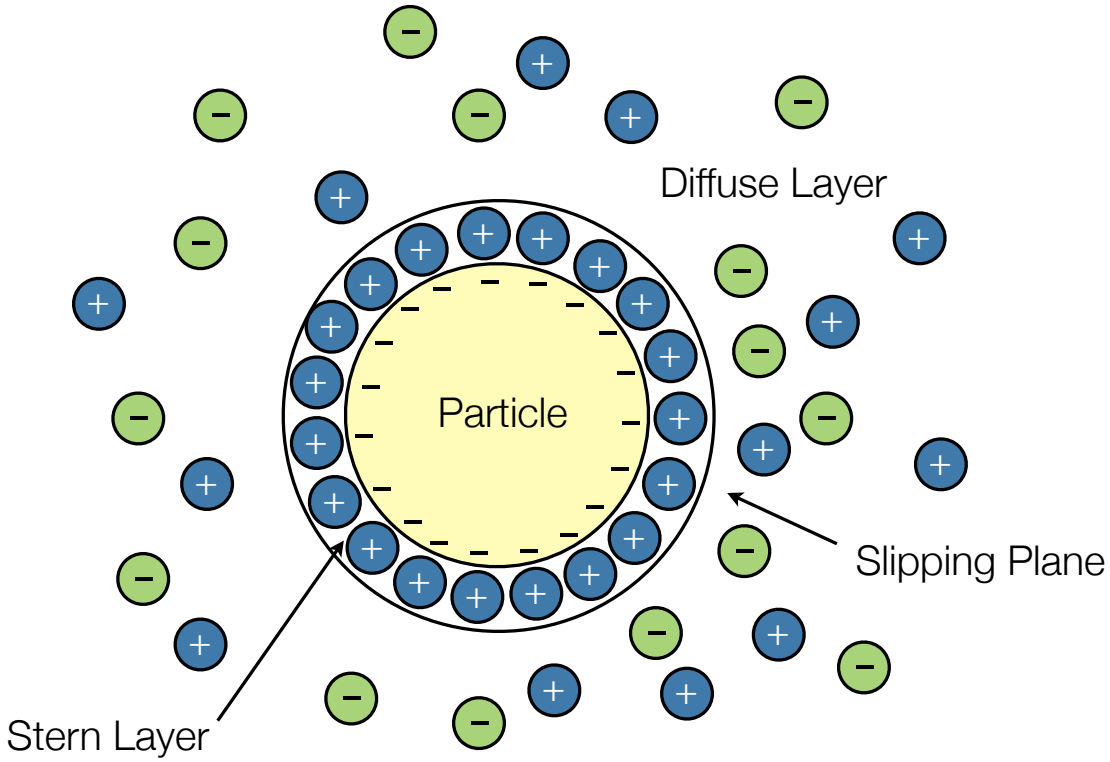


**Figure 1.19** Diagram of an electrical double layer

Zeta potential is not a parameter that is measured directly.[65] It can be calculated from the velocity of the ions at the slipping plane, also known as electrophoretic mobility, when an electric field or a voltage is applied. The electrophoretic mobility ($U_E$) of the charged particles is dependent on the strength of the electric field, the zeta potential (ζ), and the dielectric constant (ε) and the viscosity of the medium (η) they are suspended in. The Henry equation (Equation 3) illustrates how these parameters are related.

$$U_E = \frac{2\varepsilon\zeta f(\kappa a)}{3\eta} \qquad [3]$$

Henry's function, f(κa), is the ratio of the particle radius to the electrical double layer thickness.[66,67] For aqueous media and a moderate electrolyte concentration the Smoluchowski approximation may be made and f(κa) may be assumed to be 1.5. This model holds for particles that are larger than 0.2 μm in solutions of less than $10^{-2}$ M ionic strength. For particles suspended in a low dielectric constant media, the Huckel approximation can be made where f(κa) has a value of 1.0 to simplify the calculation.

Zeta potentials may be used as a predictive parameter of the colloidal stability of a system.[66,67] At large zeta potential values (greater than +30 mV or less than -30 mV), the particles are highly charged and repel one another. As a result, the system is considered to be stable and the particles will not flocculate. However, at zeta potential values that are closer to zero in value, the repulsive forces will be weakened and the particles may come together to flocculate due to attractive van der Waals forces.

Zeta potential measurements have been used in applications including the study bitumen and clay interactions in aqueous media[68], behavior of polymer suspensions[69], and the absorption of materials onto synthetic membranes.[70] Nonetheless, zeta potential is a well defined property for a given colloidal system only if the pH, solvent, electrolyte, and electrolyte concentration are fixed.[67]

## 1.6 Research Objectives

Control of water chemistry in oil sands processing is fundamental in both the extraction process and the tailings process. Ideally, the process water may be recycled through the entire operation, from extraction to tailings and back to extraction, to lessen the demand for water withdrawn from the Athabasca river. However, this remains a great challenge because the optimal water chemistry during extraction often does not align with the optimal water chemistry for tailings, as illustrated by Table 1.1.

**Table 1.1** Desired situations during bitumen extraction versus desired situations for tailings management

| Parameter | Bitumen Extraction | Tailings Ponds |
|---|---|---|
| Bitumen-mineral adhesion | Weak | Not important |
| Mineral-mineral adhesion | Not important | Strong |
| BItumen-air bubble adhesion | Strong | Not important |
| pH | High | Low |
| Divalent cation concentration | Low | High |
| Mineral particle zeta potential | Strong | Weak |
| Addition of polymer flocculants | Not important | Important |

Often, the parameters which are important to bitumen extraction are insignificant in tailings management, and vice versa. Generally, the means to achieving the desired situation required for optimal performance in either stage of the process is through the addition of chemical additives to manipulate the chemistry of the process water. These additives may be detrimental to the other phase of the operation, as exemplified in the case of pH and divalent cation concentration (Table 1.1). Treatment of process water exiting the extraction plant is required for optimal tailings ponds performance, but conversely, the water reclaimed from the tailings ponds also needs to be retreated prior to reuse in the bitumen extraction process. As a result, the current industrial practices are both energy and materials intensive, particularly with respect to recycling the process water.

The goal of this research project is to study how switchable additives developed in the Jessop group can affect model interactions found in the Alberta oil sands. Switchable additives can provide a more environmentally friendly alternative to conventional process aids, as the properties of these additives may be externally controlled through saturation/removal of $CO_2$, an economical and benign trigger. Although other switchable additive applications have been presented by other Jessop group members, the use of these compounds for oil sands applications has not been previously explored. Cationic and anionic switchable surfactants were studied in addition to switchable ionic strength additives.

Interaction forces between organic functional groups and mineral substrates were investigated by chemical force spectrometry (CFS). These experiments were

used to model bitumen/mineral interactions and study the effect of switchable additives on these interactions. Two organic functional groups were selected for this study, an aromatic phenyl group and a carboxylic acid group. Both are commonly found in bitumen. 12-phenyldodecanethiol was synthesized and characterized, whereas 12-mercaptododecanoic acid was commercially available for purchase. These two thiols were used to make self assembled monolayers (SAM) on gold AFM tips for the CFS experiments. The monolayers were characterized by surface FT-IR and by XPS. The substrates investigated include illite clay, mica, and silica. Tip/ sample interactions were analyzed as a function of pH, in the presence of divalent cations, and in the presence of switchable additives. Structures and abbreviations of the switchable additives are presented below (Table 1.1).

**Table 1.2** Switchable additives and abbreviations used

| Molecule | Abbreviation | Identification |
|---|---|---|
| 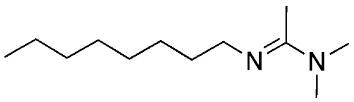 | C8 | Cationic switchable surfactant |
| 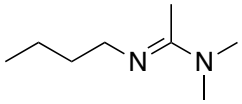 | C4 | Cationic switchable amidine |
| 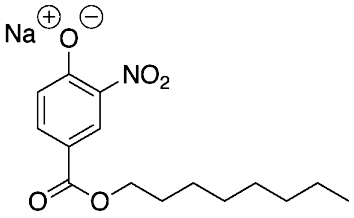 | NP-C8 | Anionic switchable surfactant |
| 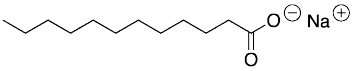 | SL | Anionic switchable surfactant |
| 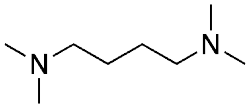 | TMDAB | Switchable ionic strength additive |
| 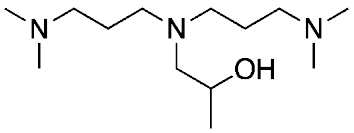 | BMDAPAP | Switchable ionic strength additive |

Inorganic/inorganic interactions were also studied by CFS and used to model mineral/mineral interactions that may be found in the oil sands. Silica AFM tips were used to probe interactions with silica and alumina substrates. As per above, tip/sample interactions were studied as a function of pH, in the presence of divalent cations, and in the presence of switchable additives.

Concurrently, the effects of switchable surfactants and switchable ionic strength additives on clay zeta potentials were studied. Three types of clays were employed in this investigation: illite, kaolinite, and montmorillonite. These are the commonly found clay fines in the oil sands. Zeta potential experiments were used as an assessment tool to determine if the switchable process aids can affect clay suspension behavior and provide a means to reversibly consolidate clays in the tailing ponds. As a supplement to the zeta potential experiments, particle size measurements and clay settling studies were conducted.

This research provided insight to changes in model oil sands interactions in the presence of $CO_2$ induced switchable additives. Potential candidates for oil sands process aids were identified. The long range goal of this project is to study how these candidates affect real oil sands systems to determine the applicability of switchable additives for large, industrial scale oil sands operations.

# 2. Experimental

## 2.1 Synthesis and Surface Preparation Methods

### 2.1.1 Source of Reagents and Supplies

$CO_2$ (Supercritical Chromatographic Grade, 99.998%, Praxair), nitrogen (Praxair, 99.998%), and argon (Praxair, 99.998%) were used as received. N,N,N′,N′-Tetramethyl-1,4-diaminobutane (TMDAB) was received from TCI. 10 wt% Pd/C was purchased from Strem Chemicals. All other reagents were purchased from Aldrich Chemical Company. Switchable surfactants were synthesized in house by previously reported methods.[46,47]

Illite, kaolinite, and montmorillonite clays were purchased from Ward's Natural Science Establishment. Muscovite mica was received from SPI Supplies. Silicon (111) substrates were purchased from Virginia Semiconductors Inc. Aluminum foil (99.999%) was received from Aldrich Chemical Company. 12-mercaptododecanoic acid was purchased from Aldrich Chemical Company. Gold coated mica substrates were purchased from Georg Albert.

All chemicals acquired from commercial sources were used as received unless specified.

### 2.1.2 Instrumentation

Solution $^{1}H$ and $^{13}C$ NMR spectra were recorded on a Bruker Advance 400 MHz spectrometer. Infrared spectra were collected for all liquid samples neat on an

Avatar 360 FT-IR spectrometer. Mass spectrometry was conducted on an Agilent HP6890 GC system.

### 2.1.3 Synthesis of 12-phenyldodecanethiol

Synthesis of 12-phenyldodecanethiol is outlined by Figure 2.1, as per previously published literature methods.[71,72,73] This is a known molecule and $^{1}$H-NMR, $^{13}$C-NMR, and mass (high res, EI$^{+}$) matches that reported in the literature.[71] The compound was subsequently used to functionalize gold coated silicon nitride AFM tips for chemical force microscopy experiments, as described below. Details pertaining to the synthesis and characterization of this molecule are presented in the Appendix.

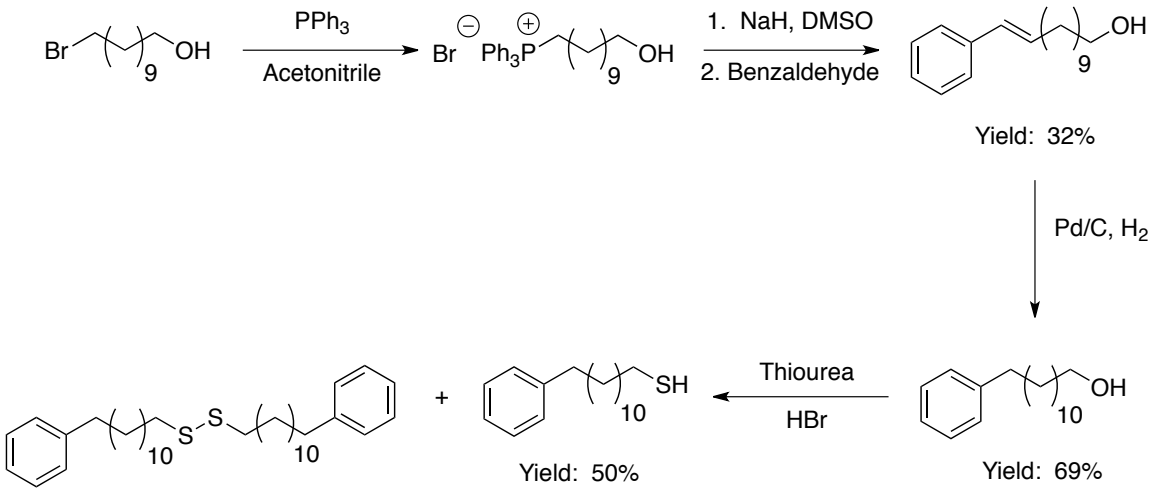


**Figure 2.1** Synthetic route to 12-phenyldodecanethiol

NMR and MS experiments show the product is a mixture of the thiol and the corresponding disulfide due to partial oxidation during the synthesis. However, it has been demonstrated in literature that disulfides also self assemble onto gold surfaces through scission of the sulfur-sulfur bond.[74,75] Therefore, this material may still be used to create the desired self-assembled monolayers on gold.

### 2.1.4 Preparation of Functionalized Gold Surfaces

To characterize the monolayer used in the chemical force microscopy experiments, epitaxial gold (111) on mica surfaces (300 nm thick) were functionalized for XPS and FT-IR experiments. Functionalized AFM tips are not conventionally used in XPS experiments, as they are too small in size and XPS elemental signals from the functionalized AFM tip will be very weak. Ideally, a 1 cm by 1 cm sample should be used for analysis to ensure that the X-ray beam irradiates the area of interest. Prior to functionalization, the Au-coated mica slide was annealed in a methane flame to smooth the gold surface layer, as well as remove surface contaminants. A blank gold on mica sample was prepared simply by flame annealing the gold on mica. The slides were submerged in a $1x10^{-3}$ M solution of 12-phenyldodecanethiol or 12-mercaptododecanoic acid in isopropanol for 24 h prior to analysis.

### 2.1.5 Preparation of Functionalized AFM Tips

Gold coated silicon nitride AFM tips (CSC-38, MikroMasch USA) were functionalized for adhesion force measurements by submerging the tips in a $1x10^{-3}$ M solution of 12-phenyldodecanethiol or 12-mercaptododecanoic acid in isopropanol for 24 h. AFM cantilevers with spring constant k=0.08 N/m, as quoted by the manufacturer, were used for these adhesion studies. The radius of the AFM tips used was <10 nm, according to the manufacturer.

### 2.1.6 Preparation of Clay Surfaces

Substrates for AFM force measurements were prepared from illite, kaolinite, and montmorillonite (Ward's Natural Science Establishment).

Illite clay was freshly cleaved with a stainless steel surgical blade. Flat, lamellar pieces were selected for the experiment. The substrate was characterized by AFM imaging and powder XPS. Sheets of illite were ground into a fine powder using a mortar and pestle, which was subsequently adhered to copper tape and analyzed using Mg Kα radiation (1253.6 eV).

Kaolinite and montmorillonite were also considered possible candidates for the AFM studies; however, these two clays are commercially available as powders, which cannot be used as substrates. Several different methods were employed in attempt to prepare flat surfaces appropriate for AFM work using these clays.

AFM substrates of precipitated metal oxides colloids have previously been prepared in the Horton group.[76,77,78] A muscovite mica slide (1 cm x 2 cm, V-4 grade, SPI Supplies) was placed in the center of a filter frit and the precipitated colloids

were suspended in water and filtered through the prepared frit. The filtration process deposited and compacted the colloids onto the mica slide, resulting in a sample that may be used for AFM measurements. This was often repeated several times to ensure adequate coverage of the slide. The procedure above was used in attempts to make kaolinite and montmorillonite substrates support on mica.

Kaolinite and montmorillonite were also pressed into discs using a handheld KBr press, used to make IR discs (International iCL Crystal Laboratories). Discs of these clays were also made using a ten tonne KBr press (International iCL Crystal Laboratories).

### 2.1.7 Preparation of Silica Surfaces

Silicon (111) wafers (Virginia Semiconductors Inc.) were cleaned and oxidized with piranha solution (3:1 concentrated $H_2SO_4$: 35 wt% $H_2O_2$ in $H_2O$) for 1 h prior to being thoroughly rinsed with deionized water and drying under a stream of $N_2(g)$.

### 2.1.8 Preparation of Mica Surfaces

Muscovite mica (V-4 grade, SPI) was freshly cleaved prior to use. Double sided tape was adhered to the surface and subsequently pulled off to reveal a new basal surface for AFM force measurements.

### 2.1.9 Preparation of Alumina Surfaces

Alumina surfaces were prepared as substrates for AFM force measurements with silicon oxide sharpened AFM tips. Two different literature preparation methods were attempted[79] and both surfaces were characterized using XPS.

*Acid Treated Aluminum*

Aluminum foil (1 cm x 1 cm, 99.999%, Aldrich) was cleaned in hot chloroform and air dried. The substrate was then immersed in a 30 vol% $HNO_3$ solution in deionized water for 30 s. Finally, the substrate was thoroughly rinsed with deionized water and dried under a stream of $N_2$(g).

*Boiled Aluminum*

Aluminum foil (1 cm x 1 cm, 99.999%, Aldrich) was immersed in boiling deionized water for 60 s and air dried.

## 2.2 Surface Characterization Methods

### 2.2.1 Atomic Force Microscopy

AFM was used to gather topographical data on the clay substrates being studied. AFM images were obtained using a PicoSPM instrument (Molecular Imaging, Tempe, AZ) and a Nanoscope IIE controller (Digital Instruments, Santa Barbara, CA). For imaging purposes, silicon nitride AFM tips (Veeco) were used.

### 2.2.2 Chemical Force Microscopy

Force measurements using thiol functionalized gold AFM tips were conducted under aqueous conditions in solutions prepared using deionized water (18.2 MΩ, Millipore). The adhesive force between the tip and the sample was determined from measuring the well depth of over 1000 force distance curves under each experimental condition. The adhesion force was measured approximately 200 times at different surface sites. At least 5 surface sites were tested for each experimental condition, but typically 15-20 sites were studied. At least 2 different tips were used in these measurements. The large number measurements were conducted to obtain a more representative value of adhesion between the tip and the sample. The reported values are an average of all the measured adhesive forces and the errors are the calculated 95% confidence intervals.

The chemical force titration experiments were conducted using freshly prepared unbuffered aqueous solutions of pH ranging from 3 to 11. To modify the pH, NaOH was used to achieve alkaline conditions and HCl was used to achieve acidic conditions. Unbuffered pH solutions were used to prevent unwanted interactions between the surface and the ionic species associated with the buffer. The pH values were checked before and after the experiment and the solutions were changed frequently to minimize changes in pH due to the dissolution of atmospheric $CO_2$.

For experiments involving $CO_2$ saturated solutions, the solutions were pretreated with $CO_2$ prior to acquiring the force curves. Ultra pure $CO_2$ (Supercritical $CO_2$ Chromatographic Grade, Praxair) was bubbled through the solutions using a syringe for 30 mins. For these force measurements, the AFM was outfitted with an

environmental cell that was filled with $CO_2$ to maintain a $CO_2$ atmosphere around the aqueous solutions during the experiments.

### 2.2.3 X-ray Photoelectron Spectroscopy

XPS experiments were conducted using a Thermo Instruments Microlab 310F surface analysis system (Hastings, U.K.) under ultrahigh vacuum conditions. A Mg Kα radiation source (1253.6 eV) was used at a 15 kV anode potential and 20 mA emission current. The binding energies of all spectra were corrected for charging effects using the C 1s line at 285.0 eV as a reference. A Shirley fit algorithm[80] was employed for spectral background subtraction and peaks were fitted using a Powell peak-fitting algorithm.[81,82]

### 2.2.4 Attenuated Total Reflection IR Spectroscopy

ATR-IR spectroscopy was conducted using a Thermo Scientific Nicolet 6700 spectrometer outfitted with a Smart Orbit diamond ATR accessory. The incident angle of irradiation was 45°.

### 2.2.5 Zeta potential measurements

Clay fines were weighed (0.025 g, Ward's Natural Science Establishment) and placed into individual vials. Kaolinite and montmorillonite were used as received, but illite clay was ground into a powder using a motar and pestle. Solutions containing additives were made with deionized water (18.2 MΩ/cm, Millipore) and

10 mL was added to the clay fines. A suspension was created using a vortex mixer and subsequently dispensed into a folded capillary cell. The zeta potential was measured using a Nano-ZS90 Zetasizer instrument (Malvern). 30 scans were collected for each measurement. The errors reported on the zeta potential values were the standard deviations of the zeta potential peaks measured.

Unless specified, all carbon dioxide treatments were conducted with the aqueous solutions prior to addition to clay fines. For applicable measurements, ultra pure carbon dioxide (Supercritical $CO_2$ Chromatographic Grade, 99.998%, Praxair) was bubbled through the solutions using a syringe. $CO_2$ treatments for switchable surfactants were conducted for 30 minutes and $CO_2$ treatments for switchable ionic strength additives were conducted for 1 h.

## 2.3 Clay Settling Experiments

Three series of clay settling experiments were conducted with 1 mM TMDAB to elucidate the ability of switchable ionic strength additive TMDAB to affect settling of clay suspensions.

### 2.3.1 Effect of TMDAB

For this series of experiments, all gas treatments were performed in the absence of the clay (Figure 2.2). Kaolinite was added after 1 mM TMDAB was treated as discussed below. This was done to elucidate switching behaviour without impedance from the clay.

Kaolinite clay fines (5 g) were added to 100 mL of 1 mM TMDAB in deionized water. The mixture was stirred for 15 minutes at 900 rpm using a magnetic stirrer prior to transferring into a 100 mL graduated cylinder, which was subsequently sealed with a rubber septum. Settling of the clay fines was monitored as a function of time using a cathetometer (Eberbach), which is an instrument used to measure vertical distances.

$CO_2$ was bubbled through 100 mL of 1 mM TMDAB using a dispersion tube (Class F, Sigma Aldrich) for 1 hour. Kaolinite fines (5 g) were added to the aqueous solution and the mixture was stirred for 15 minutes at 900 rpm prior to transferring into a 100 mL graduated cylinder and sealing with a rubber septum. Settling of clay fines was monitored.

$CO_2$ was bubbled through 100 mL of 1 mM TMDAB using a dispersion tube for 1 hour. The solution was heated to 70°C and $N_2$ was bubbled through for 1 hour. After cooling to room temperature, kaolinite fines (5 g) were added and the mixture was stirred 900 rpm for 15 minutes prior to transferring into a 100 mL graduated cylinder and sealing with a rubber septum. Settling of clay fines was monitored.

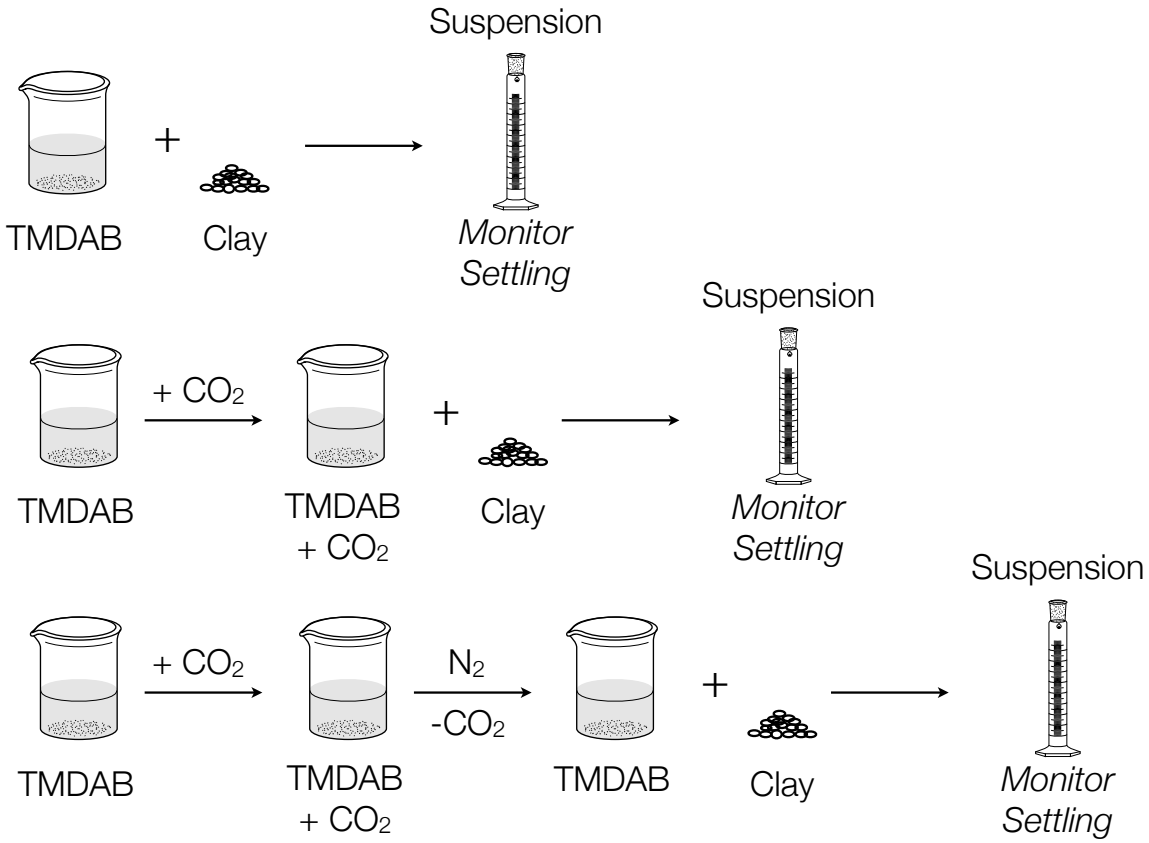


**Figure 2.2** Clay settling experimental scheme for gas treatments conducted in the absence of clay

### 2.3.2 In situ switching

For the second series of experiment, switching behaviour of 1 mM TMDAB was studied in the presence of clay fines. The same clay and TMDAB mixture was used in all three settling tests (Figure 2.3).

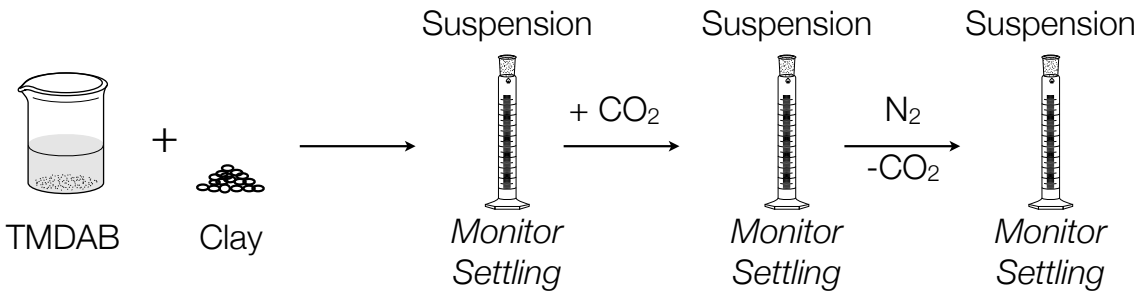


**Figure 2.3** Clay settling experimental scheme for gas treatments conducted in the presence of clay

Kaolinite clay fines (5 g) was added to 100 mL of 1 mM TMDAB in deionized water. The mixture was stirred for 15 minutes at 900 rpm prior to transferring into a 100 mL graduated cylinder, which was subsequently sealed with a rubber septum. Settling of the clay fines was monitored as a function of time.

$CO_2$ was bubbled through the suspension above. The mixture was stirred for 15 minutes at 900 rpm prior to transferring into a 100 mL graduated cylinder, which was subsequently sealed with a rubber septum. Settling of the clay fines was monitored.

The clay fines above were resuspended in the solution and the mixture was heated to 70°C. $N_2$ was bubbled through for 1 hour. After cooling to room temperature, the mixture was stirred 900 rpm for 15 minutes prior to transferring into a 100 mL graduated cylinder and sealing with a rubber septum. Settling of clay fines was monitored.

### 2.3.3 Filtrate Recycling

This experiment was conducted to determine if switchable water can be recycled after facilitating settling of clay suspensions. Clay suspensions containing TMDAB were filtered and the filtrate was collected, then treated with $CO_2$ (Figure 2.4). A clay suspension was created with the filtrate (see below) and the settling behaviour was compared to that observed in the other two series of experiments described above.

Kaolinite clay fines (5 g) were added to 100 mL of 1 mM TMDAB in deionized water. The mixture was stirred for 15 minutes at 900 rpm prior to transferring into a 100 mL graduated cylinder, which was subsequently sealed with a rubber septum. Settling of the clay fines was monitored as a function of time.

The suspension above was first filtered through a medium glass filter frit, and then through a fine glass filter frit. 90 mL of filtrate was recovered. $CO_2$ was bubbled through the filtrate for 1 hour. Kaolinite clay fines (4.5 g) were added and the mixture was stirred for 15 minutes at 900 rpm prior to transferring into a 100 mL graduated cylinder, which was subsequently sealed with a rubber septum. Settling of clay fines was monitored.

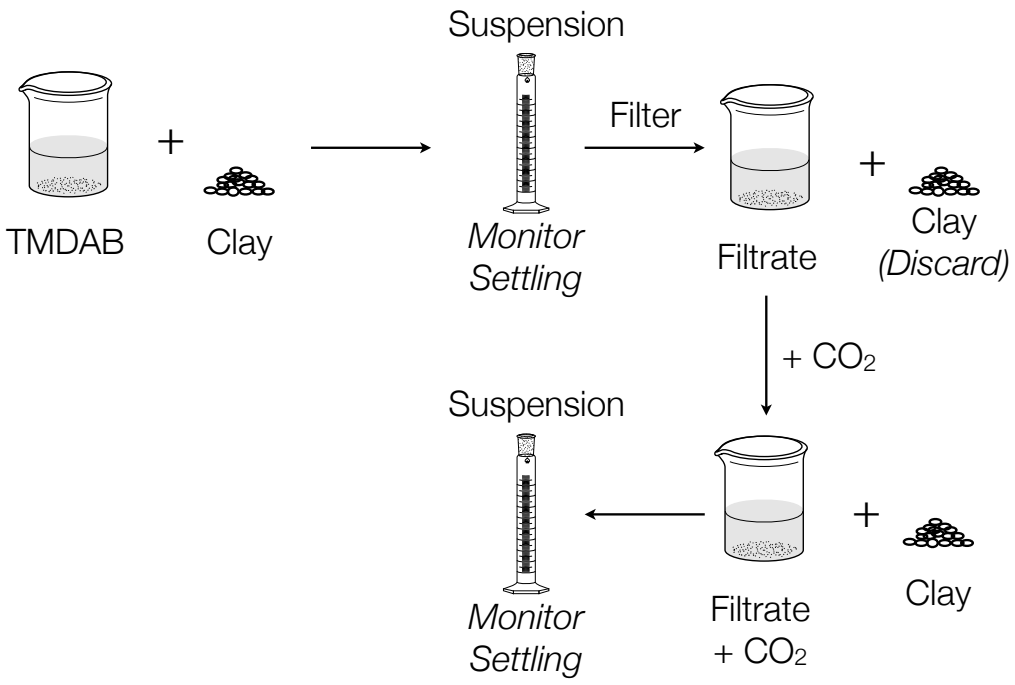


**Figure 2.4** Clay settling experimental scheme for collection and use of filtrate for settling studies

### 2.3.4 Particle Size Measurements

Clay fines were weighed (0.025 g, Ward's Natural Science Establishment) and placed into individual vials. Solutions containing additives were made with deionized water (18.2 MΩ/cm, Millipore) and 10 mL was added to kaolinite clay fines (0.025 g, Ward's Natural Science Establishment). For applicable samples, $CO_2$ was bubbled through the aqueous solution using a syringe for 1 hour prior to addition to the clay fines. Particle size measurements of kaolinite clay were determined using a Mastersizer 2000S instrument (Malvern).

### 2.3.5 Total Suspended Solids

Filter paper (#2, 2.5 cm in diameter, Whatman) was washed with deionized water and dried in the oven overnight, prior to weighing. Following the settling studies, the top 50 mL of the supernatant was drawn off and filtered through the prewashed filter. The filter paper was then dried in the oven overnight, prior to weighing. The total suspended solids was calculated by taking the difference between the two weights and dividing by the volume filtered. The final results are expressed in parts per million (ppm).

# 3. Results and Discussion: Organic/Mineral Interactions

## 3.1 Introduction

The liberation of bitumen from mineral surfaces, such as sands and clays, is governed by interaction forces between the bitumen and the mineral surface. In the current industrial process, water chemistry is manipulated through the addition of chemical additives to change the bitumen/mineral interactions to allow the bitumen to be separated from the mineral component of oil sands.[19] However, the optimal water chemistry for extraction is detrimental for the settling of tailings, which is a later step in the operation. This is problematic for the entire process as either the process water has to be purified or more chemicals must be added at the tailings stage to optimize performance. In addition, purification or more additives are required if the process water from the tailings ponds are to be recycled for extraction use.

Switchable additives may provide a more environmentally friendly alternative to conventional process aids. These chemicals can reversibly change the water chemistry through the introduction and removal of $CO_2$, which is a benign trigger. In this chapter, interaction forces between a bitumen and mineral surfaces were modeled and studied by chemical force spectrometry (CFS), particularly to investigate how switchable additives may be used to control these interactions, which are crucial to the bitumen liberation phase of the oil sands extraction process. Two organic functional groups commonly found in bitumen were selected to represent the bitumen, an aromatic phenyl group and a carboxylic acid group and

they were used to make self assembled monolayers (SAM) on gold AFM tips for CFS experiments. The mineral substrates investigated include illite clay, mica, and silica, which are all components of real oil sands systems.[6,14] Tip/sample interactions were analyzed as a function of pH, in the presence of divalent cations, and in the presence of switchable additives.

## 3.2 Surface Characterization

### 3.2.1 Characterization of 12-phenyldodecanethiol SAM

Gold coated mica substrates were functionalized with 12-phenyldodecanethiol for characterization of the self assembled monolayer that would be deposited onto the gold coated AFM tips for use in CFM experiments. The monolayer was characterized by XPS and by ATR-IR.

From the XPS data (Table 1) the sulfur to carbon ratio was calculated from the peak areas to be 28.5, greater than what is expected from the molecular stoichiometry (theoretically to be 18). This is consistent with the alkyl overlayer is attenuating the sulfur signal. The experiment was conducted in duplicate and the data is reproducible as shown (Table 3.1).

**Table 3.1** XPS characterization of 12-phenyldodecanethiol SAM

| Peak | Binding Energy (eV)[a] | Theoretical Peak Area Ratio (stoichiometry) | Experimental Peak Area Ratio |
|---|---|---|---|
| Carbon 1s | 285.0 | 18 | 28.5 |
| Sulfur 2p | 165.5 | 1 | 1 |
| Carbon 1s (Duplicate) | 285.0 | 18 | 34 |
| Sulfur 2p (Duplicate) | 163.7 | 1 | 1 |

[a]*Reported binding energies are corrected for charging effects*

The overlayer thickness of thiol modified gold on mica slides was determined using the equation below (Equation 3)

$$I = I_o e^{-d/\lambda} \qquad [3]$$

where d is the thickness of the overlayer and λ is the escape depth of a gold photoelectron (2.02 nm).[30] $I_o$ is the XPS peak intensity of a unmodified flame annealed gold on mica sample and I is the peak intensity of the gold on mica sample functionalized with 12-phenyldodecanethiol. The overlayer thickness was calculated using the above formula to be 15Å and the theoretical length of the molecule was theoretically determined using Gaussian, to be 19Å. As the overlayer thickness is less than the calculated theoretical length of the molecule, it suggests that the deposited thiol molecules are in fact not aligned perpendicular to the gold surface,

but rather, oriented in such a fashion that they are angled to the surface. Confirmation of orientation was accomplished through ATR-IR.

For ATR-IR, only molecular vibrations that result in a change in dipole moment perpendicular to the surface will give an IR absorption.[83] Therefore, the ATR-IR spectrum (Figure 3.1) may be compared with the transmission FT-IR spectrum of the free thiol (Figure 3.2) to determine the orientation of the SAM as those vibrations parallel to the surface will not be present in the spectrum.

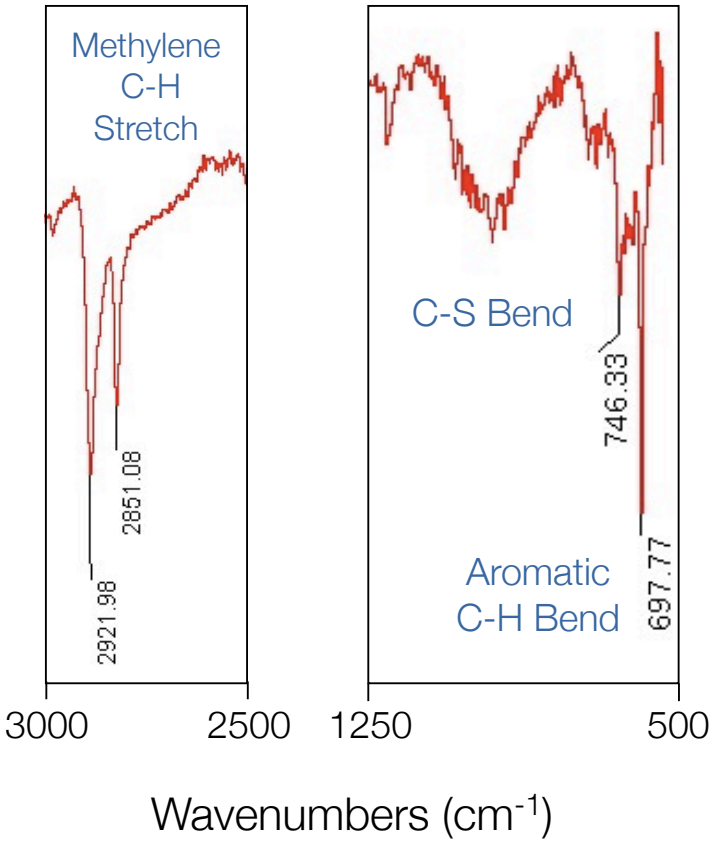


**Figure 3.1** ATR-IR spectrum of 12-phenyldodecanethiol SAM

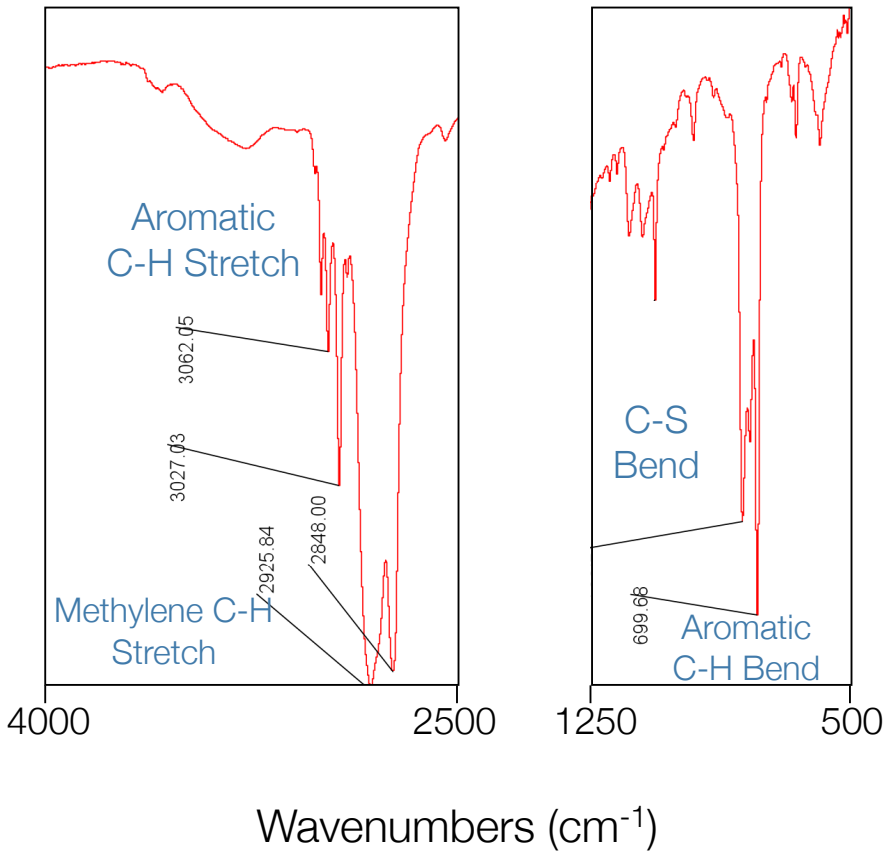


**Figure 3.2** Transmission FT-IR spectrum of 12-phenyldodecanethiol

The ATR-IR spectrum only showed peaks arising from the methylene C-H stretch, the C-S bend, and the aromatic C-H bend. The presence of the methylene C-H stretch and the aromatic C-H bend in the ATR-IR spectrum indicates that those vibrations are perpendicular to the surface. However, the peak corresponding to the methylene C-H stretch is attenuated in the ATR-IR spectrum, compared to the thiol spectrum. This suggests that the vibration occurs at an angle intermediate to a directly parallel or perpendicular vibration. The peak corresponding to the C-S bend (746 $cm^{-1}$/750 $cm^{-1}$) was also reduced in intensity in the ATR-IR spectrum in

comparison to the thiol FT-IR spectrum, again possibly because the vibration is at an angle to the surface. Disappearance of the other peaks in the thiol FT-IR spectrum, such as the one observed at 3027 $cm^{-1}$ corresponding to the aromatic C-H stretch, suggest that those vibrations are parallel to the surface.

A molecular confirmation is proposed below (Figure 3.3). Here, the molecules are angled to the surface rather than oriented perpendicularly, consistent with the XPS data. This molecular orientation is also in agreement with the observed transitions in the ATR-IR spectrum. Both the C-S bend and the aromatic C-H bend will occur perpendicular to the surface, whereas the methylene C-H stretch will be at an intermediate angle. Any aromatic C-H stretch will lie parallel and be fully attenuated.

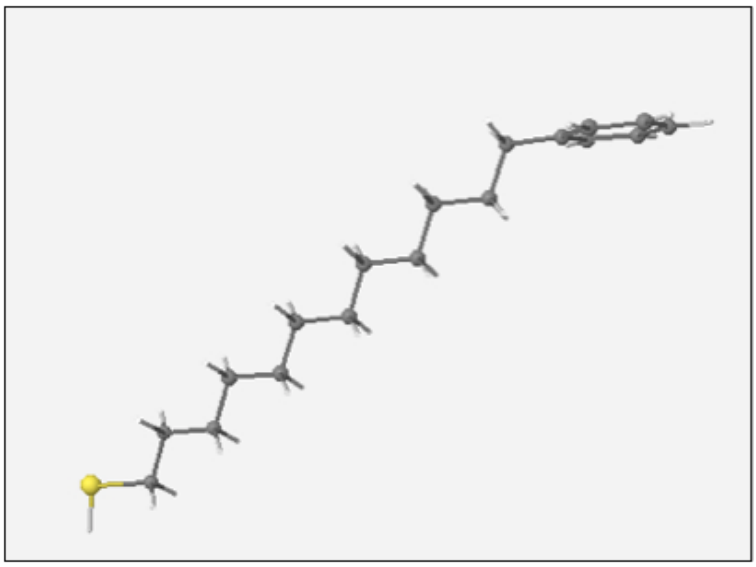

**Figure 3.3** 12-phenyldodecanethiol SAM

### 3.2.2 Characterization of 12-mercaptododecanoic acid SAM

12-mercaptododecanoic acid was self assembled onto gold to form a monolayer which was also characterized by XPS to confirm success of the deposition.

The XPS spectrum shows deposition of 12-mercaptododecanoic acid onto the Au-mica substrate (Table 3.2). Two peaks were observed in the carbon 1s spectra due to differing chemical states of the carbonyl carbon (286.3 eV) and the methylene carbon (285.0 eV) groups of the thiol molecule. The experimental peak area ratios for carbon 1s to sulfur 2p is higher than expected due to the attenuation of the sulfur signal from the alkyl overlayer. This and similar self assembled monolayers of alkanoic thiols are well known and these results are consistent with those reported extensively in the literature.[84,85,86]

**Table 3.2** XPS characterization of 12-mercaptododecanoic acid SAM

| Peak | Binding Energy (eV)[a] | Theoretical Peak Area Ratio (Stoichiometry) | Experimental Peak Area Ratio |
|---|---|---|---|
| Carbon 1s | 285.0<br>286.3 | 12 | 15 |
| Sulfur 2p | 162.1 | 1 | 1 |
| Oxygen 1s | 532.8 | 2 | 5 |

*a The reported binding energies are corrected for charging effects.*

### 3.2.3 Preparation and Characterization of Clay Surfaces

Three major types of clays, illite, kaolinite, and montmorillonite, were investigated for use as substrates in AFM force measurements. Lamellar pieces of illite were selected as substrates for the adhesion studies. AFM images (Figure 3.4) show that the illite surfaces are reasonably flat with only minor deviations (up to 18 nm) in height across the surface. Therefore, these substrates were used as is for AFM studies.

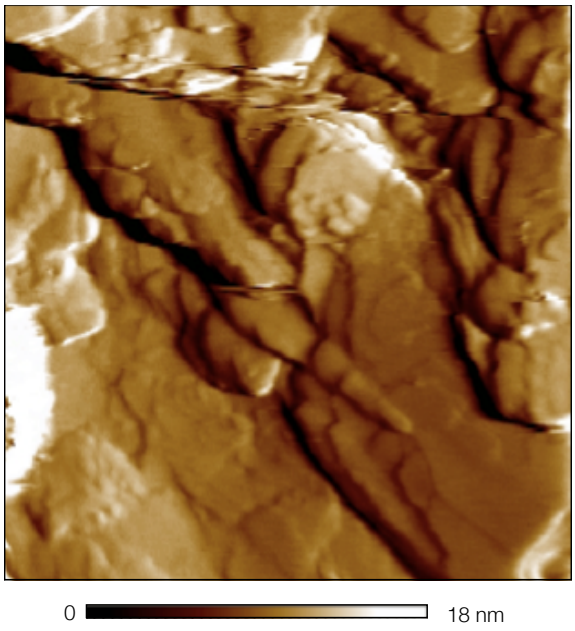


**Figure 3.4** AFM Image of Illite Clay (100 nm x 100 nm)

Kaolinite and montmorillonite were also considered possible candidates for the AFM studies; however, these two clays are commercially available as powders, which cannot be used as substrates. AFM substrates of precipitated metal oxides colloids have previously been prepared in the Horton group.[76,77,78] A muscovite mica

slide was placed in the center of a filter frit and the precipitated colloids were suspended in water and filtered through the prepared frit. The filtration process deposited and compacted the colloids onto the mica slide, resulting in a sample that may be used for AFM measurements. This was often repeated several times to ensure adequate coverage of the slide. Such a procedure was used in attempts to make kaolinite and montmorillonite substrates on mica. The slides were prepared and AFM images were collected (Figure 3.5). Both montmorillonite and kaolinite show flat topography. The kaolinite on mica shows the clay was deposited as platelet-like structures, whereas the montmorillonite is flat with few distinguishing features.

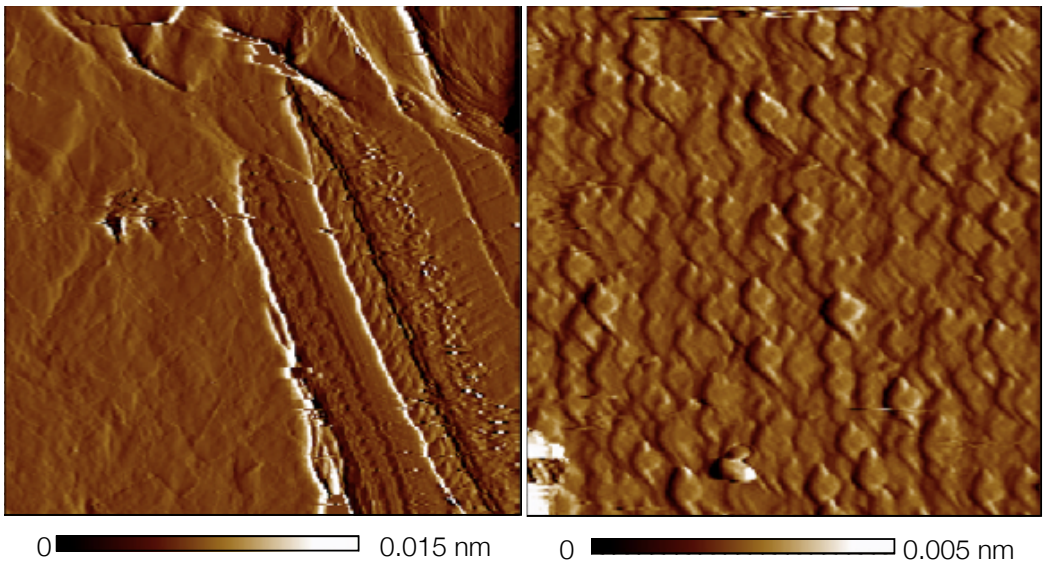


**Figure 3.5** AFM images of montmorillonite and kaolinite (250 nm x 250 nm)

However, these substrates proved to be inadequate for AFM studies. Since the experiments to be conducted require the substrate and the tip to be in an aqueous

environment, it is imperative that the substrate can withstand such conditions. When water is placed on the kaolinite on mica, the water quickly penetrates through the clay and the clay lifts off the mica surface. When water was placed on the montmorillonite clay, it was observed that the water caused the clay particles to swell and slide off the mica surface as well. AFM force measurements require that the substrate stays intact and flat for interaction forces to be measured between the tip and the surface.

Kaolinite and montmorillonite were also pressed into discs using a handheld KBr press, used to make IR discs. When water was placed onto the kaolinite disc, the water penetrated straight through the disc and the material began to disintegrate. When water was placed onto the montmorillonite disc, the disc began to warp inwards towards to droplet of water and the surface cracked. Similar behaviour was observed when discs of these clays were made using a ten tonne KBr press.

In summary, several different preparation methods were attempted in efforts to create surfaces from kaolinite and montmorillonite clay suitable for AFM force measurements. However, none of the methods proved to be successful for the intended purpose. As a result, only illite clay was used in the adhesion force measurement experiments.

## 3.3 Chemical Force Spectrometry Experiments

### 3.3.1 pH Force Titrations with Illite Clay

$CO_2$ switchable chemistry is in essence mediated by changes in solution pH due to the dissolution of $CO_2$ and the formation of carbonic acid. Thus, establishing the effects of solution pH on the interactions between a chemically functionalized AFM tip and the illite clay surface was integral to understanding the effects of switchable additives on our investigated systems.

The adhesion force between 12-phenyldodecanethiol modified AFM tips and illite clay were studied in aqueous solutions of varying pH conditions (Figure 3.6).

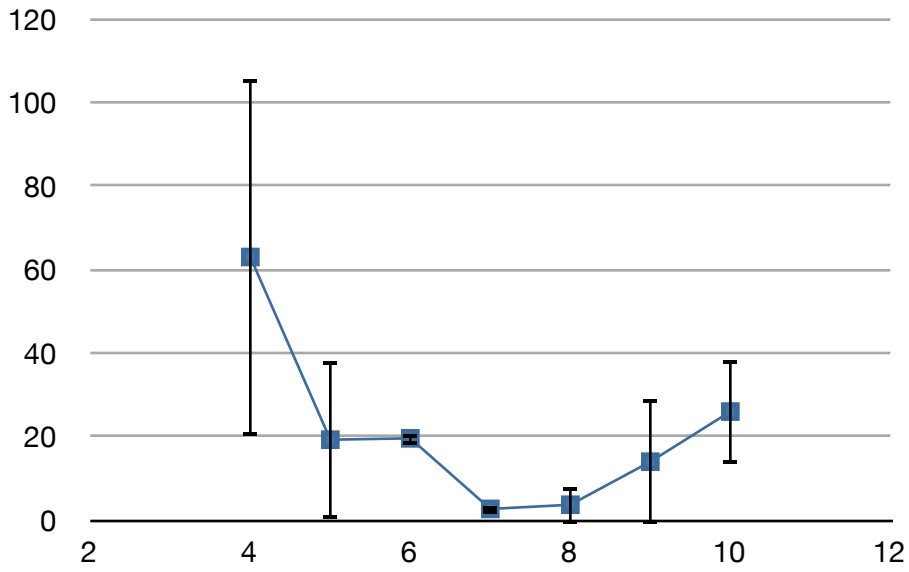


**Figure 3.6** Measured adhesion force between 12-phenyldodecanethiol AFM tip and illite clay as a function of pH

However, the results above were irreproducible. The experiment was conducted again using the same experimental conditions and procedures, but this yielded an entirely different set of data. The second experiment showed that the adhesion force was consistently low, on the order of 0-1 nN in magnitude, a finding that contradicts the data presented in Figure 3.6. Also, unlike the original results, there was very little adhesion force dependence on pH. Therefore, a variety of subsequent experiments were conducted to investigate the reproducibility of the collected data.

XPS studies were conducted a second time, to determine if the thiols are still assembling on the AFM tips. It is expected that thiols will oxidize with time to give disulfides and although it has been shown that disulfides still self assemble onto gold surfaces through scission of the sulfur-sulfur bond[74,75] perhaps the disulfides were not functionalizing the AFM tips. The XPS results were presented in Table 3.1 and it was confirmed that the thiols are still self-assembling onto the gold surface, even as disulfides.

XPS experiments confirm the deposition of thiol SAMs onto gold on mica substrate, which is used to determine if they will deposit onto the AFM tips. Functionalized AFM tips are not conveniently used in XPS experiments, as they are minuscule in size and XPS elemental signals from the functionalized AFM tip will be very weak. To confirm deposition of the thiol onto the AFM tips, AFM force measurements were conducted using gold on mica functionalized with 12-phenyldodecanethiol as substrate. The substrate was prepared in the same manner as the XPS samples. The adhesion forces between the functionalized AFM tip and the

functionalized gold on mica substrate were measured in the presence of deionized water. Adhesion of the tip to the substrate is expected under these conditions due to hydrophobic interactions between phenyl groups.

It was observed that there are measurable adhesion forces between the tip and the sample (Table 3.3). Contrary to the AFM studies using illite clay as substrate, these adhesion forces are very reproducible between trials. From the results in this experiment, it can be concluded that functionalization of the AFM tips is occurring normally; therefore, the irreproducible results involving the illite clay substrates is not attributed to this factor.

**Table 3.3** Measured adhesion forces between 12-phenyldodecanethiol AFM tip and 12-phenyldodecanethiol functionalized Au-mica substrate in deionized water

| | **Adhesion Force (nN)** |
|---|---|
| Trial 1 | 1.80 ± 0.21 |
| Trial 2 | 2.41 ± 0.23 |
| Trial 3 | 1.95 ± 0.02 |
| Trial 4 | 2.03 ± 0.15 |
| Average | 2.04 ± 0.22 |

The data collected from the pH titrations between the phenyl terminated AFM tip and the illite clay showed that the substrate was difficult to work with and yielded irreproducible results. The problematic nature of these surfaces may be a result of a variety of factors. Firstly, the clay surface itself is heterogeneous in nature.

It has both a basal surface and an edge surface, both which have unique acid-base properties. Although illite is reported to have a perfect basal cleavage plane, it is possible that through random selection of lamellar substrate pieces, the CFS experiments could have been performed with both types of surfaces. Even within the same face of the clay surface, it is heterogeneous in nature. Within the silica network, there are random substitutions of alumina sites, which gives rise to entirely different molecular interactions to be measured between the tip and the substrate. Finally, the clay surfaces were not entirely stable under aqueous conditions. It was observed that over time, the surfaces would become soft and lose integrity, making measurements difficult. Thus, it was concluded that these substrates were not suitable for the systems to be studied and further work was discontinued.

### 3.3.2 pH Force Titrations with Mica and Silica

Given the difficulty with work with the clay systems and the irreproducibility of the results obtained, working with the illite clay was halted and more well behaved systems, silica and mica, were investigated. Like clays, mica is also a phyllosilicate. Illite clay, the substrate previously discussed, is very similar to mica with the differentiation of having a higher silicon content in its crystal lattice and having a lower potassium content.[87] Mica was used to model the clay component, whereas silica was used to model the sand component of the oil sands.

The silica surfaces used in these experiments are amorphous silica surfaces. On the surface, is a two dimensional tetrahedral silicon-oxygen array, where some of

the oxygens are shared between two silicon cations (-Si-O-Si-) and some are hydroxyl groups.[88] The hydroxylated sites on the surface contribute to the acid base chemistry observed with these substrates. The point of zero charge for these surfaces is pH 2. Above this pH the silanol groups are deprotonated and the surface becomes increasingly negatively charged.

For muscovite mica substrates, the acid-base properties of the surface are a combination of the aluminol and the silanol sites that are present.[89] Like on the silica substrates, the silanol groups are increasingly negatively charged above pH 2. For the aluminol sites, they are protonated under acidic and neutral pH conditions because the pKa of these groups are approximately 8-9.[90] Although both the silanol and the aluminol sites contribute to the acid-base properties of muscovite mica, the basal surface is generally considered to be negatively charged in aqueous solutions due to $Al^{3+}$ isomorphous substitution in the tetrahedral silicon-oxygen sheet of the crystal lattice.[17]

The chemical force spectrometry experiments were conducted using AFM tips functionalized with 12-mercaptododecanoic acid ("acid tip") and 12-phenyldodecanethiol ("phenyl tip"). The adhesion forces measured between silica substrate and the acid tip were multiplied by 10 so the data may be plotted on the same graph as the adhesion forces measured between the silica substrate and the phenyl tip (Figure 3.7). This was done to facilitate comparison of trends observed in the two experimental sets.

The interaction force varied across the four different experimental sets. For the carboxylic acid terminated AFM tip, hydrogen bonding effects were the

dominating interactions found for the silica substrate (Figure 3.7). At a pH equal to its pKa, the maximum number of ionic hydrogen bonds may be formed, as the tip will be half protonated and half deprotonated. As the pKa of the acid is approximately 4, this is the region in which the strongest interactions are to be found. Indeed we observe that for the silica substrate, the maximum adhesion between the tip and the surface occurs near pKa of the tip. Above the pKa, the adhesion force diminishes sharply with increasing pH, as would be expected because the tip is becoming increasingly negatively charged and it is interacting with a negatively charged substrate. Interestingly, the adhesion force between the silica substrate and the acid tip is low under alkaline conditions, but increases again slightly at pH 11. This was a reproducible trend, seen in independent experiments. A possible explanation for this observation may be provided by considering the increase in sodium concentration from the increase in sodium hydroxide required to achieve this high pH. Both the silica substrate and the acid tip are expected to be negatively charged at pH 11 and the presence of sodium cations may serve to screen the two negatively charged surfaces, thus increasing adhesion.

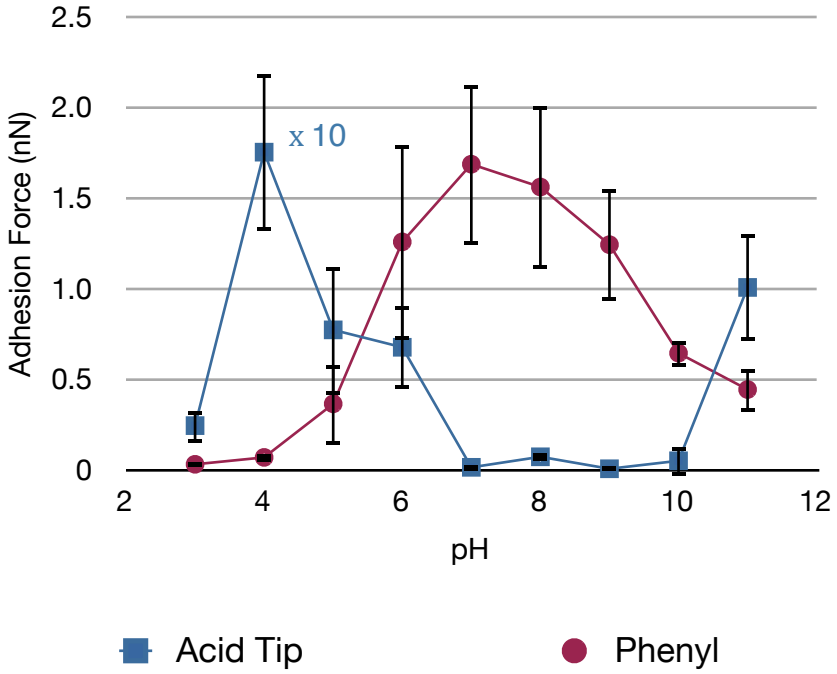


**Figure 3.7** pH force titrations with silica substrate

In contrast to the trends seen with the acid AFM tip, adhesion between silica and the phenyl tip is dominated by electrical double layer effects. Under near neutral pH conditions the adhesion between the tip and the surface is the strongest and at the extreme pH values, the adhesion is the weakest. This is a result of the changes in width of the electrical double layer with changes in ion concentration from pH modification. The electrical double layer is most diffuse near neutral pH values, as this is the region of lowest ionic strength. Under strongly acidic or strongly alkaline conditions, the electrical double layer collapses due to the increase in ionic strength of the solution.

Interactions between the mica substrate and the acid tip were also measured as a function of pH (Figure 3.8). Here, the adhesion force is strongest under acidic conditions and decreases with increasing pH. Like the interactions measured between the silica surface and the acid tip, this trend is attributed to hydrogen bonding interactions between the substrate and the surface. The pKa of this tip is approximately 4 and above this pH the tip is becoming increasingly negatively charged. The negatively charged tip experiences electrostatic repulsion with the negatively charged surface which results in the decrease in adhesion force observed.

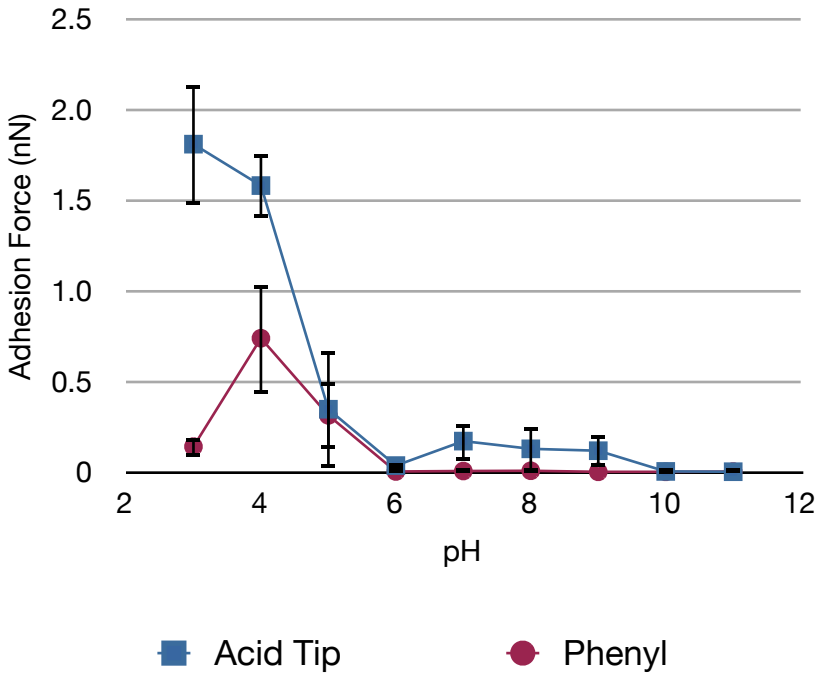


**Figure 3.8** pH force titrations with mica substrate

For the pH force titration involving mica and the phenyl tip, it was observed that the adhesion forces were mainly weak through the entire pH range (Figure 3.8).

The main contributing interaction arises from hydrophobic interactions between the organic tip and the sample. In this case, electrical double layer effects and hydrogen bonding effects are not observed.

### 3.3.3 Effect of $Ca^{2+}$

The literature from researchers in oil sands chemistry indicates that divalent cations decrease bitumen recovery through increasing bitumen and sand adhesion. The divalent cation both collapses the electrical double layer and shields the two negatively charged surfaces to increase adhesion.[88,89] Calcium sulfate, a common additive to oil sands tailings, were used in CFS studies to investigate how well our model systems would serve in mimicking real oil sands systems.

An upward trend with increasing $Ca^{2+}$ ion concentration was seen for the carboxylate tip on silica substrate (Figure 3.9). This result shows agreement with the oil sands literature. Liu, Xu, and Masilyah have previously shown that bitumen and silica can coagulate in solution containing greater than 0.1 mM calcium ions.[91] This finding was similar to that reported by Takamura and Chow.[92] With the phenyl tip, the interactions appear less dependent on calcium concentration than in the acid tip case. Because the tip cannot be ionized, the mechanism of adhesion discussed above does not apply in this system, which explains why the adhesion force does not increase with increasing divalent cation concentration.

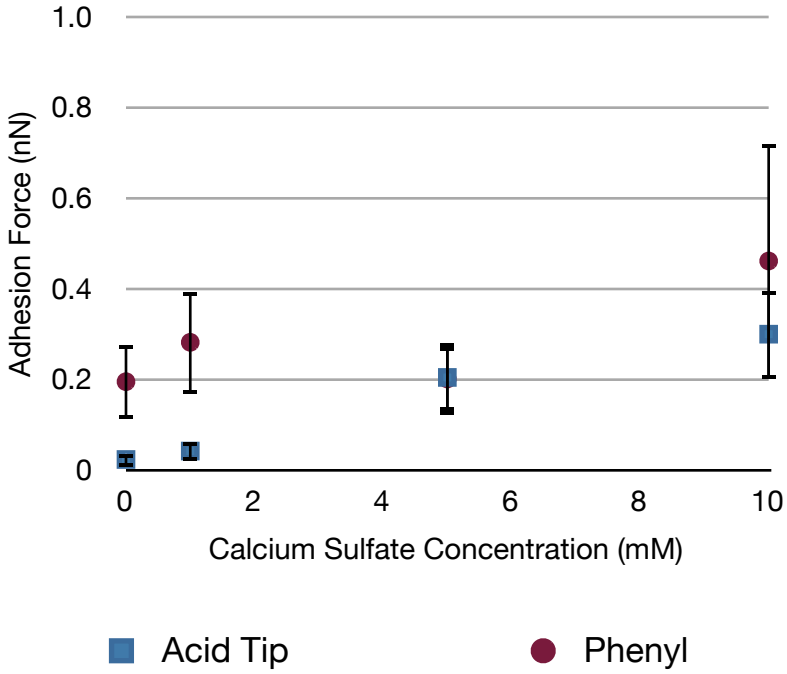


**Figure 3.9** Calcium sulfate CFS experiments with silica substrate

Unlike the results from the calcium experiments with silica, on mica there was no systematic dependence of adhesion force on calcium concentration with either AFM tip (Figure 3.10). Instead, the adhesion force initially increases with the introduction of calcium, but decreases at higher calcium concentration. This trend is likely a result of cation exchange between the potassium on the surface of the mica substrate and the calcium in solution.

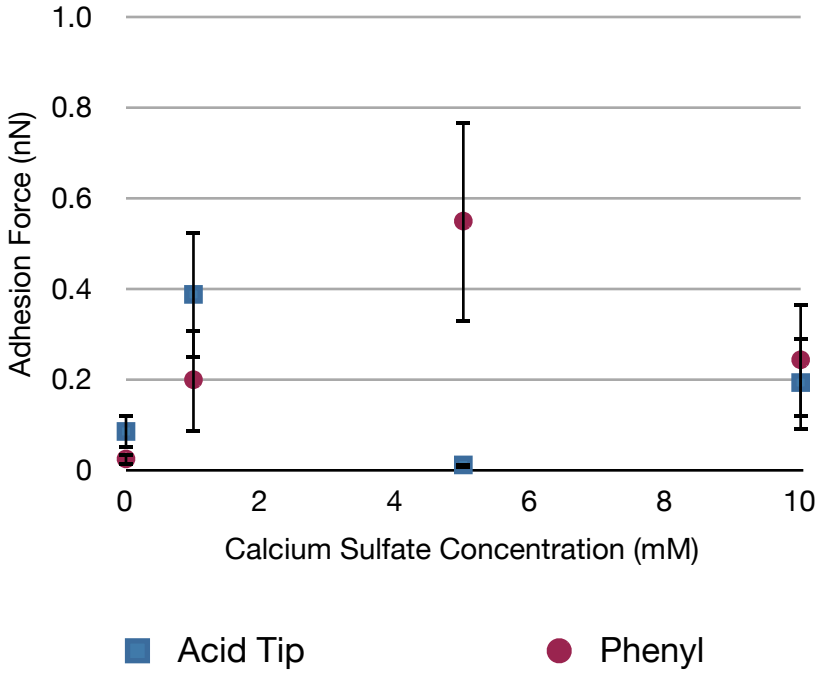


**Figure 3.10** Calcium sulfate CFS experiments with mica substrate

Exchange of surface ions on mica has previously been reported in literature[93] and it was confirmed experimentally through XPS (Figure 3.11). The substrates were submerged into calcium sulfate solutions for 15 minutes, rinsed thoroughly with deionized water, and dried prior to analysis. The XPS spectra show that the mica substrate surface was devoid of calcium before this treatment, but upon exposure to solution containing $Ca^{2+}$ a calcium 2p peak appears and then grows in intensity with increasing calcium sulfate concentration.

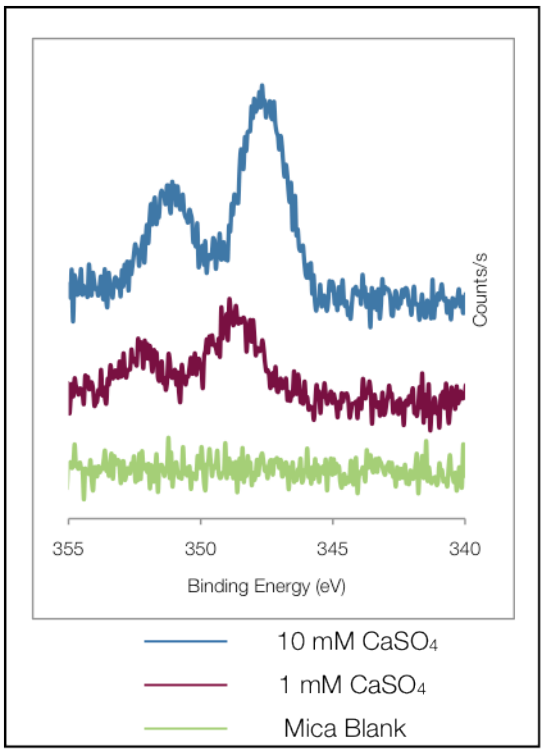


**Figure 3.11** Calcium 2p XPS spectra of mica

### 3.3.4 Effect of $CO_2$

As the switchable surfactants to be studied use $CO_2$ as a trigger, it is imperative to study the effects of $CO_2$ on the adhesion force in these systems.

The results from the $CO_2$ CFS experiments were compared with the results obtained from the pH force titrations at the same pH, but using HCl as a pH modifier. The results presented in Table 3.4 show that regardless of the acid, carbonic acid or hydrochloric acid, used to mediate the pH, the results are the same at pH 4. Therefore, $CO_2$ only serves to change the pH of the solution and no other effects are observed. This experiment serves as a control for the switchable chemistry discussed in the following sections.

**Table 3.4** CFS Experiments with Carbon Dioxide

| | Adhesion Force (nN) | | | |
|---|---|---|---|---|
| **Additive** | **Silica and Acid Tip** | **Mica and Acid Tip** | **Silica and Phenyl Tip** | **Mica and Phenyl Tip** |
| $CO_2$ (pH 4 ± 0.2) | 0.14 ± 0.05 | 1.07 ± 0.25 | 0 | 1.14 ± 0.35 |
| pH 4 ± 0.2 HCl modified | 0.18 ± 0.04 | 1.58 ± 0.18 | 0.07 ± 0.02 | 0.74 ± 0.35 |

### 3.3.5 Cationic Switchable Surfactants

A cationic switchable surfactant, C8 (Figure 3.12), was studied via CFS for its ability to affect adhesion forces together with C4 , an amidine with a four carbon chain tail, was studied concurrently (Figure 3.13). Unlike C8, C4 is not a surfactant molecule in the presence of $CO_2$ due to its short alkyl chain length, but the molecule can still be protonated in aqueous solutions saturated with $CO_2$ to yield a positively charged amidinium head group. Therefore, C4 was studied alongside C8 to determine if the effect observed with the switchable surfactant was attributed to its surfactant capabilities or simply due to the presence of the amidine functionality.

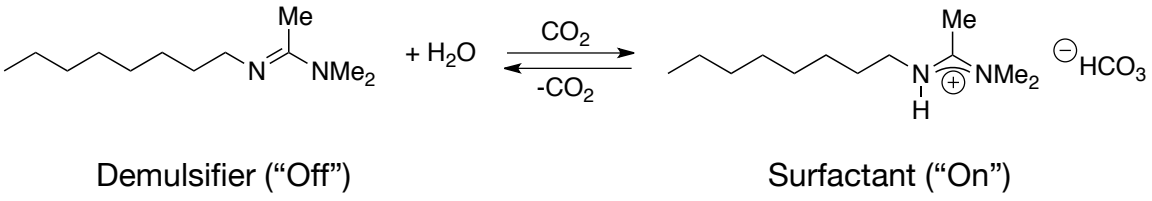


**Figure 3.12** Switchable surfactant, C8

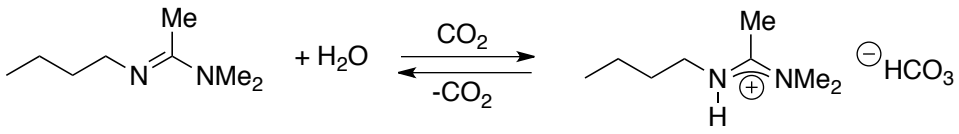


**Figure 3.13** Switchable amidine, C4

The results from the CFS experiments in the presence of C4 are presented below (Table 3.5). A consistent trend was observed for all four tip/sample pairs. In the absence of $CO_2$, there was no interaction measured between the tip and the surface. Upon saturation of the aqueous solution with $CO_2$, the adhesion force increased dramatically.

**Table 3.5** CFS experiments with C4

| | Adhesion Force (nN) | | | |
|---|---|---|---|---|
| **Additive** | **Silica and Acid Tip** | **Mica and Acid Tip** | **Silica and Phenyl Tip** | **Mica and Phenyl Tip** |
| 1 mM C4 (pH 11 ± 0.2) | 0 | 0.01 ± 0.01 | 0 | 0.01 ± 0.01 |
| 1 mM C4 + $CO_2$ (pH 5 ± 0.2) | 0.73 ± 0.11 | 0.63 ± 0.23 | 1.54 ± 0.28 | 1.05 ± 0.92 |
| pH 11 ± 0.2 NaOH modified | 0.10 ± 0.04 | 0 | 0.64 ± 0.09 | 0 |
| pH 5 ± 0.2 HCl modified | 0.08 ± 0.05 | 0.31 ± 0.30 | 0.36 ± 0.26 | 0.35 ± 0.46 |

The results from the CFS experiments using C4 were compared with the results obtained from the pH force titrations at the same pH, but using HCl and NaOH

as a pH modifier. These comparisons were made to determine if the changes in adhesion force observed in the presence of C4 may be attributed to the presence of the amidine additive or simply due to changes in pH arising from the introduction of $CO_2$ into the aqueous systems. Table 3.5 indicates the former. For the four tip/ sample pairs, the increase in adhesion force is observed in the presence of C4 is not comparatively observed when the solution pH is modified by HCl or NaOH, suggesting that the observed modifications in adhesion force are not attributed to pH changes.

The observed trends for interactions involving the carboxylic acid tip in the presence of C4 may be driven by electrostatic interactions with the protonated version of the amidine molecules. It is important to note that the solution pH of the amidines is higher than the pKa of the acid tip (approximately 4), both in the presence and the absence of $CO_2$ (pH 5 and pH 11 respectively). Therefore, in both cases the tip is negatively charged, as is the substrate surface. When the amidine is protonated, an electrostatic attraction may exist between the negatively charged tip and the positively charged additive head group. The amidinium cation may similarly be attracted to negatively charged sites on either substrate surface under these pH conditions. Such surfactant interactions with both mica and silica have previously been discussed in the literature.[94, 95] Sharma, Basu, and Sharma have shown through AFM imaging that distinct aggregates of a commercial cationic surfactant cetyltrimethylammonium bromide (CTAB) can absorb on the surface of mica at 1 mM concentration levels.[94] Gu and Zhu have similarly showed that non-ionic surfactant Triton X-100 can absorb onto silica surfaces.[95] Thus, the interactions

measured through CFS may be a combination of ionic attraction and hydrophobic interactions between the alkyl chains of the amidine molecules absorbed onto both the tip and the substrate surface (Figure 3.13).

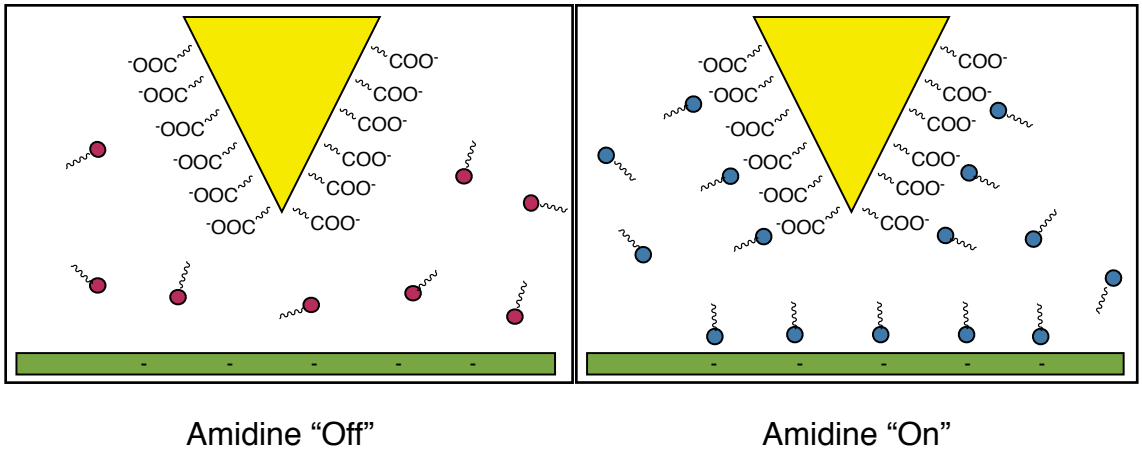


**Figure 3.13** Carboxylic tip and sample interaction in the presence of C4

A similar interaction between a phenyl tip and a sample surface decorated with alkyl groups may also be envisioned (Figure 3.14). Here, the tip is already a hydrophobic surface. Upon $CO_2$ activation of C4, electrostatic attraction of the positively charged amidine head group to the negatively charged sample surface can expose the hydrophobic tails to the tip resulting in the measurement of hydrophobic forces between the tip and sample.

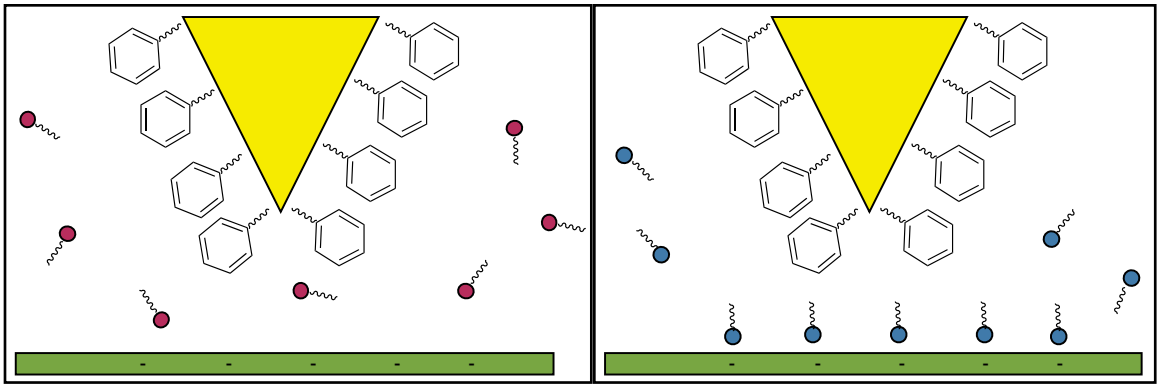


**Figure 3.14** Phenyl tip and sample interaction in the presence of C4

These trends hold for the shorter chain C4 molecule, but the increase in adhesion force is not as strong for the C8 surfactant molecule (Table 3.6). It was observed that even in the absence of $CO_2$ some attraction is observed between the tip and the sample when C8 is used.

**Table 3.6** CFS experiments with C8

| | Adhesion Force (nN) | | | |
|---|---|---|---|---|
| **Additive** | **Silica and Acid Tip** | **Mica and Acid Tip** | **Silica and Phenyl Tip** | **Mica and Phenyl Tip** |
| 1 mM C8 (pH 11 ± 0.2) | 0.39 ± 0.20 | 0.23 ± 0.28 | 0.97 ± 0.33 | 1.97 ± 0.19 |
| 1 mM C8 +$CO_2$ (pH 5 ± 0.2) | 1.53 ± 0.19 | 1.94 ± 0.23 | 1.05 ± 0.38 | 0.41 ± 0.20 |
| pH 11 ± 0.2 NaOH modified | 0.10 ± 0.04 | 0 | 0.64 ± 0.09 | 0 |
| pH 5 ± 0.2 HCl modified | 0.08 ± 0.05 | 0.31 ± 0.30 | 0.36 ± 0.26 | 0.35 ± 0.46 |

The results from the CFS experiments in the presence of C8 were compared with the results obtained from the pH force titrations at the same pH, but using HCl and NaOH as a pH modifier (Table 3.6). In all four tip/sample pairs, the changes in adhesion force that occur as a result of $CO_2$ triggered switching of C8 are not observed by modifications in solution pH using HCl and NaOH. This indicates that like C4, C8 in solution is affecting adhesion force by means other than pH modification.

As noted earlier, interactions between the tip and the sample were observed in all four cases when C8 was present in solution as a demulsifier. This is unlike what was noted in the C4 case, where in the absence of $CO_2$, no attraction between the tips and the samples were observed. These longer chain amidine molecule may self assemble at the surface to some extent due to van der Waals interactions,

leading to the adhesive interaction forces measured (Figure 3.15). The orientation of the self assembled C8 are uncertain and this is reflected in the illustration below.

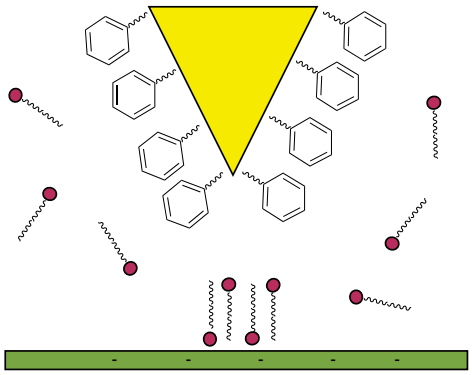

**Figure 3.15** Phenyl tip and sample interaction in the presence of a self assembled C8

Introduction of $CO_2$ to these aqueous systems protonates the C8 molecule and may cause a rearrangement the surfactant molecules on the surface, resulting in an electrostatic interaction between the positively charged amidinium head group and the negatively charged substrate surface. The orientation of molecules on the surface may be similar to that depicted for the "on" form in Figure 3.13 and 3.14.

For interactions between the acid tip and both the silica and mica substrates the presence of C8, an increase in adhesion force was observed when the aqueous solutions were $CO_2$ saturated. This is believed to be due to absorption of the switchable surfactant onto the surface of both the substrate and the tip, similar to that discussed for the C4 additive. However, the increase in adhesion force is not as

strong when C8 is used compared to C4, possibly because of interactions that already exist if C8 in its demulsifier form self assembles onto the substrate surface.

However, when the phenyl tip is in the presence of C8 the trends do not hold. Interactions with the silica substrate do not change with addition of $CO_2$, whereas addition of $CO_2$ decreases adhesion between the phenyl tip and the mica substrate. This suggests that the interactions between phenyl tip and the self assembled C8 in the absence of $CO_2$ is stronger than that of the phenyl tip and the absorbed surfactant molecules, thus producing the adhesion trends observed from these CFS experiments.

### 3.3.6 Anionic Switchable Surfactants

The effects of two different anionic switchable surfactants, sodium laurate (SL) and NP-C8, on the adhesion force between organic and mineral surfaces were studied by CFS.

Although some switching behaviour was observed using NP-C8 (Table 3.7) these two surfactants were not ideal candidates for AFM work. Upon $CO_2$ treatment to generate the neutral form of the surfactant, both SL and NP-C8 precipitate out of solution. This made it difficult to measure force distance curves as a result of dispersion of the laser signal from the particulate matter suspended in the solution. Therefore, this class of switchable surfactants was not further studied by AFM.

**Table 3.7** CFS Experiments with Anionic Surfactants

| | Adhesion Force (nN) | | | |
|---|---|---|---|---|
| **Additive** | **Silica and Acid Tip** | **Mica and Acid Tip** | **Silica and Phenyl Tip** | **Mica and Phenyl Tip** |
| 1 mM SL | 0 | 0 | - | - |
| 1 mM SL + $CO_2$ | 0.32 ± 0.50 | 0.10 ± 0.11 | - | - |
| 1 mM NP-C8 | 1.88 ± 0.81 | 0 | 0.01 ± 0.01 | 0 |
| 1 mM NP-C8 + $CO_2$ | 0.74 ± 0.60 | 0 | 0 | 0.40 ± 0.13 |

### 3.3.7 Switchable Water Additives

Switchable ionic strength additive BMDAPAP was employed in CFS studies to determine if adhesion force is dependent on ionic strength. In the presence of 0.8 molal of BMDAPAP, no adhesion force was observed in all four systems studied. Furthermore, no observable change in adhesion force was observed by increasing the ionic strength of the solution through application of $CO_2$. The same observations were made using 0.8 molal TMDAB as an additive.

This trend may be a result of the high pH of solutions containing these additives. In the absence of $CO_2$, the pH of these solutions are approximately 13. Upon saturation of the solution with $CO_2$, the pH is still strongly alkaline at a value of 10. Original force titrations (Figure 3.7 and Figure 3.8) show that in all four

experimental cases studied, low to no adhesion force is observed in this pH range. Therefore, adhesion in these systems may either be independent of ionic strength or more strongly dependent on solution pH.

## 3.4 Conclusions

CFS experiments were conducted to determine if $CO_2$ switchable chemistry may be used to mediate adhesion force between mineral substrates and organic functional groups. The effects of pH, presence of divalent cations, switchable cationic and anionic surfactants, and switchable ionic strength additives were studied.

Original CFS studies using illite clay as substrate proved to be difficult due to surface instability in aqueous conditions. However, mica and silica surfaces were shown to be more compatible with the systems of interest.

All systems under investigation show pH dependence on adhesion force. Hydrogen bonding effects between the tip and the substrate dominated force titrations with carboxylic functionalized AFM tips, whereas hydrophobic effects and electrical double layer effects were observed using the phenyl functionalized AFM tips.

For silica and carboxylic acid interactions, an increase in adhesion force was detected with increasing calcium sulfate concentration. This finding is consistent literature reports that indicate that the presence of divalent cations can collapse the electrical double layer and shield two negatively charged surfaces to increase adhesion.[88,89] The divalent cation effect is observed in oil sands chemistry between bitumen and mineral surfaces and results in a decrease in bitumen recovery. A similar, although less pronounced effect was observed when the carboxylic acid tip was replaced with the phenyl tip. This suggests that these model systems are consistent with real oil sands systems. For CFS studies employing mica as substrate,

cation exchange was observed between the surface potassium ions and the solution calcium ions. This was confirmed through XPS investigations.

Of the switchable additives used in these experiments, the greatest success in modifying adhesion force was observed through the use of C4, which were molecules containing amidine functionality, with no surfactant capabilities. In all systems studied, a switch from no adhesion to adhesion was observed when $CO_2$ was added to aqueous solutions containing C4. This experimental finding demonstrates that these compounds may be useful for applications desiring control of mineral and organic interactions.

# 4. Results and Discussion: Mineral/Mineral Interactions

## 4.1 Introduction

In the previous chapter, the interaction forces between organic functional groups and mineral surfaces were investigated in the context of the bitumen liberation phase of oil sands processing. While organic/mineral interactions are important to bitumen extraction, the interaction forces between mineral surfaces, such as clays and sand, with other mineral surfaces are crucial to the tailings disposal phase of the process. For tailings disposal, the settling of sand and clays are desired to clear up the solids content within the process water so that it may be recycled for further use.[37,38] However, mineral fines such as clays form stable suspensions in process water optimized for bitumen liberation from mineral surfaces. To circumvent this issue, current industrial practices to accelerate settling of fines include addition of polymer flocculants or gypsum. The problem with such additives is that they need to be removed if the water is to be recycled for further cycles of bitumen extraction. An alternative to these conventional process aids may be $CO_2$ triggered switchable additives.

In this chapter, the interaction forces between silica-silica and silica-alumina surfaces are investigated in the presence of switchable additives using chemical force spectrometry. Clay minerals are phyllosilicate materials that are made up of layers of tetrahedral silica-oxygen sheets and octahedral aluminum-oxygen sheets, so the study of silica-silica and silica-alumina interactions is a fundamental investigation into mineral-mineral interactions that exist in oil sand tailings. In these

studies a silica AFM tip was used to probe interactions with amorphous silica and alumina surfaces. Tip/sample interactions were analyzed as a function of pH, in the presence of divalent cations, and in the presence of switchable additives.

## 4.2 Surface Characterization

### 4.2.1. Characterization of silica surfaces

Silicon (111) wafers were used as substrates in these experiments. Prior to use, they were cleaned with piranha solution (3:1 concentrated $H_2SO_4$: 35 wt% $H_2O_2$ in $H_2O$) to remove surface contaminants. The surface was characterized by XPS (Table 4.1).

**Table 4.1** XPS characterization of silicon wafers

| Peak | Binding Energy[a] (eV) | Experimental Elemental Ratio |
|---|---|---|
| Oxygen 1s | 532.8 | 0.35 |
| Silicon 2p | 99.1<br>103.1 | 1 |

[a]*Reported binding energies are corrected for charging effects*

Two silicon 2p peaks were observed, arising from the bulk silicon (at 99.1 eV) and silicon oxide (at 103.1 eV).[96] The elemental ratio of oxygen to silicon was experimentally determined to be 0.4:1, which is expected. For the surface oxide

layer, an elemental ratio of 2:1 is expected for $SiO_2$, but if bulk silicon is included in the calculation, as per above, then the elemental ratio of oxygen to silicon should be lower than 2:1. However, the peak area ratios of oxygen 1s to silicon oxide 2p peak is 2.4 which is closer to the expected 2:1 ratio for $SiO_2$. Carbon 1s contaminants were also observed in the XPS peak, which is not unusual for XPS data. The carbon to silicon ratio was determined to be 0.15.

### 4.2.2. Characterization of alumina surfaces

Several methods for preparation of alumina surfaces have been presented in the literature by van der Brand et al.[79] Two different methods for cleaning and preparation were adapted from the procedures discussed by van der Brand,[79] one employed a nitric acid treatment to clean and oxidize the aluminum foil surfaces and the other was accomplished by submerging the foil into boiling deionized water. Substrates were prepared using both methods and characterized by XPS. An untreated sample was also analyzed in the same manner.

The XPS spectra of the untreated aluminum sample showed two Al 2p peaks, indicating that two chemical states are present in the sample (Figure 4.1). The peak at 72.9 eV corresponds to the bulk aluminum, whereas the peak observed at 75.6 eV arises from the native oxide layer that presides on the metal surface. Treating the sample with dilute nitric acid showed no changes to the spectra (Figure 4.2), and thus, no changes to the native oxide layer. However, a simple treatment with boiling deionized water showed modification of the oxide overlayer through the formation of a thick oxide layer (Figure 4.3).

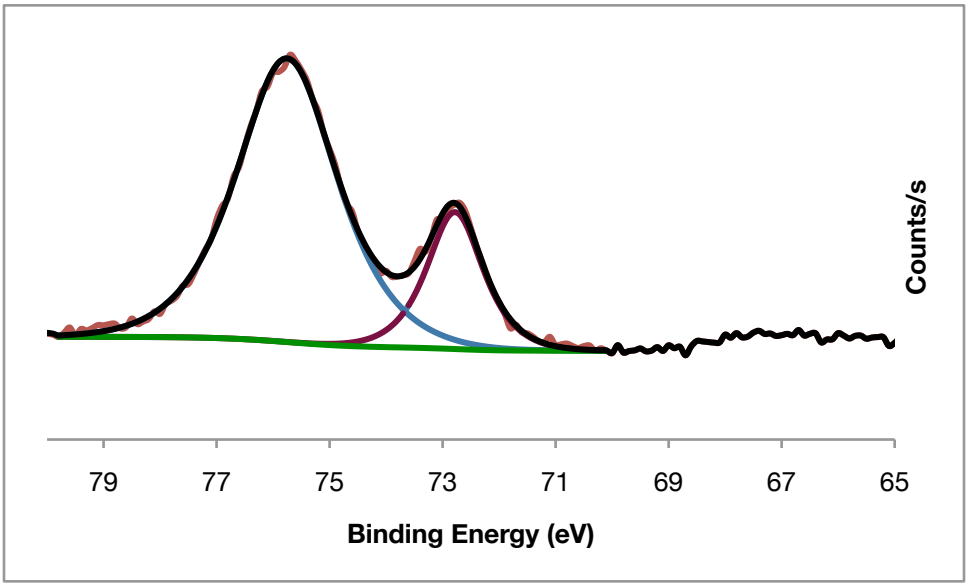


**Figure 4.1** Blank aluminum 2p XPS peak

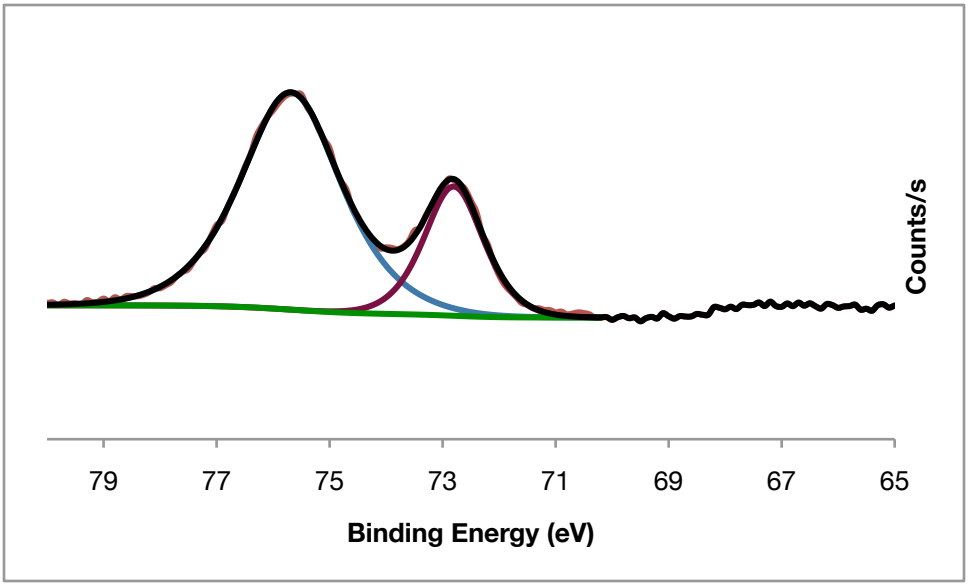


**Figure 4.2** Acid treated aluminum 2p XPS peak

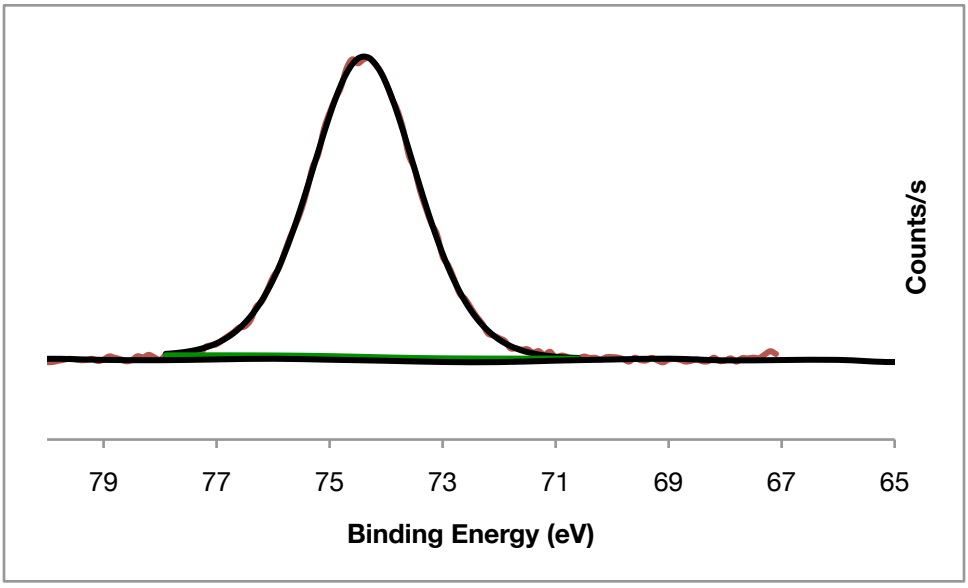


**Figure 4.3** Boiled aluminum 2p XPS peak

The new oxide overlayer formed from boiling the aluminum foil is so thick that the peak corresponding to the bulk aluminum disappears. This indicates that the new overlayer is so thick that XPS can no longer probe the bulk aluminum layer. The surface modification also reduces the conductivity of the sample, resulting in an XPS charging effect. Comparing the uncorrected binding energies of the Al 2p peak of the boiled sample with those of the blank and the acid treated sample, it is observed that sample charging of approximately 10 eV is observed. Also, a reduction in peak area of the carbon 1s peak was observed with this preparatory method, suggesting that some organic contaminants were also removed in the process. Thus, preparation of the alumina surfaces used in CFS was accomplished simply through immersion into boiling deionized water.

## 4.3 Chemical Force Spectrometry Experiments

### 4.3.1 pH Force Titrations

The interactions between the silica AFM tip and silica and alumina substrate were studied as a function of pH. These experiments provide characterization of surface acid base chemistry and were used to interpret the results obtained in CFS experiments with switchable additives.

CFS experiments with silica substrate and the silica AFM tip show no significant changes in adhesion force with varying pH over the majority of the pH range studied (Figure 4.4). Amphoteric silanol groups on silica is reported to have a low pKa (~2);[88] therefore, it is expected that in these experiments both the tip and the substrate are negatively charged. The main tip/sample interactions observed in this series of force measurements were electrical double layer effects. At the alkaline range of the pH scale, it is observed that the adhesion force decreases at the highest pH due to the increase in ionic strength of the solution. This compresses the width of the electrical double layer and thus, the electrostatic repulsive charges of the tip and the sample are no longer being screened by the electrical double layer. This is not observed at the lowest pH tested because it is closer to the pKa of the tip. At these pH values, protonation of the silica surfaces begin to occur, increasing the degree of attractive H-bonding.

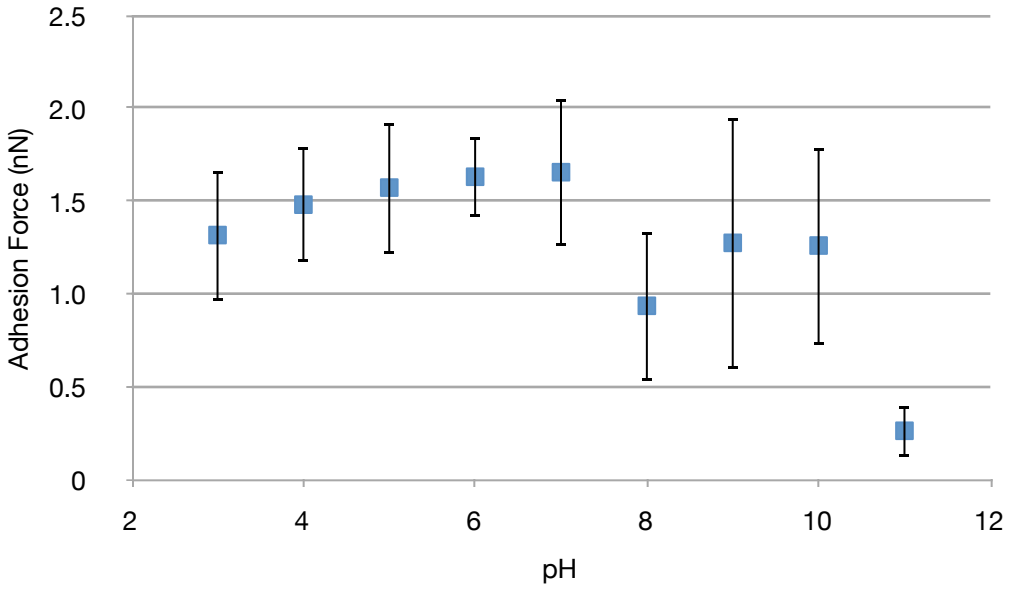


**Figure 4.4** pH force titrations with silica substrate

CFS experiments with the alumina substrate and silica AFM tip show that at the lower, more acidic range of the pH scale, the adhesion force does not vary significantly with varying pH (Figure 4.5). A maximum adhesion force is observed at pH 8-9 and a drop is observed as the pH is further increased.

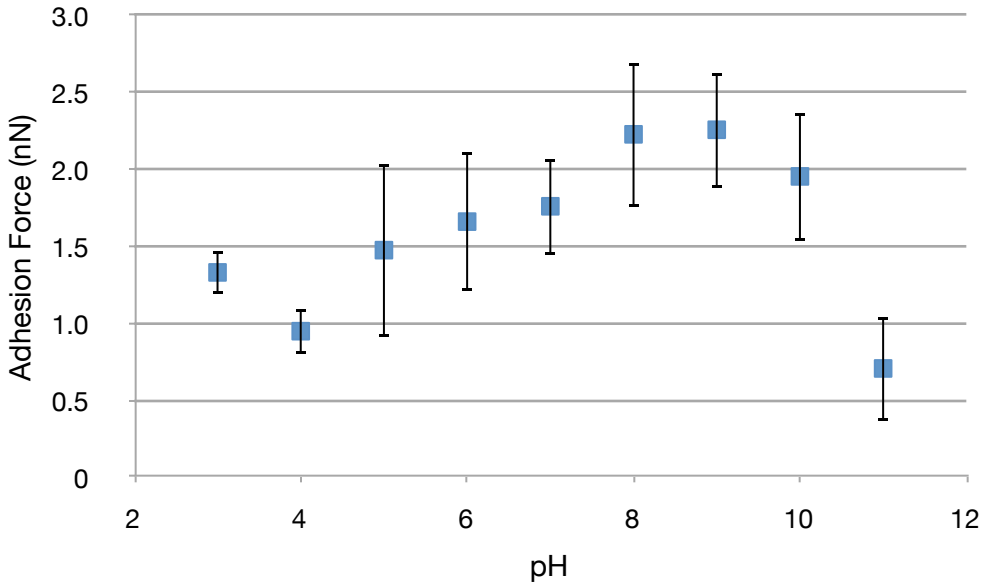


**Figure 4.5** pH force titrations with alumina substrate

Alumina is expected to be protonated under acidic conditions due to a higher, more basic pKa, whereas the silica AFM tip is expected to be deprotonated due to its lower, more acidic pKa. Therefore, the interactions observed between the tip and the sample in the acidic pH range is believed to arise from ionic hydrogen bonding. The strongest interactions between tip and sample are observed at pH 8-9 close to the pKa of alumina.[89] Beyond the pKa in the more alkaline range of the pH scale, the adhesion force is increasingly diminished as both the tip and the substrate are negatively charged and electrostatic repulsion is observed.

In summary, a silica AFM tip exhibits an interaction with both a silica surface and an alumina surface. However, whereas silica silica interactions are dominated by electrical double layer effects, alumina silica interactions are mainly attributed to ionic hydrogen bonding for most of the pH range studied.

### 4.3.2 Effect of $Ca^{2+}$

As discussed in the previous chapter, divalent cations have been shown to decrease bitumen recovery through increasing adhesion between bitumen and mineral surfaces. These additives collapse the electrical double layer and serve to shield electrostatic repulsion between two similarly charged surfaces. This results in an increase in adhesion between the two surfaces. Previous experiments have shown that this trend holds for a negatively charged organic functional groups and negatively charged surface (see Section 3.2.3). Chemical force spectrometry experiments were conducted in the presence of calcium sulfate to ascertain how the presence of divalent cations influence adhesion between two mineral surfaces.

CFS experiments showed that the addition of divalent cations has no effect on the adhesion force between two silica surfaces (Figure 4.6). This data is contrary to what was expected. Addition of calcium should have increased adhesion force between the tip and the substrate by screening the electrostatic repulsion from the two similarly charged surfaces. This trend was observed with previous CFS experiments between silica and a carboxylic acid AFM tip. Although this is not the expected outcome, this difference may be due to the differences in charge density of the AFM tip when comparing the organic functionalized tip with the silica tip. The surface coverage of the SAM may be more dense, thus providing more charged sites, relative to the silica AFM tip. Charged sites on silica are a result of deprotonated surface hydroxyl groups, which are distributed randomly across the surface.

Therefore, if there are fewer acidic sites on the silica AFM tip, an increase in adhesion with increasing calcium concentration may not be observed.

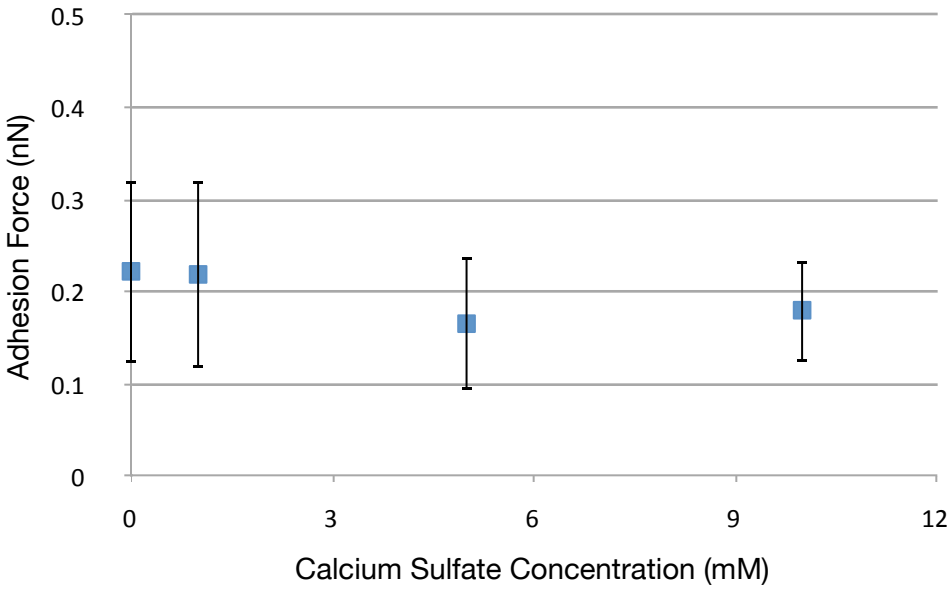


**Figure 4.6** Calcium sulfate CFS experiments with silica substrate

CFS measurements between an alumina substrate and a silica AFM tip also showed no calcium dependence on adhesion force (Figure 4.7). However, this might be expected as the alumina substrate is protonated at the pH (approximately 7) that these experiments are conducted at. Therefore, what is observed is an interaction between a negatively charged tip and a protonated surface. Although the electrical double layer is collapsed, there is no shielding of electrostatic repulsive surfaces. In addition, the same issues with density of charged sites on the silica AFM tip may apply in these experiments, as per above with the silica substrates.

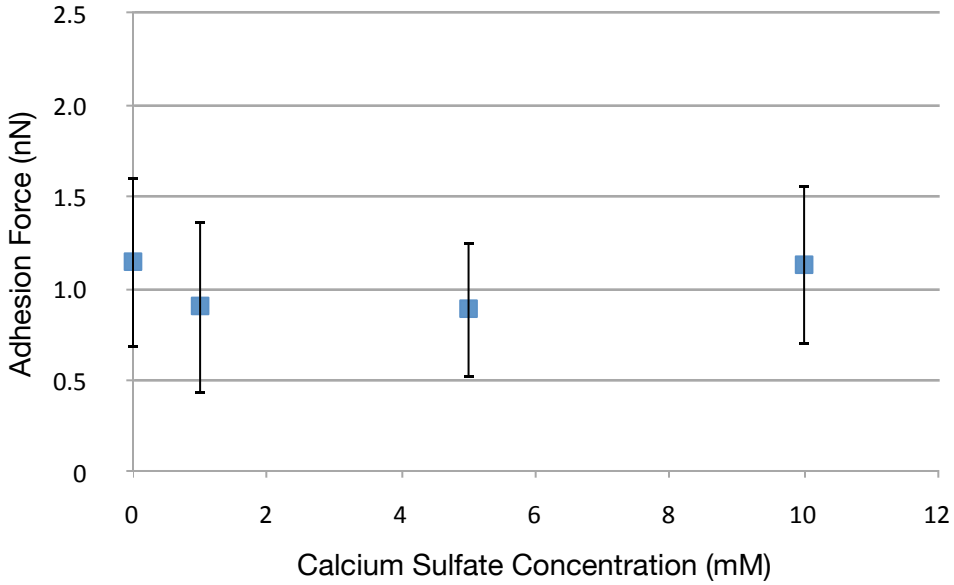


**Figure 4.7** Calcium sulfate CFS experiments with alumina substrate

### 4.3.3 Effect of $CO_2$

Adhesion forces were measured in the presence of carbonated deionized water to study the effects of $CO_2$ on the interactions between the substrates and the silica AFM tip. These experiments serve as control experiments for the switchable additives by illustrating the sole effect of $CO_2$ on these systems.

**Table 4.2** CFS experiments with $CO_2$ saturated water

| | Adhesion Force (nN) | |
|---|---|---|
| **Additive** | **Silica Substrate** | **Alumina Substrate** |
| $CO_2$ (pH 4 ± 0.2) | 0.56 ± 0.64 | 1.28 ± 0.50 |
| pH 4 ± 0.2 (modified with HCl) | 1.48 ± 0.31 | 0.95 ± 0.15 |

The results show that the adhesion force measured in the presence of $CO_2$ saturated water are within experimental error of that measured at the same pH (pH 4) for the pH titration experiments. This demonstrates that saturation of water with $CO_2$ only serves to mediate the solution pH and no further changes in adhesion force are observed with the change in anion present in the solution.

### 4.3.4 Switchable Surfactants

Cationic switchable surfactant C8 was investigated for its ability to change the adhesion force between a silica AFM tip and silica and alumina substrates. Much like the approach described in the previous chapter, a switchable additive, C4, with no surfactant capabilities was studied concurrently to determine if any observable changes in the adhesion force were a result of the amidine functionality of the switchable surfactant or a result of the surfactant capabilities of the molecule. The results from these CFS experiments were compared with the results obtained from the pH force titrations at the same pH, but using HCl and NaOH as a pH modifier.

These comparisons were made to determine if the changes in adhesion force observed in the presence of C4 and C8 were attributed to the presence of an amidine additive or to the changes in pH arising from the introduction of $CO_2$ into the aqueous systems.

The solutions containing C4 and C8 are initially alkaline (pH 11), but become slightly acidic (pH 5) upon saturation with $CO_2$. In both cases, the solution pH is higher than the reported pKa of silica (~2),[90] thus it is expected that the tip and the surface are both negatively charged. For the alumina substrates, pH 11 is above the pKa of the aluminol sites on the surface(~8-9);[89] therefore, in the presence of C4 and C8, the surface is deprotonated and negatively charged. When aqueous solutions of C4 and C8 are treated with $CO_2$, the solution pH is below that of of the pKa of aluminol and those sites will be protonated, resulting in an overall neutral substrate surface.

In the presence of C4, attractive interactions between the silica substrate and the silica AFM tip were stronger when the solution was saturated with $CO_2$ relative to the solution with no $CO_2$ (Table 4.3). That is, the protonated amidine molecule is increasing adhesion relative to the unprotonated version. Similar trends were also observed in previous CFS studies between a negatively charged carboxylic acid functional group and the silica surface (see Chapter 3.3.5).

**Table 4.3** CFS experiments with C4

| | Adhesion Force (nN) | |
|---|---|---|
| **Additive** | **Silica Substrate** | **Alumina Substrate** |
| 1 mM C4 (pH 11 ± 0.2) | 0.38 ± 0.13 | 1.88 ± 0.64 |
| pH 11 ± 0.2 modified with NaOH | 0.26 ± 0.14 | 0.71 ± 0.34 |
| 1 mM C4 + $CO_2$ (pH 5 ± 0.2) | 1.28 ± 0.26 | 1.46 ± 0.70 |
| pH 5 ± 0.2 modified with HCl | 1.57 ± 0.36 | 1.48 ± 0.57 |

The results from the CFS experiments using C4 were compared with the results obtained from the pH force titrations at the same pH, but using HCl and NaOH as a pH modifier. These comparisons were made to determine if the changes in adhesion force observed in the presence of C4 were attributed to the presence of the amidine additive or to the changes in pH arising from the introduction of $CO_2$ into the aqueous systems. Table 4.3 indicates that the changes in adhesion force may be dominated by changes in pH with the introduction of $CO_2$, as the results for the CFS experiments in the presence of C4 are consistent with the results obtained at the same pH in the pH force titrations.

The general trend observed in these CFS experiments with C4 are similar to the trends observed with analogous CFS studies using a carboxylic acid functionalized AFM tip and a silica surface in the presence of the same additive. That

is, in the presence of C4, attractive interactions between the silica substrate and the silica AFM tip were stronger when the solution was saturated with $CO_2$ relative to the solution with no $CO_2$. For the silica-silica CFS experiments, these changes may be a result of changes in solution pH with the introduction of $CO_2$, but the model used to explain the interactions observed between a carboxylic acid functionalized AFM tip and silica surfaces may also be applied (see Chapter 3.3.5).

In the presence of a negatively charged surface and a negatively charged tip, electrostatic repulsion is expected. In the presence of $CO_2$ self assembly of the protonated amidine molecule onto the negatively charged surfaces may occur through electrostatic attraction. Thus, the measured adhesion forces may arise from hydrophobic interactions between the alkyl tails of the amidine molecules assembled onto the silica surfaces.

For the alumina substrate, no change in adhesion force was observed with in the presence of C4 regardless of the presence or the absence of $CO_2$. When compared to the results obtained from pH force measurements at the same pH, the silica-alumina adhesion forces measured in the presence of C4 are stronger. However, when $CO_2$ is added to aqueous systems containing C4, the adhesion force is the same as solutions at the same pH without the additive. For the alumina substrates, pH 11 is above the pKa of the aluminol sites on the surface(~8-9);[89] therefore, in solutions containing C4, the surface is deprotonated and negatively charged. In this case, there may be some absorption amidine additives onto the surface of the alumina prior to the saturation of the aqueous system with $CO_2$. With the introduction of $CO_2$, the solution pH is below the pKa of aluminol, which remains

protonated. Therefore, no electrostatic interaction is observed between the surface and the positively charged amidine head group and the trends observed with the silica substrate are not evident.

As in the case with C4, in the presence of C8, attractive interactions between the silica substrate and the silica AFM tip were stronger when the solution was saturated with $CO_2$ relative to the solution with no $CO_2$ (Table 4.4). However, as with the carboxylic acid tip and silica surface experiment, the increase is much larger for the C4 case than the C8. This may be a result in some self assembly of the surfactant molecules even prior to the saturation of $CO_2$.

**Table 4.4** CFS experiments with C8

| | Adhesion Force (nN) | |
|---|---|---|
| **Additive** | **Silica Substrate** | **Alumina Substrate** |
| 1 mM C8 (pH 11 ± 0.2) | 0.79 ± 0.35 | 1.22 ± 0.34 |
| pH 11 ± 0.2 modified with NaOH | 0.26 ± 0.14 | 0.71 ± 0.34 |
| 1 mM C8 + $CO_2$ (pH 5 ± 0.2) | 1.39 ± 0.40 | 1.45 ± 0.28 |
| pH 5 ± 0.2 modified with HCl | 1.57 ± 0.36 | 1.48 ± 0.57 |

In general, the results from the silica-silica and alumina-silica CFS experiments with C8 are consistent with the results obtained at the same pH in the

pH force titrations. This is similar to the results from the CFS experiments exploring the effects of C4. Although surfactant absorption is possible for these systems as with the organic/mineral CFS experiments discussed in Chapter 3 of this thesis, these mineral/mineral interactions appear to be dominated by solution pH changes and not by the presence of the switchable surfactant.

### 4.3.5 Switchable Ionic Strength Additives

Switchable ionic strength additives were studied for their ability to affect the interactions between a silica AFM tip and selected substrates (Table 11).

No change in adhesion force was observed between the silica AFM tip and silica substrate when the ionic strength of the solution was increased through dissolution of $CO_2$. In oboth cases, no adhesion was observed despite the fact that a strong adhesion was observed at pH 10 and pH 8 in the pH titration experiments. These switchable ionic strength additives appear to be ineffective at screening the negatively charged surface and tip from one another, as compared with the sodium cations from the pH force titrations.

For the alumina substrate an increase in adhesion force was observed with the increase in ionic strength through the addition of $CO_2$. This may be a result of changes to the pH of the solution with application of $CO_2$. The adhesion force observed in the presence of 1 mM TMDAB is comparable to that observed at the same pH when NaOH is used as a pH mediator. This is also the case for 1 mM TMDAB saturated with $CO_2$. Therefore, it is believed that the switchability in

adhesion force with TMDAB observed with the alumina substrate is a pH effect rather than an ionic strength effect.

**Table 4.5** CFS experiments with switchable water additives

| | Adhesion Force (nN) | |
|---|---|---|
| **Additive** | **Silica Substrate** | **Alumina Substrate** |
| 1 mM TMDAB (pH 11 ± 0.2) | 0 | 0.93 ± 0.40 |
| pH 11 ± 0.2 modified with NaOH | 0.26 ± 0.14 | 0.71 ± 0.34 |
| 1 mM TMDAB + CO2 (pH 8 ± 0.2) | 0.01 ± 0.01 | 1.86 ± 0.61 |
| pH 8 ± 0.2 modified with NaOH | 0.93 ± 0.41 | 2.23 ± 0.47 |

## 4.4 Conclusions

CFS experiments were conducted to determine if $CO_2$ switchable chemistry may be used to mediate adhesion force between a silica AFM tip and silica and alumina substrates. The effects of pH, presence of divalent cations, switchable cationic surfactants, and switchable ionic strength additives were studied.

Silica-silica pH force titrations show that the system is dominated by electrical double layer effects, whereas alumina-silica pH force titrations are mainly influenced by ionic hydrogen bonding in the pH range studied.

Cationic switchable amidine additives were successful in mediating silica-silica adhesion force, but no observed changes to alumina-silica interactions were observed. Silica-silica adhesion force was low in the presence of a switchable amidine, but increased upon saturation with $CO_2$. Between the two amidines studied, the non-surfactant C4 showed greater switchablity in adhesion force when compared to the surfactant C8. The observed changes in adhesion force are attributed to possible surfactant absorption onto the substrate and tip surface, but are likely dominated by changes in solution pH due to the use of $CO_2$ as a switching trigger.

The switchable water additives show no changes in adhesion force in the case of silica-silica interactions. In addition, no adhesion force was observed due to poor screening of electrostatically repulsive surfaces. However, the switchable water additives demonstrate ability to mediate alumina-silica interactions. This switchability is attributed changes in pH with saturation of $CO_2$ rather than changes in solution ionic strength.

# 5. Results and Discussion of Zeta Potential Experiments

## 5.1 Introduction

Zeta potential may be used as an indicator of the stability of a colloidal suspension. At large zeta potential values (greater than +30 mV or less than -30 mV), the particles are highly charged and repel one another. As a result, the system is considered to be stable and the particles will not flocculate. However, at zeta potential values that are closer to zero in value, the repulsive forces will be weakened and the particles may come together to flocculate.[64,65]

During the tailings disposal phase of oil sands processing, the settling of sand and clays is desired to clear up the solids content in the process water so that it may be recycled for further use.[37,38] However, mineral fines such as clays form stable suspensions in process water optimized for bitumen liberation from mineral surfaces and other chemical additives such as gypsum and polymer flocculants must be added to accelerate settling. Further treatment of the tailings pond water is required if the water is to be recycled for further use in the extraction process. This can be both costly in materials and energy. A more economical alternative to conventional process aids may be $CO_2$ triggered switchable additives.

In this chapter, the effect of $CO_2$ switchable additives on the colloidal stability of clay suspensions is studied through zeta potential measurements. These experiments are complementary to the AFM experiments presented in Chapter 4 of this thesis as AFM is used to measure adhesion of two surfaces whereas zeta potential measurements may be used to determine repulsion between two surfaces.

The clays studied in this investigation are illite, kaolinite, and montmorillonite, which are all clays found in oil sands.[6] The effect of pH, $Ca^{2+}$, cationic and anionic switchable surfactants, and switchable ionic strength additives were investigated. The best candidates to affect colloidal stability as predicted by zeta potential measurements were identified and used in subsequent experiments to determine if they can affect the stability of clay suspensions by accelerating the settling of clay fines.

## 5.2 Zeta Potential Experiments

### 5.2.1 pH Effects

The zeta potentials of illite, kaolinite, and montmorillonite clay were measured as a function of solution pH (Figure 5.1, Figure 5.2, and Figure 5.3 respectively). Modification of pH was accomplished through addition of NaOH to reach alkaline pH conditions and HCl to reach acidic pH conditions.

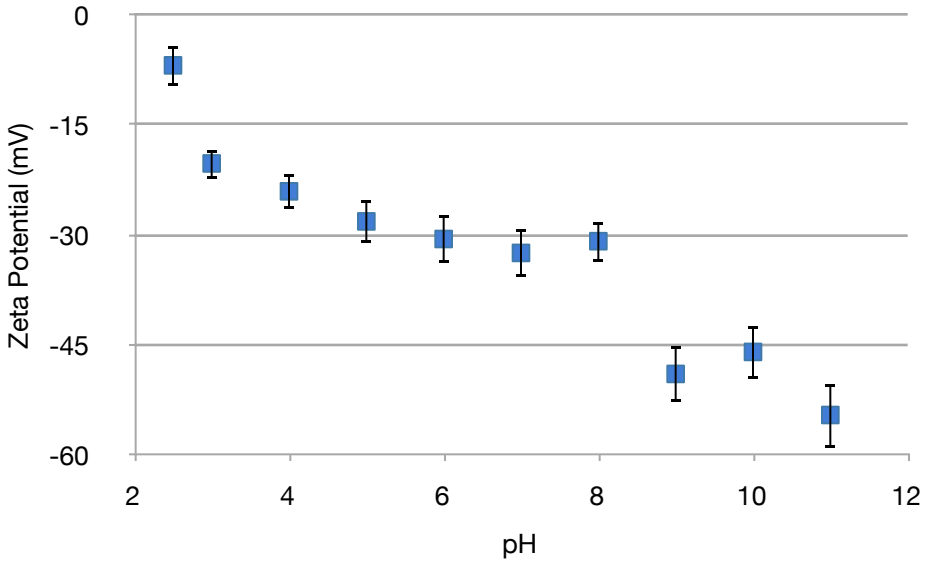


**Figure 5.1** Zeta Potential of Illite Clay vs. pH

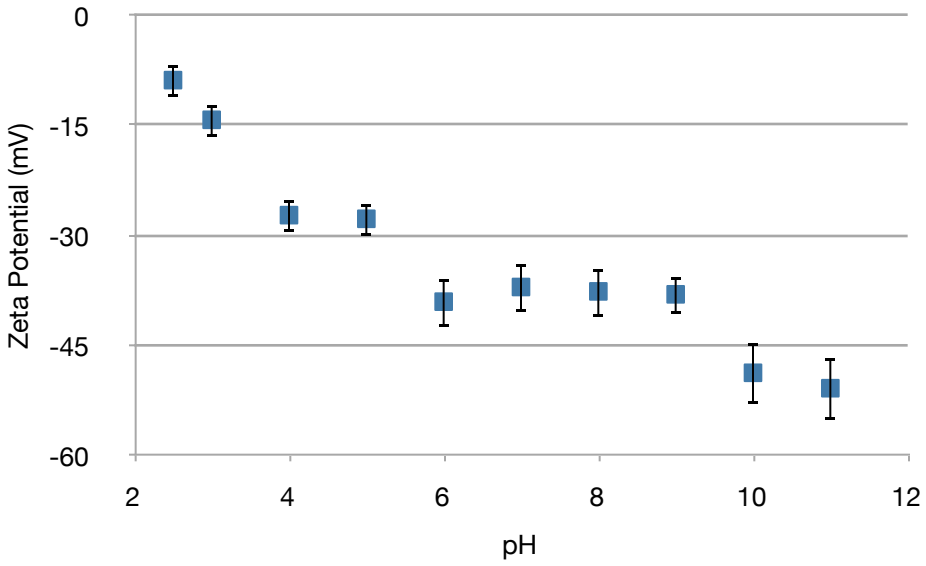


**Figure 5.2** Zeta Potential of kaolinite clay vs. pH

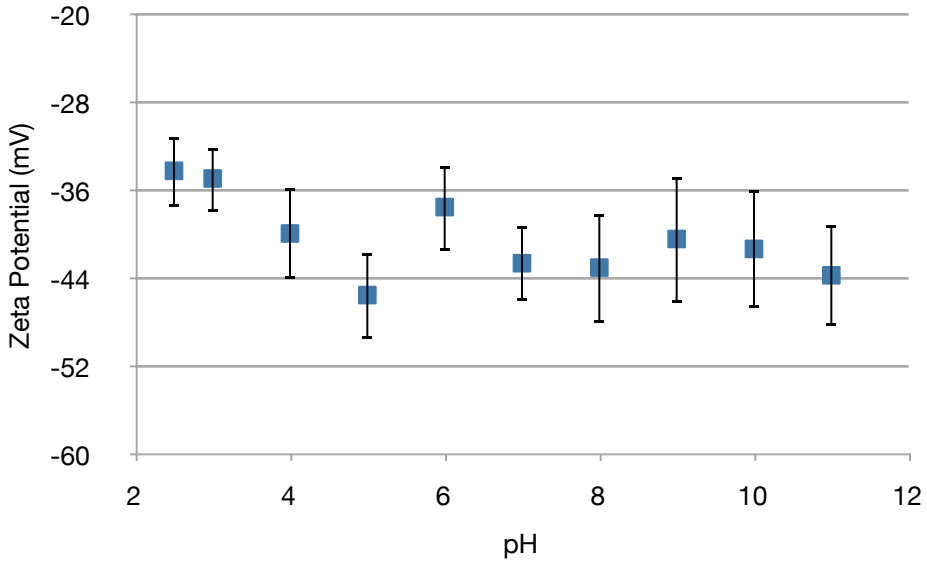


**Figure 5.3** Zeta potential of montmorillonite clay vs. pH

The results from these experiments show that the clay surfaces are negatively charged over a wide range of pH values. Both illite and kaolinite show a zeta potential dependence as a function of solution pH, but montmorillonite displays a relatively constant negative zeta potential over a range of pH values. These trends are consistent with previously reported literature values.[97,98,99]

Montmorillonite exhibits unique pH independence on zeta potential due to constant surface charge of its basal plane.[13] The amphoteric sites of this clay are situated on the edge surfaces, which make up approximately 1% of the total surface area. Therefore, it is expected that the observed changes in zeta potential with pH will not be as evident as in the case with the illite and the kaolinite clay where amphoteric sites may be found on the basal plane.

### 5.2.2 $CO_2$ Experiments

Zeta potential experiments were conducted in the presence of $CO_2$ saturated deionized water to study the effects of $CO_2$ in the absence of switchable additives.

Saturation of deionized water with $CO_2$ decreases the pH of the water to approximately pH 4, due to the formation of carbonic acid. The zeta potentials obtained in $CO_2$ saturated deionized water were compared with the measured zeta potentials of the same clays at the same pH, using HCl as a pH modifier (Table 5.1). It was observed that both carbonic acid and HCl give comparable results within experimental error for all three clays, indicating that the effects observed are pH effects and independent on the type of acid present in the solution.

**Table 5.1** Zeta potentials of clays in the presence of $CO_2$

| | Zeta Potential (mV) | | |
|---|---|---|---|
| **Additive** | **Illite** | **Kaolinite** | **Montmorillonite** |
| $CO_2$ (pH 4 ± 0.2) | -15 ± 6 | -23 ± 5 | -40 ± 8 |
| pH 4 ± 0.2 modified with HCl | -24 ± 5 | -27 ± 5 | -38 ± 9 |

### 5.2.3 Effect of Switchable Surfactants

The zeta potentials of clays were measured in aqueous solutions containing switchable surfactants. The effect of cationic switchable surfactant C8 was studied

and the results are summarized in Table 5.2. The results for the cationic switchable surfactant zeta potential experiments were compared with the measurements conducted at the same pH in the absence of any chemical additives except for HCl and NaOH as pH modifiers. This comparison is used to determine if the zeta potential changes observed during switching of the surfactants should be attributed to changes in the pH of the solution due to the introduction of carbonic acid or to changes in the surfactant capabilities of the additive.

**Table 5.2** Zeta potentials of clays in the presence of C8

| | Zeta Potential (mV) | | |
|---|---|---|---|
| | **Illite** | **Kaolinite** | **Montmorillonite** |
| 1 mM C8 (pH 11 ± 0.2) | -33 ± 3 | -40 ± 3 | -37 ± 4 |
| 1 mM C8 + $CO_2$ (pH 5 ± 0.2) | -12 ± 3 | -25 ± 3 | -30 ± 3 |
| pH 11 ± 0.2 modified with NaOH | -55 ± 4 | -51 ± 4 | -44 ± 5 |
| pH 5 ± 0.2 modified with HCl | -28 ± 3 | -28 ± 2 | -46 ± 4 |

This experiment demonstrates that with the cationic switchable surfactant, there is a change in zeta potentials of the clays for illite and kaolinite, but the zeta potential of montmorillonite clay is not significantly altered by the activation of the surfactant in aqueous solution.

The switchability observed for the kaolinite clay appears to be a result of pH changes that occur with exposure of the surfactant solution to 1 atm of $CO_2$. However, the zeta potential of kaolinite prior to $CO_2$ treatment is lower than that of the clay at the same pH, modified through the addition of NaOH. This may be due to absorption of C8 to the surface of the clay particles through hydrophobic or van der Waals interactions. After turning the surfactant on with $CO_2$, the zeta potential is the same as that of the zeta potential measured at the same pH due to modifications with HCl. This suggests that the amidine/clay interactions previously observed are disrupted upon activation of the surfactant capabilities of the amidine molecule.

The zeta potentials of illite in the presence of the switchable surfactant were significantly smaller in magnitude than the zeta potentials of the clay at the same pH. This was consistent for both the demulsifier form of the C8 molecule and the surfactant form. Like kaolinite, in the absence of $CO_2$ some interaction of C8 with the surface of the clay particles may be observed leading to the observed changes in the zeta potential. However, unlike kaolinite, the magnitude of the zeta potentials of illite with the protonated form of C8 remain lower than that of the clay at the same pH modified with HCl. This may be due to differences in the clay structure between illite and kaolinite. That is, illite contains more cations that can readily exchange with the protonated amidine molecule than kaolinite and this may lead to the decrease in magnitude of zeta potential that is observed.[11,12]

For montmorillonite, the charge compensating cations that can exchange are located within the layers of the clay lattice and not on the surface.[11,12] Also, there are fewer amphoteric sites on the surface.[41] Therefore, the same surfactant interactions

that were observed with kaolinite and illite clay, are not observed with montmorillonite, which does not exhibit any switchability in zeta potential in aqueous solutions containing C8.

The effect of an anionic switchable surfactant on the zeta potentials of clays was also investigated Table 5.3. The results also show that the presence of the surface active form of NP-C8 has no affect on zeta potentials of clays. For both kaolinite and illite, the exposure of the anionic surfactant to $CO_2$ results in a zeta potential greater in magnitude than that of the zeta potential measured at the same pH, modified with HCl. As in the case with the cationic switchable surfactant, this may be a result of surfactant interactions with the surface of these clays. However, with montmorillonite, no change in zeta potential was observed, possibly again due to the unique structural properties of this swelling clay.

**Table 5.3** Zeta potentials of clays in the presence of NP-C8

| | **Zeta Potential (mV)** | | |
|---|---|---|---|
| | **Illite** | **Kaolinite** | **Montmorillonite** |
| 1 mM NP-C8 (pH 11 ± 0.2) | -60 ± 2 | -57 ± 4 | -49 ± 6 |
| 1 mM NP-C8 + $CO_2$ (pH 6 ± 0.2) | -54 ± 3 | -48 ± 4 | -37 ± 4 |
| pH 11 ± 0.2 modified with NaOH | -55 ± 4 | -51 ± 4 | -44 ± 5 |
| pH 6 ± 0.2 modified by HCl | -46 ± 3 | -39 ± 4 | -38 ± 4 |

### 5.2.4 Effect of switchable ionic strength additives

The zeta potentials of clays were measured in the presence of switchable ionic strength additives. Two different tertiary amines were screened as candidates for this experiment. The results are summarized on Table 5.4.

**Table 5.4** Zeta potentials of clays in the presence of switchable ionic strength additives

| | Zeta Potential (mV) | | |
|---|---|---|---|
| | **Illite** | **Kaolinite** | **Montmorillonite** |
| 0.8 molal BMDAPAP (pH 13 ± 0.2) | -19 ± 4 | -24 ± 2 | -17 ± 5 |
| 0.8 molal BMDAPAP + $CO_2$ (pH 10 ± 0.2) | -2 | -4 | -3 |
| 0.8 molal TMDAB (pH 13 ± 0.2) | -26 ± 7 | -17 ± 4 | -26 ± 5 |
| 0.8 molal TMDAB + $CO_2$ (pH 10 ± 0.2) | -4 | +2 | -6 |
| pH 11 ± 0.2 modified with NaOH | -55 ± 4 | -51 ± 4 | -44 ± 5 |
| pH 10 ± 0.2 modified with NaOH | -30 ± 3 | -49 ± 4 | -41 ± 5 |

The zeta potentials measured in the switchable ionic strength solutions were compared to those measured at the same pH due to addition of NaOH to serve as a control and aid with data interpretation. However, the zeta potentials of clays were

not measured at NaOH solutions with pH 13, due to the fact that the high concentration of NaOH required to achieve this pH value would have damaged the measuring equipment. Therefore, the results for clays in aqueous solutions of pH 11 modified by NaOH are presented for comparison with 0.8 molal of the switchable ionic strength additive. For illite and kaolinite, it is expected that the zeta potentials for pH 13 will be more negative those that reported for pH 11, due to the trends observed in Figures 5.1 and 5.2. Montmorillonite exhibits no zeta potential pH dependence (Figure 5.3), thus, it can be expected that the zeta potential at pH 13 will be quite similar to that reported for pH 11.

The switchable ionic strength additives demonstrate that upon the addition of $CO_2$ the magnitude of the zeta potential is approximately 0. This trend is observed with both switchable ionic strength additives and with all three of the clays tested and is not an observed pH effect if these results are compared with potentials at similar pH, modified by NaOH. This change in zeta potential is attributed to the contraction of the electrical double layer due to the increase in ionic strength of the solution when it is saturated with $CO_2$.

Differences in zeta potential between the $CO_2$ free solutions of the switchable ionic strength additives and the NaOH solutions at the similar pH may also be a result of ionic strength. In this case, solutions containing the diamine have essentially zero ionic strength whereas the solutions containing NaOH have a non-zero value.

Both BMDAPAP and TMDAB were equally effective additives for modification of zeta potential, further experiments were conducted preferentially with TMDAB as

it has a lower molecular weight and therefore is more efficient on a per weight basis compared to BMDAPAP.

### 5.2.5 Concentration of Switchable Ionic Strength Effects

The initial zeta potential experiments were performed at a 0.8 molal concentration of additive to be consistent with previous work performed in the Jessop group.[7] However, this level of loading is very high and requires the use of a lot of material. Lower loading levels would make these additives more suitable for industrial applications through reduction of cost and risk associated with chemical use. Further work was performed at 1 mM and 10 mM levels in efforts to minimize the amount of material required.

**Table 5.5** Zeta potentials of clays in varying concentrations of TMDAB

| | Zeta Potential (mV) | | |
|---|---|---|---|
| | **Illite** | **Kaolinite** | **Montmorillonite** |
| 1 mM TMDAB | -40 ± 6 | -40 ± 7 | -40 ± 7 |
| 1 mM TMDAB + $CO_2$ | -5 ± 4 | -5 ± 4 | -3 ± 5 |
| 10 mM TMDAB | -48 ± 7 | -51 ± 13 | -24 ± 6 |
| 10 mM TMDAB + $CO_2$ | -3 ± 7 | -3 ± 8 | 9 ± 4 |
| 0.8 molal TMDAB | -26 ± 7 | -17 ± 4 | -26 ± 5 |
| 0.8 molal TMDAB $CO_2$ | -5 | +2 | -6 |

Zeta potentials of clays in varying concentrations of TMDAB indicate that a similar effect is observed at the high and the low concentrations of diamine for all of the three clays studied. Upon addition of $CO_2$ to TMDAB, the absolute value of the zeta potential is reduced, regardless of TMDAB concentration. This implies that for this application, the relatively minor change in ionic strength of solution at 1 mM of TMDAB is enough to compress the electrical double layer and suppress the zeta potential as observed.

### 5.2.6 *In Situ* $CO_2$ Treatments

The work discussed above showed that clay zeta potential can be tuned through application of $CO_2$ to water containing TMDAB. However, for these experiments, all gas treatments were performed on the solutions before the clay was added. To address concerns that switching behaviour may be impeded by the presence of clays, gas treatments were conducted on switchable water containing kaolinite fines (Table 5.6).

**Table 5.6** Zeta potential experiments with *in situ* switching of TMDAB

| | Zeta Potential (mV) | |
|---|---|---|
| **Additive** | **Switching Externally** | **Switching *in situ*** |
| 1 mM TMDAB | -40 ± 7 | -39 ± 8 |
| 1 mM TMDAB + $CO_2$ | -5 ± 4 | 0 ± 4 |
| 1 mM TMDAB + $CO_2$ + $N_2$ | -25 ± 6 | -33 ± 6 |

It was observed that the two sets of experiments provided similar results; therefore, the clays were not interfering with the protonation of the additive. In addition, the system is reversible, as the zeta potential can be restored either partially or fully back to its original value upon treatment with nitrogen gas at 70°C.

## 5.3 Clay Settling Experiments

### 5.3.1 Effect of TMDAB

The previous sections of this thesis have described the ability of switchable ionic strength additives to affect clay zeta potentials. It was shown that tertiary diamines such as BMDAPAP and TMDAB can change clay zeta potentials from highly negative in value to near zero in value upon the use of $CO_2$ as a trigger. A near zero zeta potential value can allow particles to be close enough to one another in space for van der Waals interactions between the particles to occur.[37,38] This may result in aggregation of the particles to increase the settling rates of clay suspensions. For this reason, the ability of switchable ionic strength additives to affect the clay settling rates of kaolinite suspensions was studied.

Three individual experiments were conducted concurrently (Figure 5.4). Firstly, 1 mM TMDAB was used to create a suspension with kaolinite fines and the settling of the clay was monitored using a cathetometer to measure the sediment line as a function of time. A second experiment was conducted where the 1 mM TMDAB solution was treated with $CO_2$ for 1 h prior to the creation of a suspension with kaolinite. Again, the settling of the clay suspension was monitored. Finally, 1 mM TMDAB was treated with 1 h of $CO_2$ followed by 1 h of $N_2$ at 70°C. The solution was allowed to cool prior to addition of kaolinite clay and monitoring of the settling rate. All the gas treatments were conducted in the absence of clay to ensure that the protonation and deprotonation of TMDAB occurred fully without any impedance from the clay.

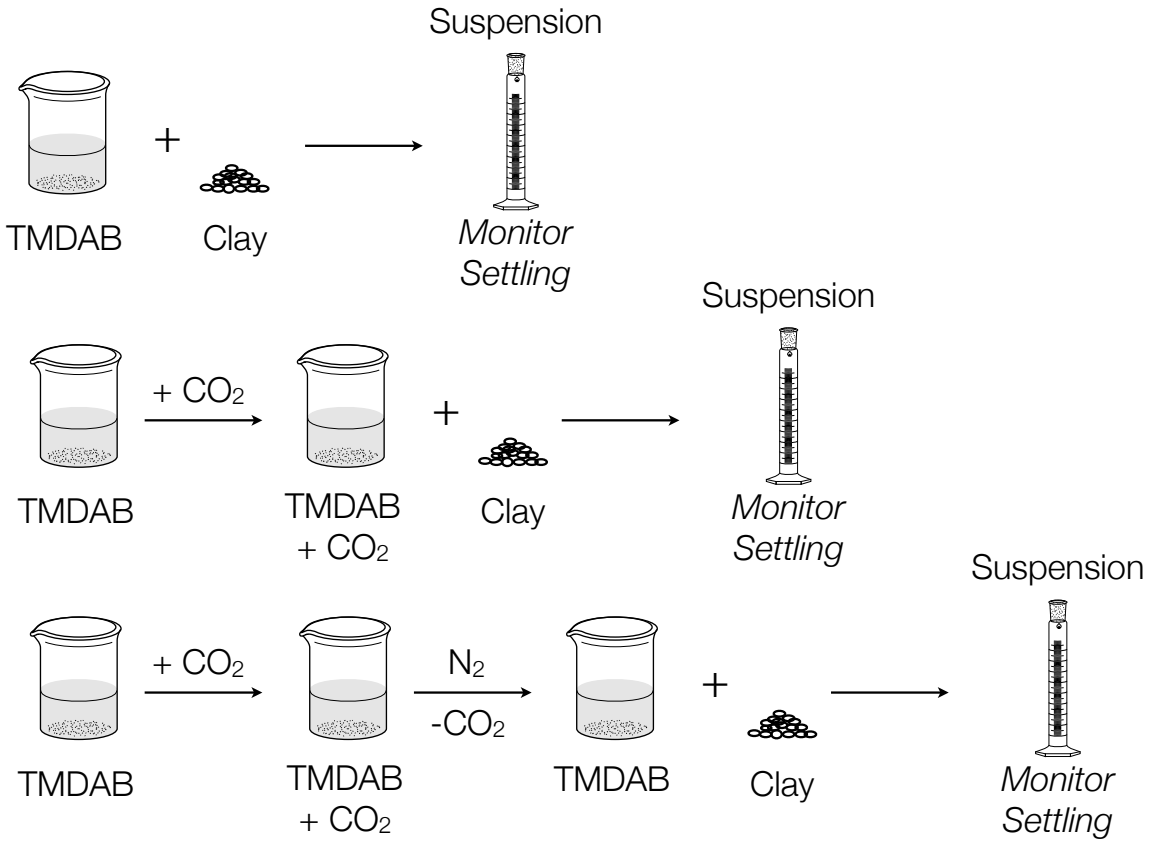


**Figure 5.4** Experimental scheme used to determine the effect of TMDAB on settling rates of kaolinite suspensions

From the experiments above, the following observations were made. A stable suspension was formed when kaolinite clay was added to 1 mM TMDAB (Figure 5.5). However, kaolinite clay with $CO_2$ treated TMDAB resulted in the settling of clay with a clean supernatant and a clear sediment line. A stable suspension was also formed with kaolinite clay and 1 mM of TMDAB treated with 1 h of $CO_2$ followed by 1 h of $N_2$ treatment.

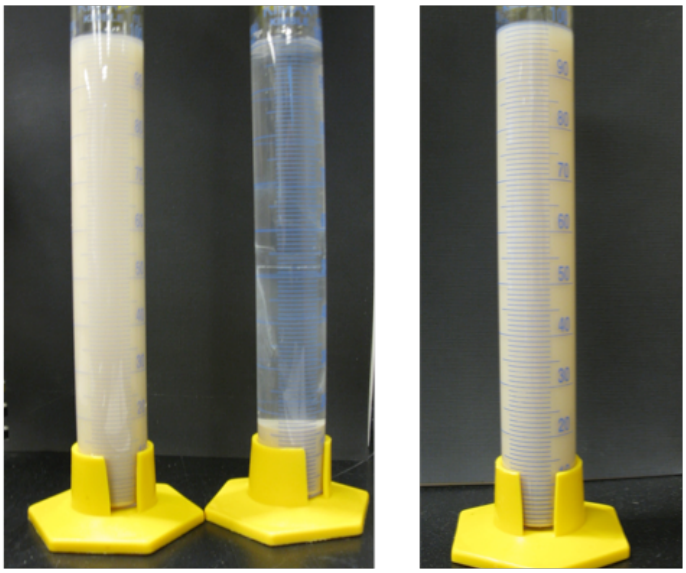


**Figure 5.5** Photos of settling behaviour of kaolinite in 1 mM TMDAB after 1 h

The settling behaviour of the kaolinite suspension treated with 1 h of $CO_2$ was plotted as a function of time (Figure 5.6). These results illustrate that the majority of the settling occurs within the first 15 minutes of the observation phase and after 1 h no further changes were observed.

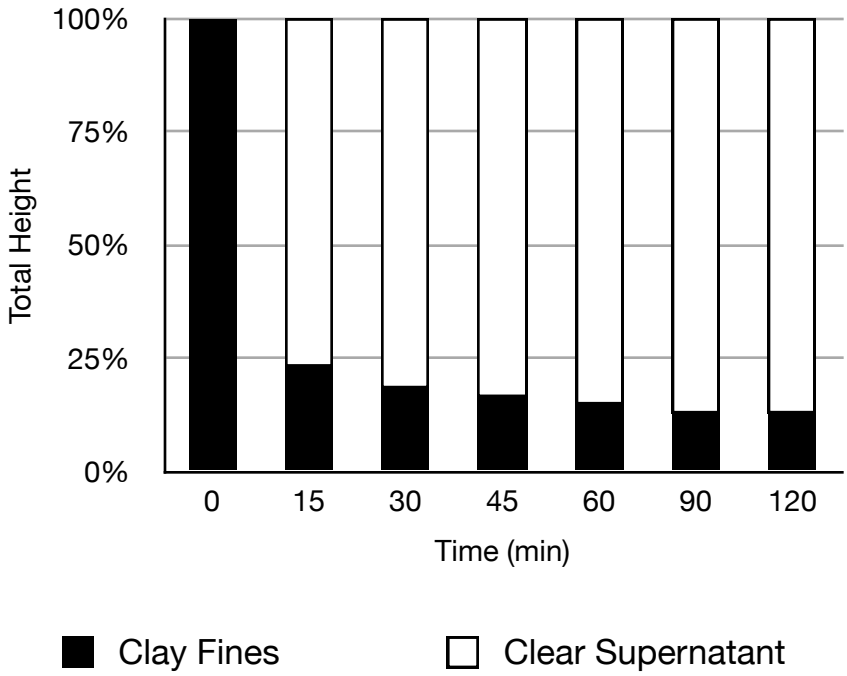


**Figure 5.6** Settling behaviour of kaolinite in 1 mM TMDAB treated with $CO_2$

The results presented above demonstrate that TMDAB is a switchable additive that has the ability to affect kaolinite clay suspensions. Clay settling behavior can be mediated by the addition and removal of $CO_2$ in the presence of 1 mM TMDAB. This result is consistent with the data collected in the zeta potential experiments involving clay and TMDAB (Chapter 5.2.5). For kaolinite clay, the zeta potential of the clay in 1 mM TMDAB was -40 ± 7, but was diminished to -5 ± 4 when the solution was saturated with $CO_2$. Initially, the surface of the clay is negatively charged and electrostatic repulsion prevents the particles from approaching each other. However, upon exposure of the solution to 1 atm of $CO_2$, the electrostatic repulsive forces are weakened by the increase in ionic strength of the solution and

the particles can come together. The suspension is no longer stable and the particles settle, as observed.

### 5.3.2 In situ switching

TMDAB has been identified as a switchable additive which can affect clay settling behaviour through the addition and removal of $CO_2$. However, for the experiments discussed in the previous section, all gas treatments were performed on the solutions before the clay was added. To determine if protonation and deprotonation of TMDAB will still occur in the presence of clays, the following series of experiments were conducted.

The same clay and TMDAB mixture was used in all three settling tests depicted below (Figure 5.7). A kaolinite clay suspension was created with 1 mM of TMDAB and the settling rate was monitored. This was followed by 1 h treatment of $CO_2$, conducted in the presence of kaolinite. The settling behaviour of this suspension was monitored and afterwards, the clay fines were resuspended into solution and the settling behaviour was monitored once again.

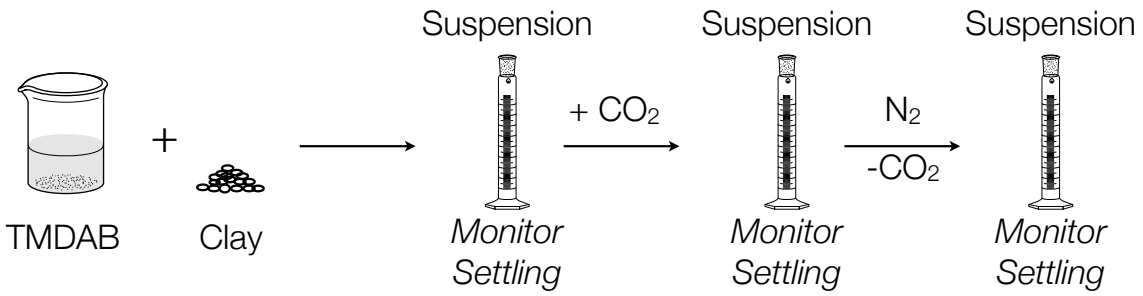


**Figure 5.7** Experimental scheme used to determine the effect of *in situ* $CO_2$ and $N_2$ treatments on settling rates of kaolinite suspensions

The behavior observed for this series of experiments was similar to that discussed in section 5.4.1. Kaolinite clay and 1 mM TMDAB were initially mixed to give a stable suspension. This suspension was treated with $CO_2$, which resulted in the settling of the clay fines with a clean supernatant and a clear sediment line (Figure 5.8). The settled clay was stirred to reform a suspension, which was treated with $N_2$, after which a stable suspension was achieved.

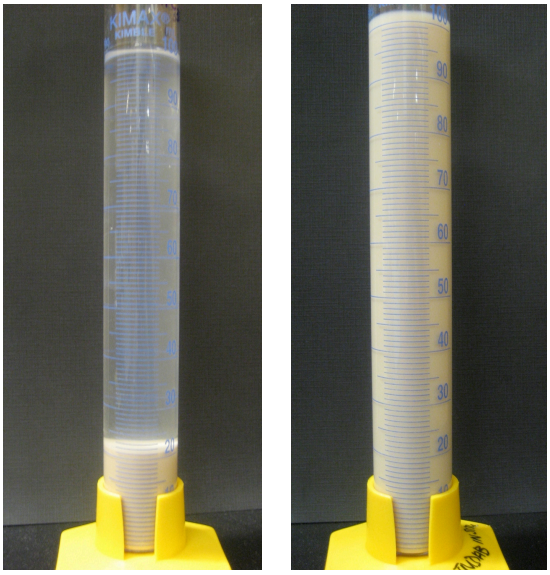

$CO_2$ $N_2$

**Figure 5.8** Photos of settling behaviour of kaolinite in 1 mM TMDAB with *in situ* $CO_2$ and $N_2$ treatment after 1 h

The settling behaviour of the kaolinite suspension treated with 1 h of $CO_2$ was plotted as a function of time (Figure 5.8). The initial settling rate of this suspension is slower when compared to the suspension treated with $CO_2$ in section 5.4.1. For the suspension treated with $CO_2$ in section 5.3.1, most of the total settling (~85%) occurs within the first 15 minutes of the observation phase and after 1 h no further changes were observed. For the experiment shown in Figure 5.8, only approximately 60% of the total settling has occurred after 15 minutes.

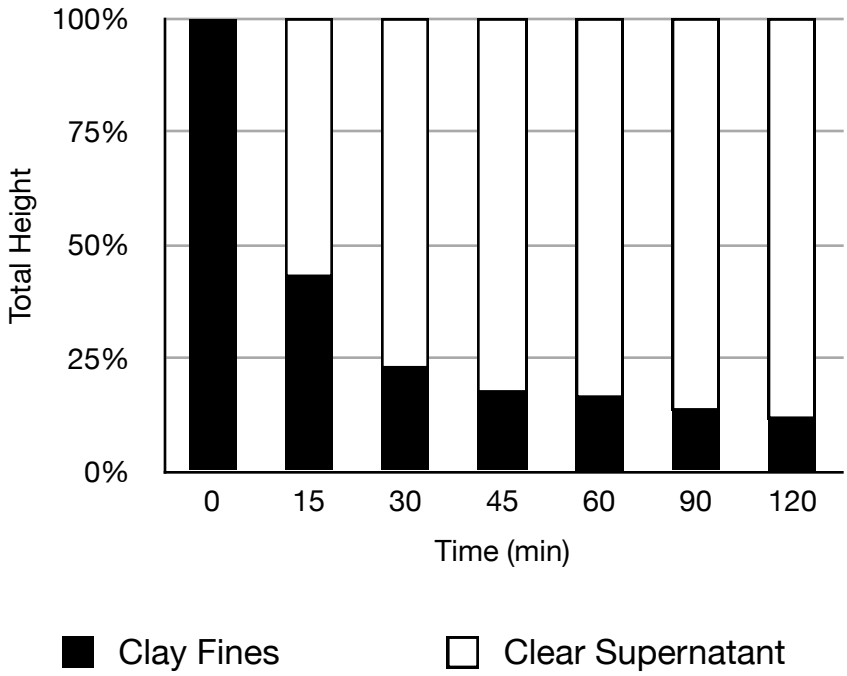


**Figure 5.9** Settling behaviour of kaolinite clay in 1 mM TMDAB with *in situ* $CO_2$ treatment

The discrepancy in settling rates may be due to the clay fines interfering with the protonation of the diamine. This contradicts the results obtained for analogous zeta potential experiments discussed in section 5.2.6. For the zeta potential experiment, there were no appreciable differences in results between kaolinite in 1 mM TMDAB samples treated with $CO_2$ in the presence of clay (0 ± 4 mV) and in the absence of clay (-5 ± 4 mV). However, the zeta potential experiments are conducted at a much lower clay loading (0.25 wt%) than the clay suspension studies (5 wt%) and such an excess of clays may be impeding complete protonation of the switchable ionic strength additive.

### 5.3.3 Filtrate Recycling

Switchable ionic strength additives have been successful at modifying clay settling behaviour through the application and removal of $CO_2$. Recycling of solutions containing these compounds would be desirable for industrial applications. The following investigation was performed to determine if the additive was adhering to the clay particles and being removed with the solids.

A clay suspension was created in 1 mM TMDAB, filtered, and the filtrate was collected and treated with $CO_2$ (Figure 5.9). Fresh clay was added and a new suspension was created and the settling behaviour was monitored.

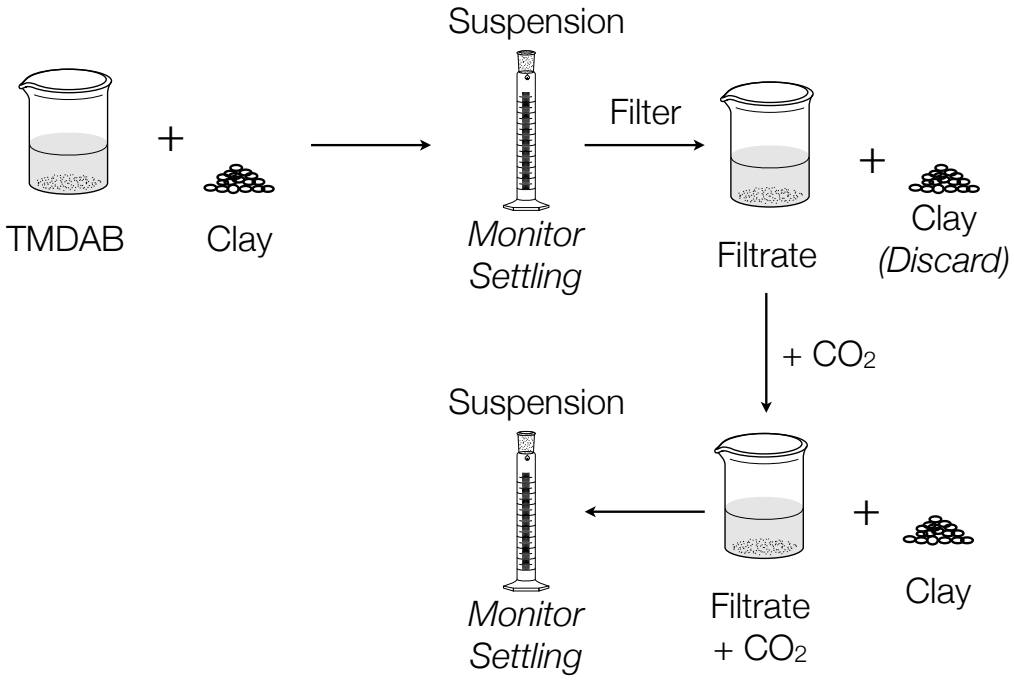


**Figure 5.10** Experimental scheme used to determine the effect of recycled TMDAB on settling rates of kaolinite suspensions

The settling behaviour of the kaolinite suspension created with the recycled filtrate was plotted as a function of time (Figure 5.11). It was observed that this suspension settled at a rate much like that observed in sections 5.3.1 and 5.3.2. A clear sediment line was observed, however, the liquid above the sediment line was turbid and still contained clay fines (Figure 5.10). This behavior was also observed with deionized water treated with $CO_2$ in the absence of any switchable water additive (Figure 5.11 and 5.12). This suggests that the additive is adhering to the surface of the clay particles and being removed with the solids.

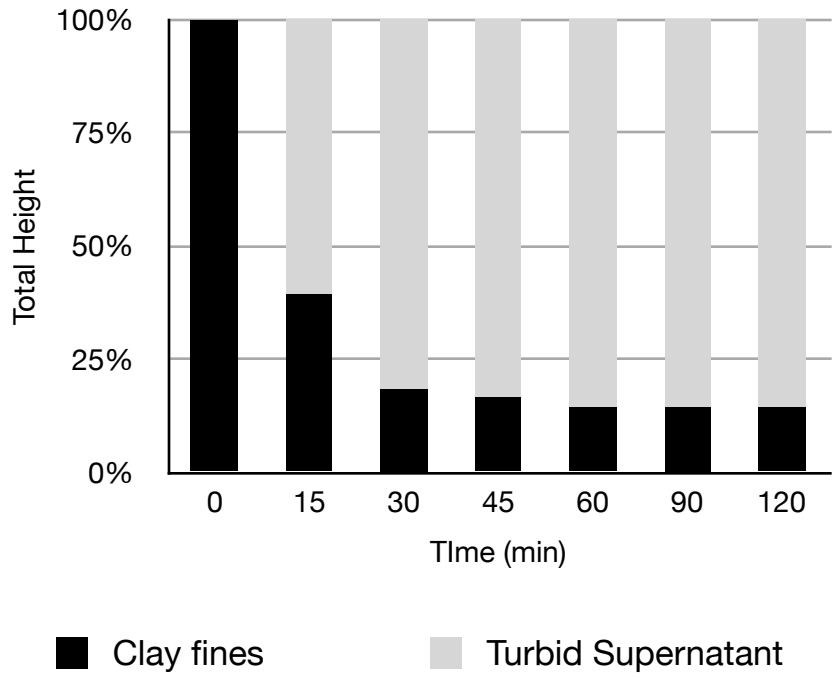


**Figure 5.11** Settling behaviour of kaolinite in $CO_2$ saturated filtrate

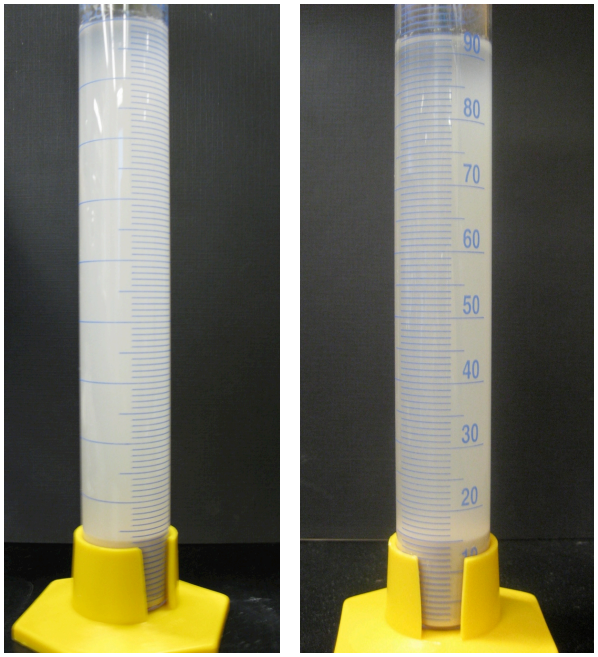


**Figure 5.12** Photos of settling behaviour of kaolinite in $CO_2$ saturated filtrate and $CO_2$ saturated water after 1 h

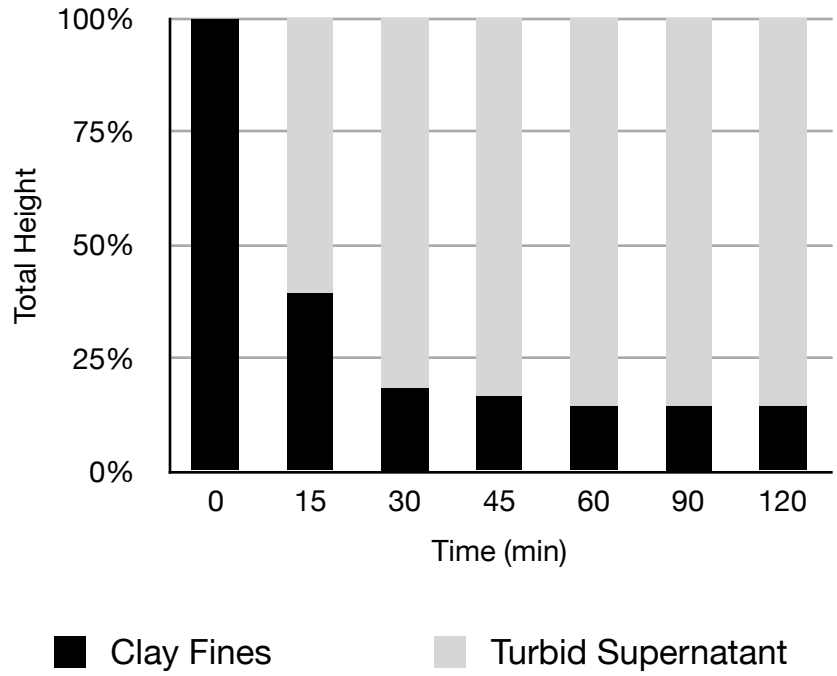


**Figure 5.13** Settling behaviour of kaolinite in $CO_2$ saturated water

### 5.3.4 Total suspended solids

Although both $CO_2$ saturated 1 mM TMDAB and $CO_2$ saturated deionized water have demonstrated the ability to accelerate settling of kaolinite suspensions, they produce visually different supernatant layers after the clay has settled. For clay suspensions in 1 mM TMDAB, a clear supernatant layer was observed, whereas for suspensions in $CO_2$ saturated deionized water, the supernatant layer is turbid. The amount of total suspended solids in these two supernatant layers were determined gravimetrically for comparison. The supernatant of the $CO_2$ saturated deionized water was found to contain 163 ppm of total suspended solids compared to 16 ppm

for the $CO_2$ treated TMDAB sample. This shows that although settling of clay suspensions is observed in the presence of $CO_2$ alone, the supernatant quality is improved through the addition of the diamine.

### 5.3.5 Particle Size Measurements

The introduction of $CO_2$ into clay fines in 1 mM TMDAB causes the zeta potentials of these clay fines to change from a strongly negative values to near zero values. When the zeta potentials of particles are near zero they are near neutral in charge and can agglomerate due to van der Waals forces.[100] Formation of larger aggregates can significantly accelerate settling rates.[101] Particle size measurements were conducted to determine if the changes in clay zeta potentials and the observed acceleration of settling of kaolinite suspensions in $CO_2$ treated solutions of 1 mM TMDAB are accompanied by changes in particle size.

Particle size measurements were conducted on kaolinite particles in 1 mM TMDAB and in 1 mM TMDAB treated with $CO_2$ (Table 5.7). Particle size measurements were also conducted on kaolinite fines in deionized water to serve as a control. No difference in size was observed between the samples in 1 mM TMDAB and the sample in deionized water.

Treatment of kaolinite fines 1 mM TMDAB with $CO_2$ showed no difference in particle size when compared to the sample without $CO_2$. The same samples were aged for 1 week prior to particle size analysis, but again, no significant difference in particle size was observed between the $CO_2$ treated sample and the $CO_2$ untreated sample.

**Table 5.7** Kaolinite particle size measurements

| Additive | Volume Weighted Mean (μm) |
|---|---|
| Deionized water | 13 |
| 1 mM TMDAB | 16 |
| 1 mM TMDAB + $CO_2$ | 18 |
| 1 mM TMDAB (Aged 1 week) | 15 |
| 1 mM TMDAB + $CO_2$ (Aged 1 week) | 23 |

The zeta potential values for clays in 1 mM of TMDAB show that electrostatic repulsion is reduced through the application of $CO_2$, but no flocculation of the clay fines was observed. Although electrostatic repulsion is an important factor of colloidal stability, the van der Waals attractive forces between two particles must also be considered. The total potential for interaction between two particles is a summation of both the long range electrostatic repulsive forces and the short range van der Waals attractive forces. Even through reduction of electrostatic repulsion, if this attractive energy is not enough to overcome the energy barrier to interaction between two clay particles, the material still will not flocculate.[102] This offers an explanation to why a change in particle size is not observed with reduction of zeta potential in these systems.

## 5.4 Conclusions

Switchable additives were studied for their ability to affect the zeta potential of illite, kaolinite, and montmorillonite clay fines. Cationic switchable surfactants show a reduction in zeta potential magnitude upon the addition of $CO_2$, whereas anionic switchable surfactants show little to no change. The greatest effect was observed with switchable ionic strength additives. These tertiary diamines can reduce the magnitude of the zeta potential to nearly zero upon the addition of $CO_2$. This is reversible upon removal of $CO_2$ through the application of heat and $N_2$. In addition, this effect can be observed in the presence of as little as 1 mM of the additive.

Kaolinite suspension settling tests were used to determine if the reduction in zeta potential magnitude results in sedimentation of the clay fines. These experiments show that settling of a stable suspension of clay in 1 mM TMDAB can be induced through the application of $CO_2$. $CO_2$ saturated deionized water was also able to induce settling of clay fines, but the presence of TMDAB results in a cleaner supernatant with lower solids content.

Particle size measurements were conducted to determine if suppression of clay zeta potential observed with TMDAB and $CO_2$ can cause particle aggregation. No change in particle size was observed, even through aging of the samples.

# 6. Conclusions and Future Work

This thesis describes an investigation of how carbon dioxide triggered switchable additives affect model colloidal interactions found in oil sands, in an effort to identify potential candidates for industrial use. Organic/mineral interactions and mineral/mineral interactions were studied by chemical force spectrometry in the presence of cationic and anionic switchable surfactants and switchable ionic strength additives. The effect of switchable additives on zeta potentials of real clay systems was concurrently investigated.

The results from the chemical force spectrometry experiments show that of the additives studied, cationic switchable amidine C4 showed the greatest change in adhesion force between solutions free of $CO_2$ and solutions saturated with $CO_2$. This was true of both the organic/mineral and the mineral/mineral systems studied. The general trend observed was an increase in adhesion force with the introduction of $CO_2$ into solutions containing C4. Similar trends were observed with solutions containing C8 as an additive, but the changes in adhesion force were weaker.

The results from the CFS experiments suggest that switchable amidines such as C4 and C8 could be potential candidates for oil sands extraction. In aqueous solutions containing these additives, the adhesion force between the organic functionalized tips and the mineral surfaces are low, or zero in the case of C4. This suggests that these additives, particularly C4, may be useful for decreasing adhesion between bitumen and mineral surfaces, thus facilitating bitumen liberation and floatation. However, the systems studied in this thesis are model systems and a

subset of possible systems to study as real oil sands are complex multicomponent and multiphase systems.

Future work for this research project would include new CFS experiments that use tips functionalized with other organic groups found in bitumen. This may include, but is not limited to, straight alkane chains, phenols,[103] and nitrogen containing heterocycles.[104] Other mineral substrates can also be used.

The effect of switchable additives may also be investigated using CFS and real bitumen and clay systems.[105] This requires the use of specialized nanofabrication equipment, but single clay particles may be glued on AFM tips to create colloidal probes. Bitumen may be spin coated onto a solid support to be used as substrate in CFS experiments with clay probes.

The suggestions above could provide more fundamental insight to how switchable additives may affect bitumen liberation from mineral surfaces. A more applied approach would be to use switchable additives such as C4 and C8 in small scale batch extractions using real oil sands. Such experiments could demonstrate in a more practical manner how bitumen liberation is affected by these potential process aids.

CFS experiments conducted in this thesis also showed that $CO_2$ saturated solutions containing switchable amidines increase adhesion force between model mineral/mineral surfaces. This result suggests that the protonated forms of these additives may be useful in the tailings disposal phase of oil sands processing, where the adhesion of mineral particles to other particles and solids are desired for rapid settling of fines.

Future work to investigate the use of C4 and C8 for tailings disposal would be to study the interaction forces between real clay particles in the presence of these additives. This may be done through CFS. A colloidal probe approach could be used to attach clay particles onto an AFM tip.[106] For the substrate surfaces, real clays may be used if new methods to making clay covered substrates suitable for force measurements under aqueous systems may be identified. Also, clay settling studies such as those described in this thesis may also be conducted in the presence of C4 and C8 to determine if acceleration of clay fines is achieved.

The results from the CFS experiments suggest that switchable additives such as C4 and C8 may be useful and recyclable process aids for bitumen extraction. That is, the $CO_2$ free version of these aqueous solutions may be useful for the bitumen extraction phase of the process, whereas $CO_2$ saturated solutions of these additives may improve upon current tailings disposal protocols. If the future work proposed is consistent with the CFS experiments conducted, these switchable additives may be "switched" between stages of oil sands processing to give a system in which process water may be easily recycled.

The effect of switchable additives on clay suspension behavior was studied by zeta potential measurements. The greatest change in clay zeta potentials were achieved through the use of switchable ionic strength additives. In these experiments, clay zeta potentials could be suppressed to nearly zero upon exposure to $CO_2$. It was demonstrated that destabilization of clay suspensions can be achieved upon exposure of aqueous solutions containing the additives to $CO_2$, thereby accelerating the settling of clay fines. As a result, these additives have been

identified as potentially useful for tailings disposal. However, further work establishing the mechanism of action will be required, in addition to optimization of additive loading.

Although the switchable ionic strength additives have not demonstrated any effect on adhesion force in the CFS experiments, they may still be effective process aids for bitumen extraction. In all four tip/sample pairs studied, little to no adhesion force was observed when the force measurements were conducted in the presence of these additives suggesting that they may facilitate bitumen liberation from mineral surfaces. Further investigations employing TMDAB and BDMAPAP such as CFS experiments with real bitumen and clay systems or batch extractions may be useful to confirm the use of these additives as process aids. If these experiments are successful, the use of TMDAB and BDMAPAP as additives in oil sands processing may also yield a system with readily recyclable process water.

# Appendix

## Synthesis of 12-phenyl-11-dodecen-1-ol

A 100 mL round bottomed flask was charged with 11-bromo-1-undecanol (2.512 g, 10 mmol; Sigma Aldrich Batch 14826JO), triphenylphosphine (2.644 g, 10 mmol; Sigma Aldrich Batch 07221DE), and acetonitrile (HPLC grade, 50 mL). The reaction mixture was refluxed for 60 h under $N_2$, after which the solution was cooled to room temperature and the solvent was removed *in vacuo* to afford a light brown oil, which was used in the subsequent reaction without further purification.

In a flame dried 50 mL two necked round bottomed flask under argon, DMSO (10 mL, anhydrous >99.9%, degassed and dried over molecular sieves) and NaH (0.902 g, 23 mmol; 60% dispersion in mineral oil, Sigma Aldrich Batch 05716MH) was stirred together to yield a grey suspension. The reaction mixture was heated to 60˚C and stirred until evolution of $H_2$ was no longer observed (~30 minutes). A colour change from grey to yellow green was observed. The reaction mixture was cooled to 40˚C and the phosphonium salt (15 mmol) dissolved in DMSO (10 mL, dried over molecular sieves) was added dropwise to yield a dark orange solution.

After 1 h, benzaldehyde was added and the reaction was left to stir for 24 h, after which the mixture was cooled to room temperature and washed with water (50 mL). The solution was washed with diethylether (3 x 100 mL), water (1 x 50 mL), and brine (1 x 50 mL) prior to drying over anhydrous $MgSO_4$. The drying agent was filtered off and the filtrate was concentrated into a dark oil.

The oil was dissolved in hexanes (200 mL) and washed with acetonitrile (4 x 30 mL). The hexanes layer was concentrated into a yellow oil, which was purified by column chromatography (eluent 3:1 hexanes to diethylether) to yield the desired product, *12-phenyl-11-dodecen-1-ol* (0.401 g, 32 % yield).

| | |
|---|---|
| $^1$H-NMR (400 MHz, $CDCl_3$) | δ7.37-7.21 (m, 5H), 6.42-6.38 (m, 1H), 5.72-5.65 (m, 1H), 3.67-3.41 (m, 4H), 2.73-2.12 (m, 4H), 1.60-1.22 (m, 12H) |

## Synthesis of 12-phenyl-1-dodecanol

In a 150 mL round bottomed flask, 12-phenyl-11-dodene-1-ol (0.317 g, 1.22 mmol) was dissolved in hexanes (75 mL) and sparged with $N_2$. 10 wt% Pd/C (0.034 g, Strem Chemicals Batch A0368078) was added and the suspension was flushed with $H_2$ for 24 h. The reaction mixture was sparged with $N_2$ prior to filtration over Celite. $^1$H-NMR spectroscopy showed incomplete hydrogenation so the material was redissolved in hexanes (75 mL) and sparged with $N_2$. 10 wt% Pd/C (0.042 g, Strem Chemicals Batch A0368078) was added and the suspension was flushed with $H_2$ for 22 h. The suspension was sparged with $N_2$ prior to filtering over Celite. The solvent was removed *in vacuo* and the material was analyzed by $^1$H-NMR spectroscopy to show complete reduction of the vinylic protons to the desired product, *12-phenyl-1-dodecanol* (0.220 g, 69 % yield). The $^1$H-NMR spectum of the product matches that reported in the literature.[65]

| | |
|---|---|
| $^1$H-NMR (400 MHz, $CDCl_3$) | δ 7.27-7.19 (m, 5H), 3.66 (quartet, $^3J_{HH}$ = 5.6 Hz, 2H), 2.61 (t, $^3J_{HH}$ = 8.0 Hz, 2H), 1.61 (m, 4H), 1.29 (m, 16H) |

## Synthesis of 12-phenyldodecanethiol

A 10 mL round bottomed flask was charged with 12-phenyl-1-dodecanol (0.630 g, 2.40 mmol), thiourea (0.185 g, 2.43 mmol, Sigma Aldrich Batch 125K2506), and HBr (48% wt in $H_2O$, 0.85 mL). The biphasic reaction mixture was heated to 100 ˚C and stirred for 20 h, after which 2.5 M (10 wt%) NaOH(aq) was added and $N_2$(g) was passed over the reaction. Stirring was halted and the reaction was left heating at 100˚C for 2 h. The reaction mixture was cooled to room temperature and the aqueous layer was washed with diethyl ether (3 x 5 mL). The organic layers were combined and the solvent was removed *in vacuo* to yield a brown oil, identified by $^1$H-NMR spectroscopy to be *12-phenyl-1-bromododecane.*

| | |
|---|---|
| $^1$H-NMR (400 MHz, $CDCl_3$) | δ 7.28-7.19 (m, 5H), 3.43 (t, $^3J_{HH}$ = 6.8 Hz, 2H), 2.62 (t, $^3J_{HH}$ = 7.9 Hz, 2H), 1.87 (quintet, $^3J_{HH}$ = 7.1 Hz, 2H), 1.61 (quintet, $^3J_{HH}$ = 6.6 Hz, 2H), 1.29 (m, 16H) |

12-Phenyl-1-bromododecane (0.050 g, 0.15 mmol), thiourea (0.012 g, 0.16 mmol, Sigma Aldrich Batch 125K2506), and ethanol (0.1 mL) were heated to a reflux in a 10 mL round bottomed flask for 3 h. 2.5 M NaOH (aq) (0.1 mL) was added and the reaction was heated at a reflux for 2 h under $N_2$(g). The reaction mixture was cooled to room temperature and acidified with dilute $H_2SO_4$ dropwise until the pH was 2. The aqueous layer was washed with diethyl ether and the organic extract were combined, dried over $MgSO_4$, and concentrated to yield *12-phenyldodecanethiol*

(0.045 g, quantitative yield). $^{1}$H-NMR, $^{13}$C-NMR, and mass (high res, EI$^{+}$) of the final product matches that reported in the literature.[65]

| | |
|---|---|
| $^{1}$H-NMR (400 MHz, $CDCl_3$) | δ 7.21-7.19 (m, 5H), 2.64 (t, $^{3}J_{HH}$ = 7.5 Hz, 2H), 2.54 (quartet, $^{3}J_{HH}$ = 7.2 Hz, 2H), 1.64-1.61 (m, 4H), 1.38-1.25 (m, 16H) |
| $^{13}$C-NMR (400 MHz, $CDCl_3$) | δ 143.0, 128.4 (2C), 128.2 (2C), 125.6, 39.2, 36.0, 34.1, 29.6 (2C), 29.5 (2C), 29.4, 29.2, 29.1, 28.4, 24.7 |
| MS (High Res, EI$^{+}$) | 544.36 (disulfide), 278.19 (thiol) |
| IR ($cm^{-1}$) | 3027 (aromatic C-H stretch), 2926 (methylene C-H stretch), 2848 (methylene C-H stretch), 1599 (aromatic ring stretch), 1454 (aromatic ring bend), 750 (C-S bend), 700 (aromatic C-H bend) |

## Works Cited


[1] N. Berkowitz and J. Speight. *Fuel.* **1975**, 54, 138-148.

[2] T. Kasongo, Z. Zhou, Z. Xu, J. Masliyah. *Can. J. Chem. Eng.* **2000**, 78, 674-681.

[3] L.L. Schramm (ed). Surfactants: Fundamentals and Applications in the Petroleum Industry, Cambridge University Press, 2000.

[4] National Energy Board (September 2004), "Canada's Oil Sands: Opportunities and Challenges to 2015," www.neb.gc.ca, (January 8, 2009).

[5] M. Gray, Z. Xu, and J. Masilyah. *Phys. Today* **2009**, 31-35.

[6] K. Takamura. *Can. J. Chem. Eng.* **1982**, 60, 538-545.

[7] J. Czarnecki, B. Rodoev, L.L. Schramm, and R. Slavchev. *Adv. Colloid Interface Sci.* **2005**, 114-115, 53-60.

[8] K. Clark. *Trans. Can. Inst. Min. Metall.* **1944**, 47, 257.

[9] M. Ball. *Bull. Am. Assoc. Pet. Geol.* **1935**, 19, 153.

[10] K. Takamura. *Can. J. Chem. Eng.* **1982**, 60, 538-546.

[11] R. Ciese and C. van Oss. Colloid and Surface Properties of Clays and Related Minerals, Marcel Dekker, Inc., 2002.

[12] B. Velde (ed). Origin and Mineralogy of Clays. Springer-Verlag B, 1995.

[13] J. Liu, Z. Xu, and J. Masilyah. *AlChE J.* **2004**, 50, 1917-1927.

[14] V. Gupta and J. D. Miller. *J. Coll. Inter. Sci.* **2010**, 344, 362-371.

[15] X. Ding, C. Repka, Z. Xu, and J. Masliyah. *Can. J. Chem. Eng.* **2006**, 84, 643-651.

[16] Q. Du, Z. Sun, W. Forsling, and H. Tang. *J. Coll. Interface Sci.* **1997**, 187, 221-231.

[17] T.J. Senden, C.J. Drummond. *Colloids Surf., A.* **1995**, 94, 29-51.

[18] J. Read and D. Whiteoak. Shell Bitumen Handbook, 5th ed., Thomas Telford Publishing, 2003.

[19] J. Masilyah, Z. Zhou, Z. Xu, J. Czarnecki, and H. Hamza. *Can. J. Chem. Eng.* **2004**, 82, 628-654.

[20] G.D. Mossop. *Science* **1980**, 207, 145-152.

[21] L.L. Schramm, C. Morrison, and E.N. Stasiuk. *Fuel Process Tech*. **1998**, 56, 243-261.

[22] U.G. Romanova, H.W. Yarranton, L.L. Schramm and W.E. Shelfantook. *Can. J. Chem. Eng.* **2004**, 82, 710-722.

[23] K. Clark and D. Pasternack. *Ind. Eng. Chem.* **1932**, 24, 1410-1416.

[24] J. Long, J. Drelich, Z. Xu, and J. Masliyah. *Can. J. Chem. Eng.* **2007**, 85, 726-738.

[25] J. Hupka, J. Miller, and A. Coretz. *Mining Eng.* **1983**, 35, 1635-1641.

[26] J. Long, Z. Xu, and J. Masilyah. *Energy Fuels* **2005**, 19, 1440-1446.

[27] Z. Zhou, T. Kasongo, Z. Xu, and J. Masilyah. *Can. J. Chem. Eng.* **2004,** 82,696-708.

[28] L.L. Schramm and R. Smith. *Colloids Surf., A.* **1985**, 14, 67-85.

[29] L.L. Schramm and R. Smith. *Can. J. Chem. Eng.* **1987**, 65, 799-811.

[30] Q. Dai and K. Chung. *Fuel* **1996**, 75, 220-226.

[31] J. Liu, Z. Xu, and J. Masliyah. *Langmuir* **2003**, 19, 3911-3920.

[32] T. Kasongo, Z. Zhou, Z. Xu, and J. Masliyah. *Can. J. Chem. Eng.* **2000**, 78, 674-681.

[33] J. Liu, Z. Xu, and J. Masliyah. *Colloids Surf., A* **2005**, 260, 217-228.

[34] J. Liu, C. Repka, Z. Xu, and J. Masliah. *AlCHE J.* **2004**, 50, 1917-1927.

[35] E. Sanford. *Can. J. Chem. Eng.* **1983**, 61, 554-567.

[36] A. Rowe, R. Counce, S. Morton, M. Hu, and D. DePaoli. *Ind. Chem. Eng. Res*. **2002**, 41, 1787-1795.

[37] F. Camp. *Can. J. Chem. Eng.* **1977**, 55, 581-592.

[38] T. Burchfield and L. Hepler. *Fuel* **1979,** 58, 745-747.

[39] J. Long, Z. Xu, and J. Masliyah. *Colloids Surf., A.* **2006**, 281, 202-214.

[40] Schramm, L.L. (ed.) Suspensions: Fundamentals and Applications in the Petroleum Industry, Advances in Chemistry Series #251, American Chemical Society Publication, 2002.

[41] S. Renault, C. Lait, J. Zwiazek, and M. MacKinnon. *Environ. Poll.* **1998**, 102, 177-184.

[42] J. Long, H. Li, Z. Xu, and J. Masliyah. *AlCHE J.* **2006**, 52, 371-382.

[43] H. Li, J. Long, Z. Xu, and J. Masilyah. *Can. J. Chem. Eng.* **2008**, 86, 177-186.

[44] H. Li, J. Long, Z. Xu, and J. Masliyah. *Energy Fuels* **2005**, 19, 936-943.

[45] A. Sworska, J. Laskowski, and G. Cymerman. *Int. J. Miner. Process.* **2000**, 60, 143-152.

[46] Y. Liu, P. Jessop, M. Cunningham, C. Eckert, C. Liotta. *Science* **2006**, 313, 958-960.

[47] P.G. Jessop, C. Liang, and J. Harjani. Patent pending, 2010.

[48] T. Brown, H. LeMay Jr., B. Bursten, and J. Burdge. Chemistry: The Central Science 9th Ed., Pearson Education, 2003.

[49] J. Wijmans and R. Baker. *J. Membrane Sci.* **1995**, 107, 1 – 21.

[50] P. Gross. *Chem Rev.* **1933**, 13, 91-101.

[51] S.M. Mercer and P.G. Jessop. *Chem. Sus. Chem.* **2010**, 3, 467-470.

[52] E. Meyer *Prog. Surf. Sci.* **1992**, 41, 3-49.

[53] F. Giessibl. *Rev. Mod. Phys.* **2003**, 75, 949-983.

[54] R. Garcìa and R. Pérez. *Surf. Sci. Rep.* **2002**, 47, 197-301.

[55] T. Albrecht, P. Grütter, D. Horne, and D. Rugar. *J. Appl. Phys.* **1991**, 69, 668-673.

[56] A. Noy, D. Venzenov, C. Lieber. *Annu. Rev. Mater. Sci.* **1997**, 27, 381-421.

[57] T. Han, J. Williams, T. Beebe, Jr. *Anal. Chim. Acta* **1995**, 365-376.

[58] J. Drelich and K. Mittal (Ed). Atomic Force Microscopy in Adhesion Studies, Koninklijke Brill NV, 2005.

[59] B. Cappella and G. Dietler. *Surf. Sci. Rep.* **1999**, 34, 1-104

[60] C. Brundle, C. Evans, Jr. and S. Wilson. Encyclopedia of Materials Characterization, Butterworth-Heinemann, 1992.

[61] D. McQuarrie. Quantum Chemistry, University Science Books, 2008.

[62] D. Briggs and J. Grant. Surface Analysis by Auger and X-ray Photoelectron Spectroscopy, 2003.

[63] R.J. Hunter. Zeta Potential in Colloid Science: Principles and Applications. Academic Press, 1988.

[64] T. Cosgrove. Colloid Science-Principles, Methods, and Applications. Blackwell Publishing, 2005.

[65] D. Everett. Basic Priciples of Colloid Science, Royal Society of Chemistry, 1988.

[66] "Zeta Potential: An Introduction in 30 Minutes", Malvern Instruments.

[67] A. Delgado, F. González-Caballero, R. Hunter, L. Koopal, and J. Lyklema. *Pure Appl. Chem.*, **2005**, 77, 1753-1805.

[68] J. Liu, Z. Zhou, Z. Xu, and J. Masilyah. *J. Colloid Inter. Sci.* **2002**, 252, 209-218.

[69] Z. Chen, R. Ring, and J. Lemaitre. *J. Am. Ceram. Soc.* **1992**, 75, 3201-3208.

[70] C. Jucker and M. Clark. *J. Membr. Sci.* **1994**, 97, 37-52.

[71] S. Lee, A. Puck, M. Graupe, R. Colorado Jr., Y. Shon, R. Lee, and S. Perry. *Langmuir* **2001**, 7364-7370.

[72] J. Speziale. *Org. Syn. Coll.* **1963**, 4, 396-401

[73] R. Frank . and P. Smith. *J. Am. Chem. Soc.* **1946**, 68, 2103-2104.

[74] R. Nuzzo and D. Allara. *J. Am. Chem. Soc.* **1983**, 105, 4481-4483.

[75] C. Bain, H. Bieyuck, and G. Whitesides. *Langmuir* **1989**, 5, 723-727.

[76] J. Liang and J.H. Horton. *Langmuir* **2005,** 21, 10608-14.

[77] D.I. Kreller, G. Gibson, W. Novak, G.W. van Loon, and J.H. Horton. *Coll. Surf. A.* **2002**, 212, 249-264.

[78] D.I. Kreller, G. Gibson, G.W. van Loon, and J.H. Horton. *J. Coll. Inter. Sci.* **2002**, 254, 205-213.

[79] J. van den Brand, P.C. Snijders, W. G. Sloof, H. Terryn, and J.H.W. de Wit. *J. Phys. Chem. B* **2004**, 108, 6017-6024.

[80] D. A. Shirley. *Phys. Rev. B* **1972**, 5, 4709.

[81] J. M. Conney, C.J. Powell, and L.A. Currie. *Surf. Interf. Anal.* **1998**, 26, 939-956.

[82] J. M. Conney and C.J. Powell. *Surf. Interf. Anal.* **2000**, 29, 856-872.

[83] G. Attard and C. Barnes. Surfaces. Oxford University Press, 1998

[84] T. Lee, R. Carey, H. Biebuyck, and G. Whitesides. *Langmuir* **1994***, 10, 741-749.*

[85] G. Whitesides and P. Laibinis. *Langmuir* **1990**, 6, 87-96.

[86] C. Bain and G. Whitesides. *J. Am. Chem. Soc.* **1988**, 110, 3665-3666.

[87] Chemistry of Clays and Clay Minerals, A.C.D. Newman, Ed.

[88] R. K. Iler. Chemistry of Silica-Solubility, Polymerization, Colloid and Surface Properties and Biochemistry, John Wiley & Sons, 1979.

[89] M.V. Maslova, L.G. Gerasimova, and W. Forsling. *Colloid J.* **2004**, 66, 322-328.

[90] M. Kosmulski. Chemical Properties of Material Surfaces, Marcel Dekker, 2001.

[91] J. Liu, Z. Xu, and J. Masliyah. *J. Coll. Inter. Sci.* **2005**, 287, 507-520.

[92] K. Takamura and R.S. Chow. *J. Can. Pet. Technol.* **1983**, 22, 22.

[93] L. Xu and M. Salmeron. *Langmuir* **1998**, 14, 5841-5844.

[94] B. Sharma, S. Basu, ad M. Sharma. *Langmuir* **1996,** 12, 6506-6512.

[95] T. Gu and B. Zhu. *Colloids Surf.* **1990**, 44, 81.

[96] E. McCafferty and J. Wightman. *Surf. Interface Anal.* **1998**, 26, 548-564.

[97] S. Hussain, S. Demirci, and G. Ozbayoglu. *J. Colloid Interface Sci.* **1996**, 184, 535-541.

[98] J.D.G. Duran, M.M. Ramos-Tejada, F.J. Arroyo, and F. Gonzalez-Caballero. *J. Colloid Interface Sci.* **2000**, 299, 107.

[99] I. Sondi, J. Biscan, and V. Pravdic. *J. Colloid Interface Sci.* **1997**, 189, 66.

[100] J. Gregory. Particles in Water: Properties and Processes, Taylor & Francis, 2006.

[101] M.S. Zbik, R.C. Smart, G.E. Morris. *J. Colloid Interface Sci.* **2008**, 328, 73-80.

[102] H.J. Butt and M. Kappl. Surface and Interfacial Forces, John Wiley & Sons, 2010.

[103] M. Desando and J. Ripmeester. *Fuel* **2002**, 81, 1305-1319.

[104] S. Moschopedis, R. Hawkins, and J. Speight. *Fuel* **1981**, 60, 397-400.

[105] J. Liu, Z. Xu, and J. Masilyah. *Langmuir* **2003**, 19, 3911-3920.